2016

Electrospun polycaprolactone scaffolds: mechanical properties, alignment quantification, and topology induced gene expression

Timothy John Fee
University of Alabama at Birmingham

ELECTROSPUN POLYCAPROLACTONE SCAFFOLDS: MECHANICAL PROPERTIES, ALIGNMENT QUANTIFICATION, AND TOPOLOGY INDUCED GENE EXPRESSION

by

TIMOTHY JOHN FEE

JOEL BERRY, CHAIR
CRAWFORD DOWNS
ALAN EBERHARDT
HO-WOOK JUN
YONG ZHOU

A DISSERTATION

Submitted to the graduate faculty of The University of Alabama at Birmingham,
in partial fulfillment of the requirements for the degree of
Doctor of Philosophy

BIRMINGHAM, ALABAMA

2016

ELECTROSPUN POLYCAPROLACTONE SCAFFOLDS: MECHANICAL PROPERTIES, ALIGNMENT QUANTIFICATION, AND TOPOLOGY INDUCED GENE EXPRESSION

TIMOTHY JOHN FEE

BIOMEDICAL ENGINEERING

ABSTRACT

Producing tissue engineering scaffolds which mimic the structure and mechanical properties of the native extracellular matrix (ECM) is an important challenge in developing synthetic tissue replacements. Electrospinning is a frequently used technique to fabricate 3D nanofibrous scaffolds which match the dimensions of the fibrous elements of ECM. However, the mechanical behavior of electrospun materials is complex and challenging to predict. To aid in understanding the mechanical properties of electrospun materials, a microtensile testing platform was developed. This platform was used to quantify the mechanical properties of arrays of individual electrospun nanofibers. Additionally, this device permitted optical strain recording to visualize the true strain along the length of an electrospun fiber. To investigate the importance of fiber alignment within electrospun scaffolds, a metric of fiber alignment first needed to be defined. Using an image-based method, a metric for quantifying the alignment of fibers within an electrospun material was developed. It was found that this metric was correlated with the mechanical anisotropy of scaffolds fabricated under various conditions. Finally, the influence of fiber alignment on adherent cell behavior was examined. It was found that fibroblasts on aligned scaffolds elongate and reoriented to mirror the topological arrangement of their substrate. While fiber alignment does not significantly alter proliferation, the addition of 10% gelatin to the electrospun fibers did significantly increase cell proliferation compared to 100% polycaprolactone scaffolds. Additionally, it

was found that fibroblasts on aligned scaffolds express genes related to actin production, actin polymerization, and focal adhesion assembly at higher levels than fibroblasts on randomly oriented scaffolds. These results improve the ability to understand and predict the cellular response to fiber alignment in electrospun tissue engineering scaffolds.

Keywords: Biomaterials, Electrospinning, Mechanical Testing, Image Processing, Gene Expression

DEDICATION

Soli Deo Gloria

TABLE OF CONTENTS

Page

LIST OF TABLES

Table *Page*

A NOVEL DEVICE TO QUANTIFY THE MECHANICAL PROPERTIES OF ELECTROSPUN NANOFIBERS

LIST OF FIGURES

Figure *Page*

A NOVEL DEVICE TO QUANTIFY THE MECHANICAL PROPERTIES OF ELECTROSPUN NANOFIBERS

IMAGE BASED QUANTIFICATION OF FIBER ALIGNMENT WITHIN ELECTROSPUN TISSUE ENGINEERING SCAFFOLDS IS RELATED TO MECHANICAL ANISOTROPY

NANOFIBER ALIGNMENT REGULATES NIH3T3 CELL ORIENTATION AND CYTOSKELETAL GENE EXPRESSION ON ELECTROSPUN PCL+GELATIN NANOFIBERS

INTRODUCTION

Tissue Engineering

Tissue engineering has emerged from the realm of science fiction to a serious scientific discipline over the past years. Tissue engineered substitutes for skin, bone, heart valves, cartilage, and blood vessels have been reported [1]–[5]. The primary goal of tissue engineering is to produce living replacements for damaged and diseased tissues. The promise of tissue engineering is to return lost functionality without inducing harmful drug side effects (as in conventional pharmaceuticals), immune rejection, or a long-term foreign object in the body. These long-term goals are achieved by formulating an engineered tissue that replaces the damaged tissues with a biomimicking construct that recruits the patient's own cells to facilitate healing and regeneration, and implementing such a system with biodegradable materials that are naturally broken down and replaced with new tissue as the body regenerates itself [6].

A significant focus of tissue engineering has been the development of a matrix to permit cellular growth in three dimensions and provide a framework for cells to infiltrate and be supported as they produce new tissue. Frequently, biodegradable polymers are used to build scaffolds to provide this platform for 3D tissue growth and are frequently modified to promote specific cellular recruitment, adhesion, or function. Both natural and synthetic polymers have been used to produce scaffolds as well as hybrids of natural

and synthetic materials [7]. While a perfect tissue engineering system remains elusive, many researchers are progressing towards clinically acceptable tissue replacements.

Extracellular Matrix

A complicating factor for producing successful tissue engineering scaffolds is that living tissue is far more than a mass of contiguous cells; it contains substantial non-cellular components which are crucial for its function. The solid fraction of the non-cellular components of tissue is referred to as the extracellular matrix (ECM). This nanofibrous substrate produces an in vivo cellular environment which is far more complicated than cells growing in a suspension of fluid or on a smooth hard surface. Beyond the simple idea of a structural framework for cells support themselves, the ECM influences cellular behavior in many important ways. During human embryogenesis, ECM membranes are fabricated within two weeks of conception. As the embryo develops, the newly synthesized ECM aids in signaling and differentiation of stem cells into their organ precursors. As stem cells differentiate and become more specialized, the role of producing ECM is handed over to organ specific cells, such as osteoblasts and chondroblasts, but also fibroblasts which produce the ubiquitous collagen fibers. The vast majority of the ECM is composed of Collagen I [8]. Collagen I is the most massive dry component of the body and provides the primary structural component of the body. Collagen forms a nanofibrous network within the body that surrounds cells and tissues. It is believed that this nanoscale network of fibers can be influential in the overall behavior of adherent cells.

Because tissue engineering scaffolds are designed to mimic the native nanostructured environment of the ECM, nanoscale fabrication methods are important. The two basic approaches of fabricating nanostructured materials are: top-down and bottom-up. The top-down approach uses large-scale, or bulk, materials and removes material producing a finished product smaller than the starting size of the material. This process is not unlike a sculptor taking a large block of stone and carefully chiseling it down to a much smaller statue. Bottom-up production of nanoscale materials uses molecular-level building blocks for the construction of larger materials. The construction of nanofibers, nanofilms, and nanospheres has been reported using a bottom-up self-assembly technique [9]. Self-assembly is achieved by altering a solution of molecular building blocks in order to induce the molecules to form ordered solid structures. Besides self-assembly, electrospinning can be thought of as another bottom-up approach that is being extensively studied for tissue engineering scaffold applications.

Electrospinning

The rediscovery of the electrospinning in the late 1970's provided a simple method to produce nanoscale fibers that mimicked the microstructure and topology of naturally occurring collagen networks. Electrospinning of collagen itself was published in 2002 by Matthews et al. [10]. The ability to fabricate scaffolds that are composed of natural materials and also mimic the in vivo structure of the native ECM induced a boon to the field of tissue engineering as it was believed that this scaffold production method would permit the fabrication of tissues ex vivo and then be implanted to replace diseased or damaged tissues. However, in 2008 a research group published that the electrospinning

process denatured the collagen material, or disrupted the tertiary and quaternary structure of the protein, and resulted in fibers which were indistinguishable from gelatin fibers [11]. Consequently, most research into electrospun materials shifted to synthetic materials over natural materials. However, there is still debate in the scientific community over the possibility of electrospinning collagen. Electrospun collagen has been shown to have a slightly higher elastic modulus than electrospun gelatin. The same group has reported differences in gene expression from cells cultured on electrospun collagen vs electrospun gelatin, which the authors attribute to the difference in substrate stiffness [12]. In addition to collagen, many synthetic polymers have been successfully electrospun. Polylactic acid, Polyethylene oxide, and polycaprolactone (PCL) are just a few of the synthetic materials which have been electrospun as a potential tissue engineering scaffold. Additionally, many of these materials have been used in FDA approved medical implants. PCL is of particular interest due to its superior viscoelastic properties as compared to other biodegradable polymers [13].

The principle of electrospinning is simple: a polymer is dissolved in a volatile solvent which is extruded through a needle into a high-voltage static electric field. The combination of viscous and electrostatic forces causes the formation of a conical droplet at the end of the needle, known as a Taylor cone. From this Taylor cone, a thin stream of polymer solution is attracted towards a grounded collector some distance away. As the polymer stream moves to the collector, bending instability in the stream initiates a whipping motion of the polymer jet. Simultaneously, the volatile solvent evaporates forming solid polymeric fibers [14]. This combination of events leads to the formation of a randomly aligned non-woven mat of polymeric fibers on the collector. The

electrospinning set-up is comprised of only a syringe pump, a high-voltage power supply, and the appropriate polymers and solvents. Each of the parameters in the electrospinning process has been examined to understand how each factor influences the overall outcome. The parameters affecting the polymer solution include, polymer concentration, type of polymer, type of solvent, and viscosity of solution. Additional parameters used for customization include: polymer flow rate, diameter of needle, applied electric potential, shape of electric field, distance from needle to target, geometry of the target, and motion of the target [10], [14]. Precise control over fiber diameter has proven difficult. A recent paper by Seyedmahmoud et al. indicated that the solution viscosity was the primary driver of electrospun fiber diameter [15]. Electrospun fibers can have a large range of diameters depending on the fabrication parameters used. The fiber diameter has been shown to be as low as 200 nm for some conditions, and as large as several microns for other conditions. Additionally, electrospun fibers have been shown to have desirable mechanical properties, degradation properties, and have been functionalized to allow for binding of specific biomolecules [16], [17].

Traditionally, electrospinning is performed using a stationary conductive plate as the target. With this set-up, the electrospinning process deposits fibers in a non-aligned mat. Altering the collector geometry, collector motion, and electric field has successfully been used to induce alignment in the resulting fiber mat [14], [17], [18]. Producing aligned fibers is desirable for certain applications such as the engineering of artificial tendons and other anisotropic tissues [18], [19]. The ability to place cells in a mechanical environment that closely mimics physiological properties is a highly desired feature of

any tissue engineered implant. Electrospun scaffolds have been shown to mirror both the fibrous and anisotropic nature of naturally occurring extracellular matrix [10], [20].

Mechanical Properties of Electrospun Fibers

Because cells are known to receive biomechanical cues from their substrate, a thorough understanding of the mechanical properties of electrospun materials is required to understand the function of adherent cells. Relatively few groups have examined the mechanics of individual electrospun fibers. Tan et al. tested individual electrospun fibers of PCL using a standard tensile testing apparatus. Other groups have used AFM to deform a single electrospun fiber spanning a channel and measured nanoNewton loads [21], [22]. Fee et al. recently reported on mechanical properties of arrays of parallel electrospun fibers and showed the average behavior of an individual electrospun PCL fiber [23]. While measurements of individual fiber properties are important, the complex fiber-fiber interactions, combined with the porosity and anisotropy of 3D scaffolds necessitates mechanical characterization of full scaffolds.

The mechanical properties of electrospun scaffolds are complex. The fiber orientation, scaffold density, fiber diameter, and fiber crosslinking all influence the overall mechanical properties of the scaffold. A review by Stella et al. illustrates the scale-dependence of the mechanical response of electrospun scaffolds under load. At the macro level (on the order of millimeters), the scaffold exhibits non-linear elastic behavior similar to that of native tissue. At the meso scale (micron scale), electrospun fibers reorient under strain to go from tortuous or crimped fibers under no strain, to web like at high strain, with all the fibers stretched out and uncrimped. At the micro scale (nanometer

to micrometer), the inherent randomness of the electrospun scaffold and the fiber-fiber interactions can cause a heterogeneous strain field [24].

The macroscale tensile and viscoelastic properties of electrospun PCL specifically has been characterized by Duling et al. A constitutive model was developed using Fung's theory of quasilinear viscoelasticity. The model predicted stress values and observed stress values for a cyclic test were shown to correspond very well when the samples were preconditioned [25]. However, the scaffold density was not accounted for in this work, and no attempt at characterizing the effects of fiber alignment was made. The effects of fiber diameter and alignment have been examined with electrospun polyesterurathane urea. In this study, a computational model of electrospun materials was developed based on a neo-Hookean constitutive equation for individual fiber mechanical properties. The model agreed well with their experiments showing a decreased modulus for scaffolds composed of smaller diameter fibers [26]. It also matched the experimentally observed mechanical properties in the direction of aligned fibers. However, it failed to accurately predict the scaffold modulus when loaded perpendicular to the primary direction of fiber alignment in anisotropic scaffolds. Mechanical characterization of electrospun materials remains difficult as the microscale deformations arise from highly complex geometries and numerous fiber-fiber interactions.

Mechanotransduction

The mechanical relationship between cells and substrate is emerging as a crucial indicator of the biocompatibility of a tissue engineered construct. This process by which cells receive stimuli from mechanical cues is known as mechanotransduction. However,

many mechanotransduction signaling pathway remains elusive. Currently, two main hypotheses exist to explain the transduction of mechanical signals into the cell. The first hypothesis is called “tensegrity”, a shortening of tensional integrity. Tensegrity holds that cells use their focal adhesions as anchors and microfilaments like ropes to support tensile forces and to control cell structure and cellular morphology. Just as actin microfilaments support tensile loads, microtubules are used to support compressive loads (along their main axis) to aid in the overall cell structure in tensegrity theory [27]. This process of conducting forces along microfilaments and microtubules causes the entire cell to behave as a force transducer, that is, force on one side of the cell is transferred to the nucleus and every other part of the cell. The current alternative to the tensegrity hypothesis is the hypothesis of mechanosomes. The mechanosomes hypothesis says that only specialized regions (such as focal adhesions) transform the mechanical forces into a chemical signal [28]. It is clear that the nucleus is attached to some focal adhesions, but they claim that the mechanical signal must be transformed to a chemical one on the outside of the nucleus before alterations of gene expression occur.

The term tensegrity was coined by the architect Buckminster Fuller (designer of geodesic structures including the Epcot center) in the early 1960s, and is used to describe a structure composed of non-contacting compression elements supported by tension bearing elements [27], [29]. It is of specific interest to note that a certain tensegrity structures form a sphere in their low energy state, but when bound to a flat surface, they produce a flattened morphology, not unlike that of a cell bound to a substrate. This suggested that cell structure may be due to a tensegrity arrangement of the cytoskeleton [27]. A key point predicted by the theory is that perturbation of focal adhesions will cause

a change in distant portions of the cell, specifically the nucleus. It has been confirmed that the nucleus is displaced by the motion of focal adhesions [27], [30]. The clearest example is an experiment where the distal end of a neuron was stretched away from the cell body; the nucleus was pulled out of the cell body and into the axon [31]. Other research has been done to suggest that the actin cytoskeletal filaments are used to support the tensile forces in the cell and the microtubules are used as the compressive elements. This was indicated by measuring the force a neural axon exerts on a force gauge. When the axon was exposed to microtubule dissolving drugs, the axon exerted a tension force; when microfilaments dissolving drugs were used, the tension force relaxed [31]. Despite the evidence for cytoskeletal elements directly connecting focal adhesions and the nucleus, there is not currently data to indicate whether the nucleus can decode the mechanical information transduced on these fibers.

Substrate Topology

The influence of surface microtopology on adherent cellular morphology has been observed for decades. Studies of cells grown on surfaces with aligned microtopologies (ie micropatterning and aligned electrospun scaffolds) indicate an increased degree of cell polarization parallel to the direction of microtopographic features [32], [33]. Two main principles are used to explain this phenomenon. Firstly, the likelihood of a cell to change its shape to match topological features is termed “contact guidance”. This phenomena has been observed on micropatterned silicone, micropattered metals, and aligned electrospun materials [32]–[34]. In each case, cells prefer to orient themselves parallel to the direction of microtopography. Besides contact guidance, the mechanical anisotropy of aligned

electrospun tissues has been theorized to determine the polarization of adherent cells. It is well known from mechanical testing that aligned electrospun scaffolds exhibit highly anisotropic behavior. It has also been shown that cells seeded on anisotropic substrates tend to spread more in the stiffer direction. This result agrees well with data that indicates cells assume a more spread morphology when cultured on a stiffer substrate. Strong evidence for both contact guidance and anisotropic substrate sensing has been collected. Contact guidance has been shown on micropatterned silicon wafers which have similar mechanical properties in all directions, and anisotropic substrate sensing has been shown on smooth gels constrained uniaxially. Aligned electrospun matrices likely send both signals to cells, as the alignment of the fibers produces both topological and anisotropic mechanical cues. Beyond micropatterning, anisotropic substrates, and aligned electrospun fibers, protocols have been developed to use decellularized ECM as a substrate for cell culture [35]. While using decellularized ECM is the most accurate in vitro representation of the native ECM, the batch to batch variance and the possibility of lingering cytokines or other soluble signaling molecules necessitate a synthetic scaffold to insure consistency between samples.

Document Structure

As the development of a tissue engineering scaffold remains an important research area, this work has endeavored to improve the knowledge base for designing tissue engineering scaffolds. Initially, the mechanics of individual electrospun fibers were examined using a custom mechanical testing platform and an optical strain recording technique (Chapter 2). As larger electrospun scaffolds were considered, it became

apparent that fiber alignment induced anisotropy was a critical feature of electrospun scaffolds. Consequently, an image based descriptor of the fiber alignment within electrospun scaffolds was developed (Chapter 3). Finally, the importance of fiber alignment on the proliferation and gene expression of adherent fibroblasts was examined (Chapter 4).

A NOVEL DEVICE TO QUANTIFY THE MECHANICAL PROPERTIES OF ELECTROSPUN NANOFIBERS

by

TIMOTHY J. FEE, DERRICK R. DEAN, ALAN W. EBERHARDT, JOEL L. BERRY

Journal of Biomechanical Engineering, 124, 104503-1. DOI: 10.1115/1.4007635

ABSTRACT

Background: Mechanical deformation of cell-seeded electrospun matrices plays an important role in cell signaling. However, electrospun biomaterials have inherently complex geometries due to the random deposition of fibers during the electrospinning process. This confounds attempts at quantifying strains exerted on adherent cells during electrospun matrix deformation.

Method of Approach: We have developed a novel mechanical test platform that allows deposition and tensile testing of electrospun fibers in a highly parallel arrangement to simplify mechanical analysis of the fibers alone and with adherent cells.

Results: The device is capable of optically recording fiber strain in a cell culture environment. Here we report on the mechanical and viscoelastic properties of highly parallel electrospun poly(ε-caprolactone) fibers.

Conclusions: Force-strain data derived from this device will drive the development of cellular mechanotransduction studies as well as the customization of electrospun matrices for specific engineered tissue applications.

Keywords: Viscoelasticity, Polycaprolactone, Electrospinning, Tensile Testing

INTRODUCTION

The biomaterial poly(ε-caprolactone), (PCL), has been extensively used for electrospun tissue engineering applications [1, 2]. The appeal of PCL for tissue engineering includes its desirable mechanical properties, biodegradation time, previous use in FDA approved products, and ease of electrospinning into nanofibers. In some applications, electrospun PCL nanofibers mimic the nanofibrous nature of natural extracellular matrices thus contributing to the popularity of electrospinning as a method of producing scaffolds for tissue engineered constructs [2].

Precise characterization of the mechanical properties of electrospun materials is difficult due to the intricate network of fibers comprising bulk electrospun matrices. Previous efforts to characterize electrospun fiber mechanics have concentrated on understanding the influence of macro and micro scale features (such as porosity, fiber alignment, and fiber-fiber interactions) on the overall mechanical properties of the bulk material [3-12]. While the elaborate constitutive models developed from the testing of macro-scale electrospun materials are useful for the descriptions of the overall matrix properties, adherent cells only experience the properties of the material in their immediate vicinity [13, 14]. It remains unknown how electrospun fiber deformation affects the behavior of adherent cells.

A small number of reports exist which describe the mechanical testing of single electrospun fibers [15-21]. The majority of these reports use atomic force microscopy (AFM) to apply a strain and measure the forces of single fibers. While AFM has the

ability to accurately record nano-Newton loads, the technique is limited due to 1) restricted total deformation length, 2) fiber handling challenges, and 3) the inability to test complex fiber geometries or fiber-fiber interactions. The ability to quantify the load-strain behavior of individual electrospun fibers is a necessary pre-requisite for understanding the mechanical interaction between an electrospun substrate and adherent cells. Moreover, an understanding of the individual fiber mechanics is essential in modeling the mechanical behavior of three-dimensional networks of electrospun fibers and the strain response of cells seeded onto and within the network [22].

Multiple cell types possess an inherent contractile nature (e.g. myofibroblast, smooth muscle, cardiac). When these cells are combined with a biomaterial, the substrate mechanical properties, such as stiffness and roughness, have been shown to modulate a number of key cellular processes including gene expression, protein production, morphology, and migration [23-29]. Even in non-contractile cells, such as epithelium, it has been shown that mechanical forces have a strong influence on cellular behavior [30, 31]. The specific response of cells to deformation on electrospun materials, however, is largely unknown.

The main hindrance in studying the cellular response to deformation of electrospun substrates is the inherently complex geometry of electrospun materials. Even materials accepted to be “highly-aligned” contain fiber-fiber interactions, inhomogeneous deformation, and multi-scale mechanics [6]. Furthermore, there are no commercially available devices capable of performing mechanical testing including fiber strain measurements on electrospun materials with adherent cells. Ideally, a system for mechanical testing of electrospun materials will be capable of micron level deformations,

micro-Newton load recording, non-contact strain recording, and testing in physiological environment with samples containing cells. Additionally, a well-defined fiber geometry is needed for isolating the true mechanical properties of electrospun fibers without influence from fiber-fiber interactions or complex fiber geometry.

We therefore endeavored to produce a micro-tensile testing platform capable of performing mechanical testing on arrays of individual electrospun PCL fibers in a well-defined geometry. Here we show, for the first time, the load-strain behavior in PCL fibers generated from direct strain measurements of individual fibers. This system is ideally suited to quantify the influence of substrate deformation on adherent cell populations.

MATERIALS AND METHODS

Electrospinning

Nano-scale fibers of PCL were produced via electrospinning. PCL was purchased from Durect Polymers (Pelham, AL) with inherent viscosity =1.08 dL/g, and dissolved in a 50:50 mixture of dichloromethane and dimethylformamide (Fisher Scientific, Pittsburg, PA). The solution was extruded through a blunt tipped 25G needle at a rate of 1.0 mL/hr. The needle was charged to +17kV relative to a grounded collector (rectangular aluminum plate) located 20 cm from the end of the needle.

In order to produce highly aligned arrays of fibers, a forked metallic wand was rapidly waived just in front of the grounded target to capture individual fibers between the fork tines. From this non-aligned collection of individual fibers, all fibers were removed except one (Fig. 1A). This remaining fiber was manually deposited onto a separate set of parallel bars (representing the clamps of the tensile tester) under a stereoscopic microscope in a controlled orientation (Fig. 1B). Using this procedure, arrays of individual electrospun PCL fibers were produced and clamped for subsequent tensile testing.

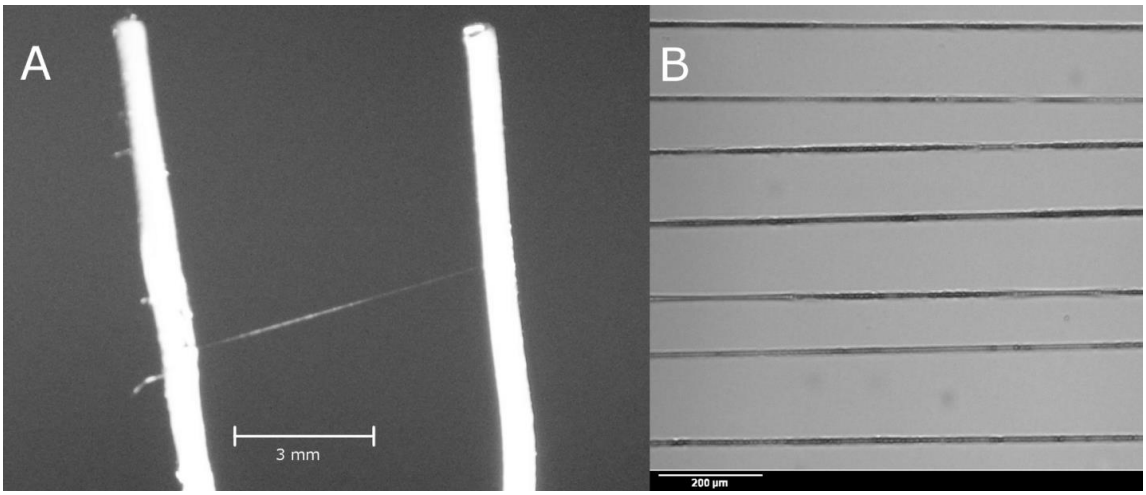

Figure 1. A) A single electrospun fiber suspended between the tines of a fork ready to be manually deposited in a parallel array. The scale bar is 3 mm. B) Micrograph of an array of parallel electrospun nanofibers, the scale bar is 200 microns.

It was anticipated that both fiber diameter and crystallinity could have a significant influence on the mechanical properties of the fibers [32]. Consequently, samples were characterized using differential scanning calorimetry (DSC, TA Instruments Q series 100 DSC, New Castle, DE, temperature was swept from -80°C to 80°C at a rate of 10°C/min) and scanning electron microscopy (SEM, FEI, Hillsboro, OR, accelerating voltage of 10kV) to quantify the polymer crystallinity and fiber diameter respectively. The reference enthalpy of fusion value used for 100% crystalline PCL was 135.44 J/g [33].

Mechanical Testing

A novel micro-tensile testing platform was fabricated (Fig. 2) utilizing a precision screw-type linear actuator (Newport TRA12-CC. Irvine, CA) and a 1.1N load cell (Futek, Irvine, CA). Both the actuator and the load cell controlled and received data from a

custom LabView program (National Instruments, Austin, TX). The specifics of the design of the novel testing platform are provided in Appendix A.

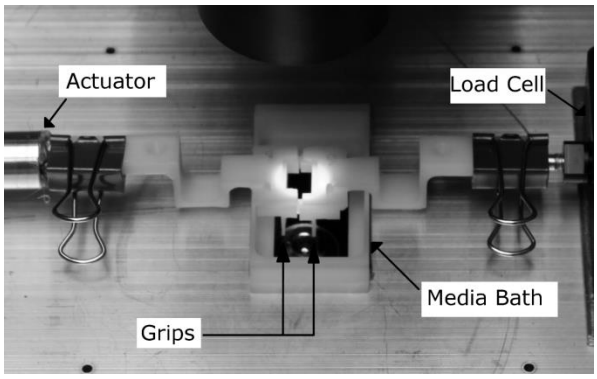

Figure 2. Image of the novel micro-tensile testing platform on the stage of an inverted microscope. The primary components of the device are identified.

Tensile testing was performed within the platform to characterize the mechanical properties of electrospun PCL. The fiber diameter, and therefore stress, could not be accurately measured using optical microscopy necessitating the need to report tensile forces as a functions of true strain ($\varepsilon_{True}=\ln[\varepsilon_{Eng}+1]$) to describe the behavior of the fibers. True strain was selected over engineering strain due to the expected large deformations. Stress relaxation testing was performed to quantify the viscoelastic properties of the electrospun samples. The stress relaxation response of the fibers was fitted to a two-term Prony series ($y[t]=a\times\exp[-t/\tau_1] + b\times\exp[-t/\tau_2]$) using a least squares algorithm.

Optical Strain Measurement

An optical tracking system was implemented to provide optical measures of the true strain present within electrospun fibers. Fluorescent micro-spheres (FluoroSphere Amine-modified 0.2 μm yellow-green, Invitrogen, Grand Island, NY) were prepared

according to manufacturer directions and diluted to a 1% (v/v) solution, then applied to the fibers via spraying.

The fluorescent strain markers on the fibers were tracked optically on an inverted fluorescent microscope. Video acquired during the test was processed using a custom MATLAB (Mathworks, Natick, MA) program which automatically tracked the motion of the fluorescent dots across the video frames. The custom MATLAB functions developed are provided in Appendix B. The location of each fluorescent dot in time relative to its reference position was used to determine the true strain along an individual electrospun PCL fiber (hereafter referred to as “optical strain”).

RESULTS

Electrospun Fiber Characterization

Electrospun PCL nanofibers were characterized using optical microscopy (for alignment), SEM (for diameter) and DSC (for crystallinity). Optical microscopy showed that the array of individual electrospun fibers were within 2 degrees of being completely parallel (Fig. 1B). The mean fiber diameter was 394nm and ranged from 310nm to 510nm (Fig. 3). The crystallinity was calculated from DSC by dividing the area under the melting curve by a reference value for 100% crystalline PCL. The crystallinity was found to be 53% (Fig. 4).

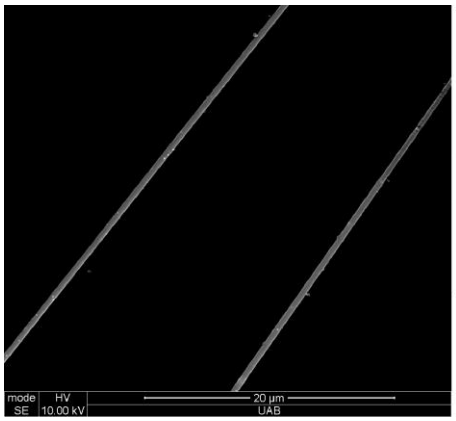

Fiber Diameter	
Mean	394 nm
Std. Dev	60.12 nm
Min	310 nm
Max	510 nm
N	15

Figure 3. Scanning Electron Microscope image of parallel electrospun PCL nanofibers. The scale bar is 20 microns. A table summarizing the distribution of fiber diameters is provided at right.

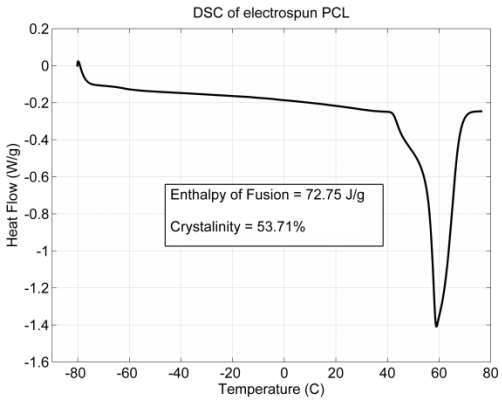

Figure 4. Differential Scanning Calorimetry of electrospun PCL. The data indicates that the PCL used for this study had a crystallinity of 53.7%.

Tensile Testing

Fluorescent strain markers were successfully applied to an array of individual PCL fibers and used to determine optical strain along the length of an electrospun fiber (Fig. 5). When optical strain is plotted against the load recorded during a tensile test, the load-strain response of the fibers was determined (Fig. 6A). It can be seen that the response of the PCL nanofibers is non-linear and hyper-elastic. By dividing the recorded load by the number of fibers present within a sample, the average load-strain response of a single PCL nanofibers can be determined (Fig. 6B).

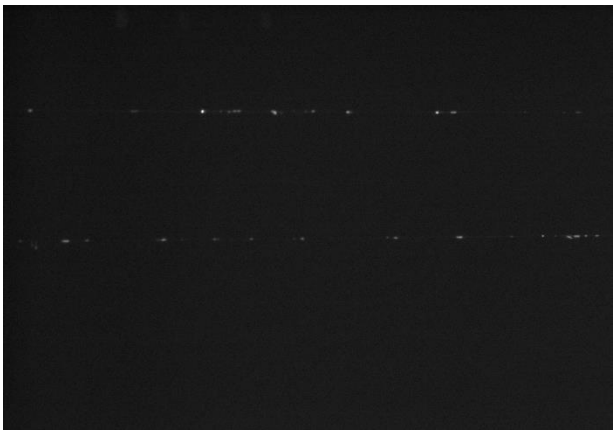

Figure 5. Fluorescent micrograph showing two electrospun PCL nanofibers with fluorescent strain markers adhered along the length of the fiber.

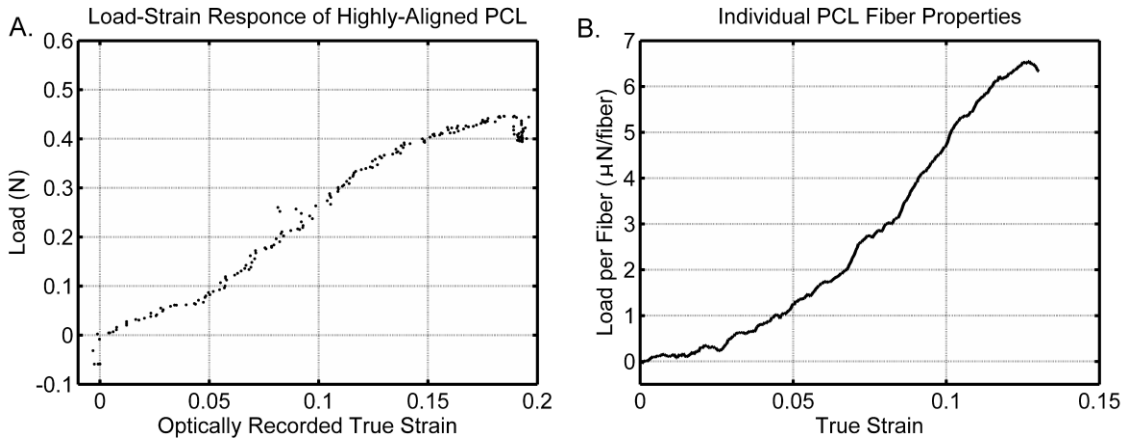

Figure 6. A) Graph showing a representative load-strain response of the highly-aligned PCL fibers. The true strain plotted on the horizontal axis was determined optically. B) A representative plot of the load-strain properties of a single electrospun PCL nanofiber in uni-axial tension.

Viscoelastic Testing

The time-dependent properties of electrospun PCL nanofibers were quantified using a stress-relaxation test. This test (performed in the absence of fluorescent strain markers), illustrates the viscoelastic nature of electrospun PCL. The viscoelastic response was modeled using a two-term Prony series linking the fiber behavior to a fast time constant and a slow time constant (Fig. 7).

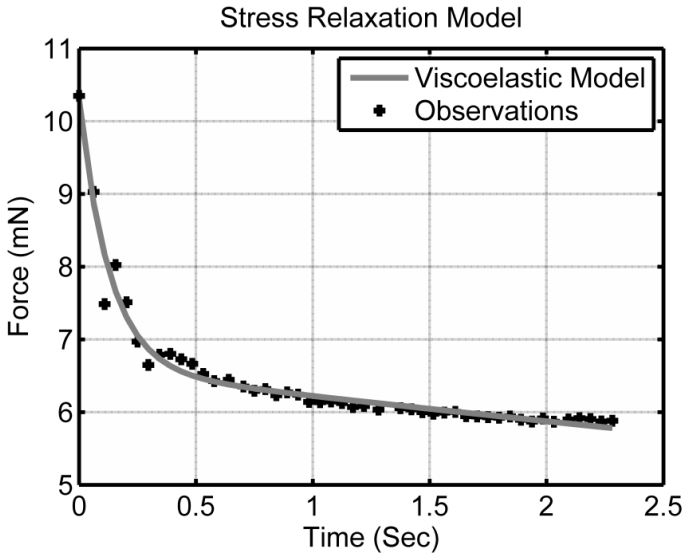

Load = a*exp(-time/b) +... ... c*exp(-time/d)	
a=	6.57
b=	17.825 seconds
c=	3.673
d=	0.1386 seconds
R^2 =	0.973

Figure 7. Stress relaxation test of highly-aligned PCL fibers. The viscoelastic response of the fibers was modeled using the two-term Prony series described in the table at right.

DISCUSSION

We have successfully produced arrays of parallel electrospun PCL nanofibers suitable for uniaxial tensile testing. The advantage to using an array of individual parallel fibers as opposed to random fibers or a thick sheet of aligned fibers is the improved accuracy of the measured fiber properties due to a) elimination of fiber-fiber interactions, b) elimination of off-axis loading, and c) higher confidence in average fiber properties due to larger sample sizes.

Additionally, we have produced a novel micro-tensile testing platform. This platform was designed to have the ability to perform a) tensile testing, b) viscoelastic testing, c) testing in physiological conditions, and d) testing with adherent cells. Electrospun PCL nanofibers were used to test the ability of the device to perform tensile and viscoelastic mechanical tests. One key benefit of using our novel testing platform is the ability to record fiber strain optically using fluorescent strain markers. To the authors' knowledge, this is the first time that strain along the length of an electrospun fiber has been directly measured. The ability to measure strain at multiple locations along a fiber is imperative in the case of testing fibers with non-uniform diameters, or non-homogeneous properties. The use of a two-term Prony series to model the stress relaxation behavior of electrospun fibers is consistent with the viscoelastic modeling of other electrospun fibers employed by other groups [19, 20]. The time constant values of τ_1=17.8 seconds and τ_2 =0.139 seconds are near the time constants reported for dry electrospun fibrinogen, τ_1=11 seconds and τ_2 =1.2 seconds [19].

Interestingly, the true strain at failure recorded using the novel testing platform and the values reported in the literature are significantly different. However, there was no significant difference in the engineering stress at failure (calculated using the average fiber diameter as determined by SEM) (Table 1). The cause for the fibers early failure remains unclear. Both SEM and DSC analysis indicated that the fiber diameter and crystallinity of the fibers were not significantly different than reported elsewhere. Additionally, the sources used to populate Table 1 were selected to match the conditions

Table 1. Mechanical properties of electrospun PCL fibers as observed and as reported in the literature.

		Eng. Stress at Failure (MPa)	**True Strain at Failure (%)**	**Sources**
Experimental Observations	Mean	50.14	17.89	
	SD	18.21	5.68	
	N	10	14	
Published Values	Mean	31.41	102.96	[18, 34, 35]
	SD	21.2	36.24	
	N	5	5	
	Significant ?*	No ($p=0.0979$)	Yes ($p<0.0001$)	

*Student's t-test, $\alpha=0.05$

used for our own tests (dry fibers at room temperature).

The data affirms that the novel micro-tensile testing platform is useful for determining the mechanical properties of ECM mimicking nanofibers frequently used in tissue engineered scaffolds. Though we have only as yet tested PCL on this platform, the same protocols can be used for testing any electrospun material. Additionally, the ability of our platform to conduct wet tests at physiological temperature permits the testing of samples with adherent cells. Though the parallel arrangement of fiber arrays does not represent the microstructure of natural tissues, understanding the properties of the components of ECM mimicking scaffolds in a defined geometry provides the foundation of knowledge that can be used to form models describing more complicated geometries.

We report the successful production of a micro-tensile testing platform with the capacities needed to perform mechanical testing on electrospun nanofibers. By using a microscope assisted optical strain recording method, the true strain along the length of an electrospun nanofibers has been directly measured. Additionally, we have generated parallel arrays of electrospun PCL fibers which allow the average load-strain response of a single PCL nanofiber to be measured. Our platform easily extends to permit testing in physiological conditions, bi-axial testing, multiple types of fibers, and testing of materials with adherent cells. This platform has implications for research into the mechanotransduction response of cells to substrate deformation.

REFERENCES

1. Baker BM, Nerurkar NL, Burdick JA, Elliott DM, Mauck RL. Fabrication and modeling of dynamic multipolymer nanofibrous scaffolds. J Biomech Eng. 131(10):101012. 2009.

2. Phipps MC, Clem WC, Catledge SA, Xu Y, Hennessy KM, Thomas V, et al. Mesenchymal stem cell responses to bone-mimetic electrospun matrices composed of polycaprolactone, collagen I and nanoparticulate hydroxyapatite. PLoS One. 6(2):e16813. 2011.

3. Amoroso NJ, D'Amore A, Hong Y, Wagner WR, Sacks MS. Elastomeric electrospun polyurethane scaffolds: the interrelationship between fabrication conditions, fiber topology, and mechanical properties. Adv Mater. 23(1):106-11. 2011.

4. Courtney T, Sacks MS, Stankus J, Guan J, Wagner WR. Design and analysis of tissue engineering scaffolds that mimic soft tissue mechanical anisotropy. Biomaterials. 27(19):3631-8. 2006.

5. D'Amore A, Stella JA, Wagner WR, Sacks MS. Characterization of the complete fiber network topology of planar fibrous tissues and scaffolds. Biomaterials. 31(20):5345-54. 2010.

6. Stella JA, D'Amore A, Wagner WR, Sacks MS. On the biomechanical function of scaffolds for engineering load-bearing soft tissues. Acta Biomater. 6(7):2365-81. 2010.

7. Driscoll TP, Nerurkar NL, Jacobs NT, Elliott DM, Mauck RL. Fiber angle and aspect ratio influence the shear mechanics of oriented electrospun nanofibrous scaffolds. J Mech Behav Biomed Mater. 4(8):1627-36. 2011.

8. Lake SP, Barocas VH. Mechanical and structural contribution of non-fibrillar matrix in uniaxial tension: a collagen-agarose co-gel model. Ann Biomed Eng. 39(7):1891-903. 2011.

9. Mauck RL, Baker BM, Nerurkar NL, Burdick JA, Li WJ, Tuan RS, et al. Engineering on the straight and narrow: the mechanics of nanofibrous assemblies for fiber-reinforced tissue regeneration. Tissue Eng B Rev. 15(2):171-93. 2009.

10. Nerurkar NL, Elliott DM, Mauck RL. Mechanics of oriented electrospun nanofibrous scaffolds for annulus fibrosus tissue engineering. J Orthop Res. 25(8):1018-28. 2007.

11. Raghupathy R, Barocas VH. Generalized anisotropic inverse mechanics for soft tissues. J Biomech Eng. 132(8):081006. 2010.

12. Raghupathy R, Witzenburg C, Lake SP, Sander EA, Barocas VH. Identification of regional mechanical anisotropy in soft tissue analogs. J Biomech Eng. 133(9):091011. 2011.

13. Stella JA, Liao J, Hong Y, David Merryman W, Wagner WR, Sacks MS. Tissue-to-cellular level deformation coupling in cell micro-integrated elastomeric scaffolds. Biomaterials. 29(22):3228-36. 2008.

14. Stella JA, Wagner WR, Sacks MS. Scale-dependent fiber kinematics of elastomeric electrospun scaffolds for soft tissue engineering. J Biomed Mater Res. 93(3):1032-42. 2010.

15. Tan EPS, Lim CT. Novel approach to tensile testing of micro- and nanoscale fibers. Rev Sci Instrum. 75(8):2581-5. 2004.

16. Tan EPS, Lim CT. Physical properties of a single polymeric nanofiber. Appl Phys Lett. 84(9):1603-5. 2004.

17. Tan EPS, Goh CN, Sow CH, Lim CT. Tensile test of a single nanofiber using an atomic force microscope tip. Appl Phys Lett. 86(7):073115. 2005.

18. Tan EP, Ng SY, Lim CT. Tensile testing of a single ultrafine polymeric fiber. Biomaterials. 26(13):1453-6. 2005.

19. Baker S, Sigley J, Helms CC, Stitzel J, Berry J, Bonin K, et al. The mechanical properties of dry, electrospun fibrinogen fibers. Mater Sci Eng C. 32:215-21. 2012.

20. Carlisle CR, Coulais C, Namboothiry M, Carroll DL, Hantgan RR, Guthold M. The mechanical properties of individual, electrospun fibrinogen fibers. Biomaterials. 30(6):1205-13. 2009.

21. Croisier F, Duwez AS, Jérôme C, Léonard AF, van der Werf KO, Dijkstra PJ, et al. Mechanical testing of electrospun PCL fibers. Acta Biomater. 8(1):218-24. 2012.

22. Stylianopoulos T, Bashur CA, Goldstein AS, Guelcher SA, Barocas VH. Computational predictions of the tensile properties of electrospun fibre meshes: effect of fibre diameter and fibre orientation. J Mech Behav Biomed Mater. 1(4):326-35. 2008.

23. Balestrini JL, Chaudhry S, Sarrazy V, Koehler A, Hinz B. The mechanical memory of lung myofibroblasts. Integr Biol (Camb). 4(4):410-21. 2012.

24. Heo SJ, Nerurkar NL, Baker BM, Shin JW, Elliott DM, Mauck RL. Fiber stretch and reorientation modulates mesenchymal stem cell morphology and fibrous gene

expression on oriented nanofibrous microenvironments. Ann Biomed Eng. 39(11):2780-90. 2011.

25. Huang X, Yang N, Fiore VF, Barker TH, Sun Y, Morris SW, et al. Matrix stiffness-induced myofibroblast differentiation is mediated by intrinsic mechanotransduction. Am J Respir Cell Mol Biol. 1(C):1-41. 2012.

26. Kurpinski K, Chu J, Hashi C, Li S. Anisotropic mechanosensing by mesenchymal stem cells. Proc Natl Acad Sci. 103(44):16095-100. 2006.

27. Mann JM, Lam RH, Weng S, Sun Y, Fu J. A silicone-based stretchable micropost array membrane for monitoring live-cell subcellular cytoskeletal response. Lab Chip. 12(4):731-40. 2011.

28. Park JS, Chu JS, Cheng C, Chen F, Chen D, Li S. Differential effects of equiaxial and uniaxial strain on mesenchymal stem cells. Biotechnol Bioeng. 88(3):359-68. 2004.

29. Park JS, Huang NF, Kurpinski KT, Patel S, Hsu S, Li S. Mechanobiology of mesenchymal stem cells and their use in cardiovascular repair. Front Biosci. 12:5098-116. 2007.

30. Tzima E, Irani-Tehrani M, Kiosses WB, Dejana E, Schultz DA, Engelhardt B, et al. A mechanosensory complex that mediates the endothelial cell response to fluid shear stress. Nature. 437(7057):426-31. 2005.

31. Zhang H, Landmann F, Zahreddine H, Rodriguez D, Koch M, Labouesse M. A tension-induced mechanotransduction pathway promotes epithelial morphogenesis. Nature. 471(7336):99-103. 2011.

32. Lim CT, Tan EPS, Ng SY. Effects of crystalline morphology on the tensile properties of electrospun polymer nanofibers. Appl Phys Lett. 92(14):141908-11. 2008.

33. Creszenzi V, Mazini G, Calzolari G, Borri C. Thermodynamics of fusion of poly-β-propiolactone and poly-ϵ-caprolactone. comparative analysis of the melting of aliphatic polylactone and polyester chains. European Polymer J. 8(3):449-63. 1972.

34. Thomas V, Jose M, Chowdhury S, Sullivan J, Dean D, Vohra Y. Mechano-morphological studies of aligned nanofiberus scaffolds of polycaprolactone fabricated by electrospinning. J Biomater Sci Polymer E. 17:969-84. 2006.

35. Kim GH. Electrospun PCL nanofibers with anisotropic mechanical properties as a biomedical scaffold. Biomed Mater. 3(2):025010. 2008.

IMAGE BASED QUANTIFICATION OF FIBER ALIGNMENT WITHIN ELECTROSPUN TISSUE ENGINEERING SCAFFOLDS IS RELATED TO MECHANICAL ANISOTROPY

by

TIMOTHY FEE, CRAWFORD DOWNS, ALAN EBERHARDT, YONG ZHOU, JOEL BERRY

Submitted to *Journal of Biomaterials Research part A*

Format adapted for dissertation

ABSTRACT

It is well documented that electrospun tissue engineering scaffolds can be fabricated with variable degrees of fiber alignment to produce scaffolds with anisotropic mechanical properties. Several attempts have been made to quantify the degree of fiber alignment within an electrospun scaffold using image-based methods. However, these methods are limited by the inability to produce a quantitative measure of alignment that can be used to make comparisons across publications. Therefore, we have developed a new approach to quantifying the alignment present within a scaffold from SEM images. The alignment is determined by using the Sobel approximation of the image gradient determine the distribution of gradient angles with an image. This data was fit to a Von Mises distribution to find the dispersion parameter κ, which was used as a quantitative measure of fiber alignment. We fabricated 4 groups of electrospun PCL+Gelatin scaffolds with alignments ranging from κ=1.9 (aligned) to κ=0.25 (random) and tested our alignment quantification method on these scaffolds. It was found that our alignment quantification method could distinguish between scaffolds of different alignments more accurately than two other published methods. Additionally, the alignment parameter κ was found to be a good predictor the mechanical anisotropy of our electrospun scaffolds. The ability to quantify fiber alignment within and make direct comparisons of scaffold fiber alignment across publications can reduce ambiguity between published results where cells are cultured on “highly aligned” fibrous scaffolds. This could have important

implications for characterizing mechanics and cellular behavior on aligned tissue engineering scaffolds.

Keywords: Electrospun, Image processing, Aligned Scaffold, Mechanical Anisotropy, Scaffold Characterization.

INTRODUCTION

The use of electrospun materials as tissue engineering scaffolds is a rapidly growing and promising area of research for generating replacements to damaged tissues. Fabrication of electrospun scaffolds only requires a simple set-up and the electrospinning parameters can be adjusted to yield highly customizable mechanical and microtopological properties. It is straightforward to produce electrospun scaffolds with customizable fiber diameters, porosities, and fiber alignments, among other features.

Fiber alignment within electrospun materials is of particular interest as it has been well shown to be a crucial modulator of many cellular behaviors. The influence of substrate microtopology and mechanical properties has been previously reviewed [1]. A few recent examples of how fiber alignment regulates cell behavior include: modulating myofibroblast differentiation, inducing alignment in nerve regeneration, and influencing proliferation of cardiac myocytes [2]–[6]. While many research groups have published on the importance of fiber alignment within electrospun scaffolds, a challenge remains in comparing the relative alignment of different scaffolds. Often times, researchers develop aligned electrospun fiber scaffolds and fail to quantify the fiber alignment in a way that can be used to compare the alignment of scaffolds across publications.

One of the most frequently cited methods of quantifying electrospun fiber alignment makes use of the fast Fourier transform (FFT) to identify directions of strong periodic behavior within a SEM image [7]. The basic concept of using of the FFT for

identifying directional components in biomedical images has been demonstrated as early as the 1980's [8]. This method has been widely used by researchers due to its ease and its use of freely available plugins and software (ImageJ by the NIH). While advantageous in that the method is simple to implement, the method relies on assumptions that make direct comparisons between images difficult. Specifically, the FFT method requires all images to be the same size, the image needs to lack large voids where no objects are present, and have symmetric boundary conditions.

The disadvantages of the FFT method were noted by researchers and an alternative approach was suggested [9]. As an alternative to the FFT, it has been suggested that using the Sobel-Feldman edge detection algorithm (often called the Sobel filter) as a method of determining edge orientation. This approach has several advantages: firstly, it is computationally faster and more sensitive than the FFT method, it ignores large voids where there are no detectable edges, and it contains some degree of robustness to image noise. However, using the Sobel filter in this way results in a data point for most of the pixels within an image. Comparing the alignment between multiple images remains challenging with such large sample sizes as significance testing is "trivial" [9].

A separate approach for measuring alignment involves an algorithm that automatically identifies fiber segments in SEM images. Where two fibers cross each other, an intersection point is defined. Researchers then quantify the orientation of fiber segments between intersection points as well as the density of fiber intersections in an SEM image [10]. While this method has been proven to be functional and mimics the intuitive approach of interactive fiber tracing methods, the morphological image

processing methods provides opportunities for reduced repeatability due to the structuring element size variability.

Another methodology that has been used cited by several research groups is the OrientationJ plugin for ImageJ [11]. The principle of the method is strongly based on the image gradient. It is advantageous in that it is easy to implement and it avoids many of the pitfalls of the FFT method. While the simple implementation is useful, the authors did not elaborate on methods for testing the significance of fiber orientation. Additionally, it is possible that using the image gradient is more sensitive to noise than the Sobel approximation of the gradient as suggested by others [9].

The currently used fiber alignment quantification methods demonstrate a lack of true “quantification” resulting in metrics that may or may not be useable for making direct comparisons across publications. In order to produce a method of truly quantifying the alignment present within an electrospun scaffold, we have undertaken the task of developing an image processing algorithm to assign a numeric value to the degree of fiber alignment within a SEM image. For such an algorithm to be successful, it must be: easy to implement, well defined mathematically, robust to image noise and number of objects, not require a priori knowledge of magnification or presumed alignment direction, provide a means of statistical significance testing between groups, and provide a simple numeric quantity for alignment strength.

Our hypothesis is that by using the Sobel approximation of the 2D image gradient and fitting the resulting orientation distribution to a Von Mises distribution will provide the coefficients needed for statistical significance testing of fiber alignment.

METHODS

Electrospinning

An electrospinning solution of polycaprolactone (PCL, Sigma, St. Louis, MO) and type A gelatin (Sigma) in a 90/10 (w/w) ratio was dissolved in Trifluoroethanol (Fisher Scientific, Pittsburg, PA) with 1% acetic acid (Fisher Scientific) it improve miscibility [12]. The PCL+Gelatin concentration was 10% (w/v). The solution was loaded into a 10 mL syringe with a 25 Gauge needle and extruded at a rate of 0.5 mL/hr into a high voltage electric field. The applied static electric potential was +17kV relative to a grounded cylindrical collector 20 cm away. The collector was rotated at various RPMs to collect fibers with various degrees of fiber alignment. Collector RPM was measured with a digital tachometer every 20 minutes throughout the 2 hours of electrospinning. All electrospinning parameters besides collector velocity were kept constant. As a control, one sample was electrospun using a stationary planar collector to produce random fibers. After electrospinning, each sample was put in a vacuum desiccator overnight to remove any residual solvent.

Mechanical Testing

Mechanical testing was performed using a RSA-G2 Dynamic Mechanical Analysis machine (TA Instruments, New Castle, DE). Sample length and width were measured using digital calipers and the sample thickness was measured using a Q-400

TMA machine (TA Instruments) with a probe capable of measuring thickness to less than 1 micron. Samples were strained in air at room temperature at a rate of 0.1 mm/sec. The strain was calculated by: $\varepsilon=\Delta\ell/\ \ell_0$, were ε is strain and ℓ is the length of the specimen. The stress was calculated by: $\sigma=F/A$, where F is the force applied and A is the cross-sectional area of the sample, which is width × thickness for a rectangular specimen. The tensile modulus was calculated from the stress-strain data by fitting a line to the stress-strain data for the first 10% strain (the biologically relevant portion of the curve) using method of least squares. For each alignment group, 7 separate samples were cut parallel to the direction of fiber alignment and another 7 were cut perpendicular to the direction of fiber alignment (N=7).

Scanning Electron Microscopy

Samples of electrospun matrices were prepared for Scanning Electron Microscopy (SEM) by sputter-coating with gold-palladium prior to imaging. Samples were imaged using a Quanta 650 FEG SEM (FEI, Hillsboro, OR) with an accelerating voltage of 10kV. At least five images were taken of each group of scaffolds (N=5).

Image Analysis

The fiber diameters of electrospun fiber matrices were determined from SEM images in ImageJ (NIH, Bethesda, MD). To quantify fiber alignment within SEM images, a novel method was developed based on estimation of the image gradient using the Sobel filter, then fitting the distribution of gradient angles to a Von Mises distribution. The Von Mises distribution parameter κ is then used as a metric for alignment strength. As a

comparison, other popular methods were implemented in MATLAB (Mathworks, Natick, MA) to validate the utility of the newly developed method. Custom MATLAB functions developed are provided in Appendix B.

Sobel filter image processing

To implement the Sobel approximation of the image gradient in MATLAB, horizontal and vertical Sobel edge detection filters were produced using the function *fspecial*. The horizontal filter ([-1,0,1;-2,0,2;-1,0,1]) and vertical filter ([-1,-2,-1;0,0,0;1,2,1]) were convolved with the input image I using the *imfilter* function in the Image Processing Toolbox ($S_{dir}=I(x,y)*Sobel_{dir}(x,y)$).The resulting matrices were combined to form an approximation of the 2D image gradient: $Grad(x,y)=S_h(x,y)\mathbf{i}+S_v(x,y)\mathbf{j}$. The gradient magnitude is: $||Grad(x,y)||=[S_h(x,y)^2+S_v(x,y)^2]^{0.5}$, and the corresponding angle of the gradient vector is calculated as: $\theta(x,y)=\arctan[S_v(x,y)/S_h(x,y)]$.

To determine the distribution of angles in the original image, the function *imhist* was used to form a histogram of the number of pixels with 180 bins of angles. The bimodal data on the range of $[0,2\pi)$ was transformed to the range of $[0,\pi)$ and then normalized such that the area under the curve was unity.

Angular Distribution Fitting

The distribution of fiber angles is produced from the normalized histogram of image gradients. The angular distribution of fibers was fitted to a Von Mises distribution using Maximum Likelihood Estimation, as implemented by the MATLAB function *mle*.

The Von Mises distribution for is given by: $f(\theta)=\exp(\kappa*\cos(2\theta-2\mu))/(\pi*I_0(\kappa))$ for $0\leq\theta\leq\pi$. Where the parameter μ is the direction strongest alignment, and the parameter κ ranges represents the angular dispersion. When κ is 0, the distribution is equivalent to a wrapped uniform distribution, and when κ is larger, the distribution approximates a wrapped normal distribution. The term I_0 is the zeroth order modified Bessel function of the first kind and is given by: $I_0(\kappa)=\Sigma\,[m!(m+1)]^{-1}(\kappa/2)^{2m}$, for $m=0,1,2,3,...,\infty$.

FFT image processing

To implement the FFT method of determining fiber alignment in an image, the method described by Ayres et al. was modified slightly to maximize performance. Firstly, the input image was multiplied by a 2D Hamm function which removes artifacts induced by non-periodic boundary conditions. Next, the MATLAB function *fft2* was used to compute the Fourier transform of the image. The resulting transformed image was re-organized into quadrants using the *fftshift* function. The intensity profile was then determined using the *improfile* function for 360 radii of a circle inscribed in the transformed image. The pixel values for each radius were summed to provide intensity values as a function of the radial angle. Finally, the angle for each radius was shifted by 90 degrees to account for the difference in the direction of periodicity and the direction of alignment within the original image. The bimodal data on the range of $[0,2\pi)$ was transformed to the range of $[0,\pi)$ and then normalized such that the area under the curve was unity.

OrientationJ processing

Quantification of fiber alignment using the OrientationJ plugin [11] was performed in ImageJ. The OrientationJ plugin outputs the data after the histogram of angles has been assembled, at which point the data was copied into MATLAB to be processed alongside the data acquired from each other method.

Statistical Analysis

Statistical calculations were performed in MATLAB statistics toolbox. Alpha was set to 0.05 for all experiments. Differences between groups were determined using one-way ANOVA with a post-hoc Tukey test for multiple comparisons. Data is displayed in figures as the mean with error bars of one standard deviation (SD).

RESULTS

Production of Aligned Electrospun Fibers

Electrospun PCL+Gel fibers were fabricated on a rotating mandrel and the surface velocity was modulated to produce scaffolds with varying degrees of fiber alignment and anisotropy. Five groups were produced with four different rotation speeds and one stationary flat collector (Figure 1 A-E). It was expected that using the lowest mandrel speed would result in a random distribution of fiber orientations. The group produced on the stationary flat collector served as a control group as it is well accepted that this technique produces randomly oriented fibers with isotropic mechanical properties. Samples from each mandrel rotation speed were imaged using SEM to quantify fiber alignment and fiber diameter. The results for each group are summarized in Figure 1F, and representative SEM images are shown in Figure 1A-E.

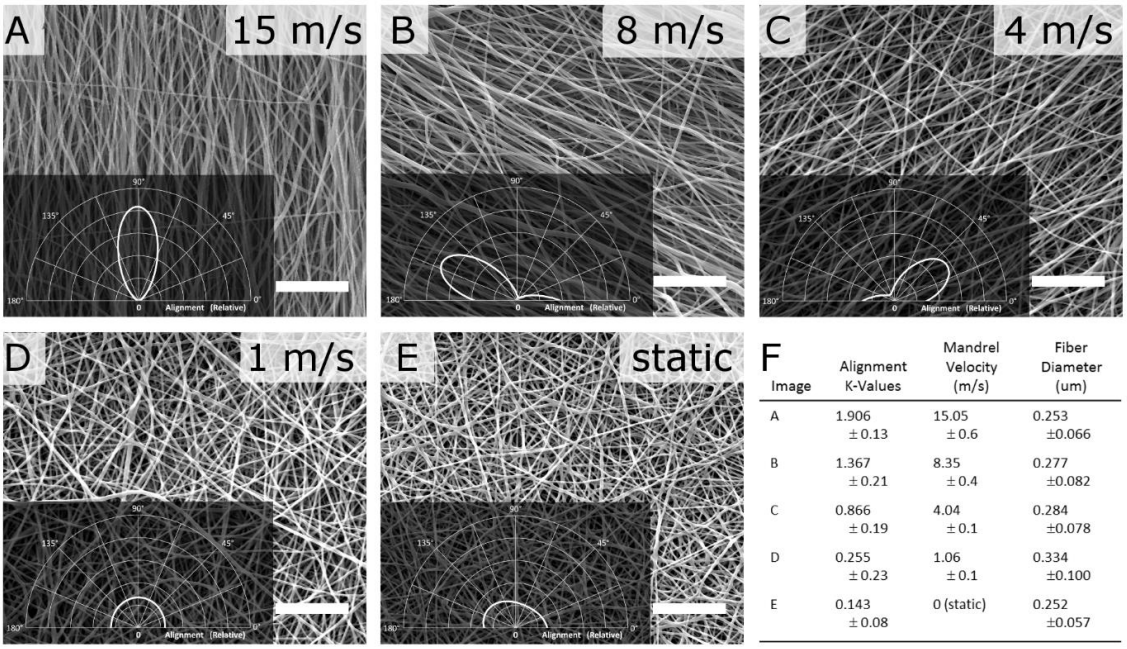

F

Image	Alignment K-Values	Mandrel Velocity (m/s)	Fiber Diameter (um)
A	1.906 ± 0.13	15.05 ± 0.6	0.253 ±0.066
B	1.367 ± 0.21	8.35 ± 0.4	0.277 ±0.082
C	0.866 ± 0.19	4.04 ± 0.1	0.284 ±0.078
D	0.255 ± 0.23	1.06 ± 0.1	0.334 ±0.100
E	0.143 ± 0.08	0 (static)	0.252 ±0.057

Figure 1. A-E) Representative SEM images of nanofibrous scaffolds produced with different collector velocities. Panels A-D are fibers collected on a rotating collector, panel E shows fibers collected on a stationary planar collector. The inset plot displays the Von Mises distribution representing the fiber alignment present within the image. Scale=10 μm. **F)** Table summarizing the alignment, collector velocity, and fiber diameter for each group of scaffolds represented in A-E (mean±SD).

Fiber Alignment Quantification

The novel method of quantifying fiber alignment from SEM images was tested against the FFT method and the 2D gradient method used by the OrientationJ plugin. Each algorithm was given the same set of images and the alignment distributions were fitted to the Von Mises distribution to determine the alignment parameter κ. The data in Figure 2 show the Sobel approximation of the gradient produces groups that are statistically different from each other and from the two randomly oriented groups. The OrientationJ method produces larger values of κ than the other methods, but only one group was statistically different than the rest. The FFT method has the smallest κ values, closest to a uniform distribution, but not all the groups were statistically different.

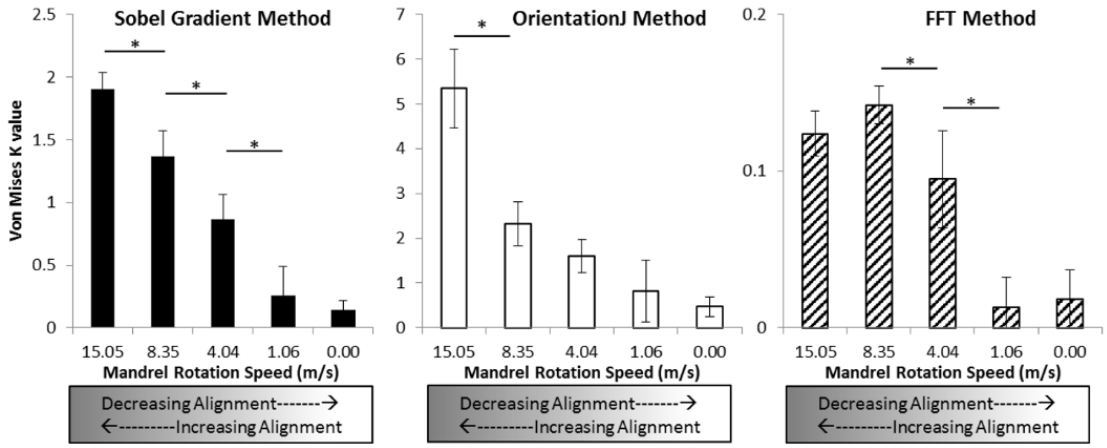

Figure 2. Comparison of alignment quantification methods. Each method was applied to the same set of images and the resulting angular distribution was fitted to a Von Mises distribution and the κ values representing quantified alignment are shown. The * denotes the indicated groups are statistically different (one-way ANOVA, Tukey post-hoc, $p<0.05$).

Mechanical Testing

The mechanical properties of scaffolds with different alignments were determined from uniaxial tensile testing. Representative stress-strain curves parallel and perpendicular to the direction of fiber alignment are shown in Figure 3 for samples from the κ=1.9 group and the κ=0.25 group. The moduli from the different groups are summarized in Figure 4. Electrospun scaffolds from the three highest collection speeds had significantly different moduli in the directions parallel and perpendicular to the direction of fiber alignment. When only the parallel direction modulus is considered, the scaffolds from the three highest mandrel speeds were statistically different from each other.

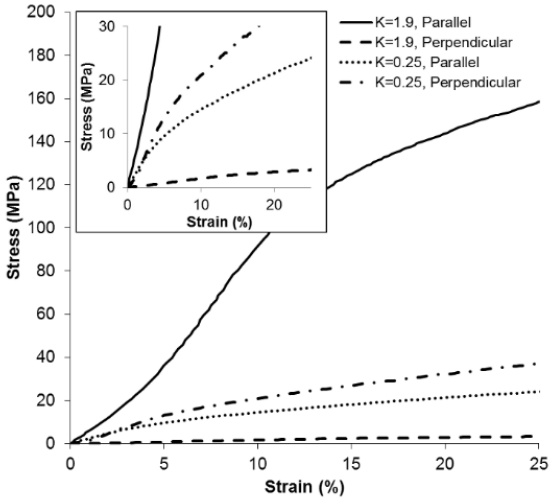

Figure 3. Representative stress-strain curves from the tensile tests performed on the most aligned group (κ=1.9) and the least aligned group (κ=0.25) both parallel and perpendicular to the direction of fiber alignment. The inset plot displays the same data, but plotted on a scale appropriate for the weaker scaffolds.

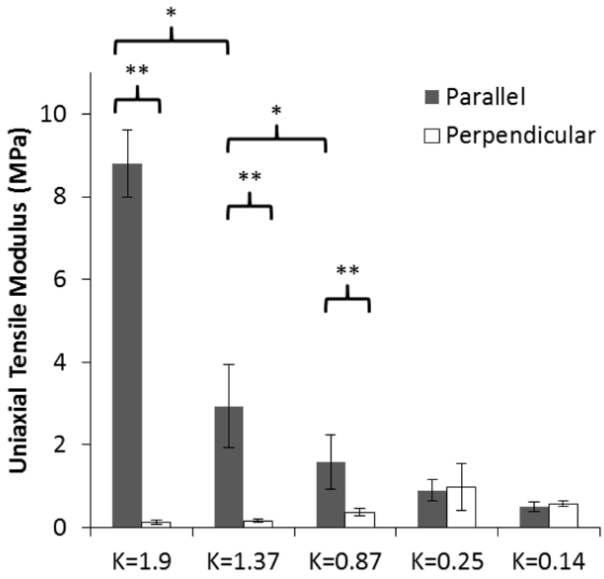

Figure 4. Summary of the uniaxial testing performed on scaffolds with different amounts of fiber alignment. Elastic modulus for the directions parallel and perpendicular to the direction of fiber alignment is shown for each group. The * indicates a statistically significant difference between the parallel moduli of the different groups (one-way ANOVA, Tukey post-hoc, $p<0.05$). The ** indicates a statistically significant difference between the moduli for the parallel and perpendicular direction within the group ($p<0.05$, 2-sample t-test).

Mechanical Properties Related to Fiber Alignment

It is well known that fiber alignment influences the observed mechanical properties of a fibrous material. The relationship between the alignment quantification parameter κ and the tensile mechanical properties of nanofibrous scaffolds is shown in Figure 5. It is apparent from the data that a linear relationship exists between κ and the log of the tensile modulus parallel to the direction of fiber alignment and also the log of the ratio of the moduli in the parallel and perpendicular directions.

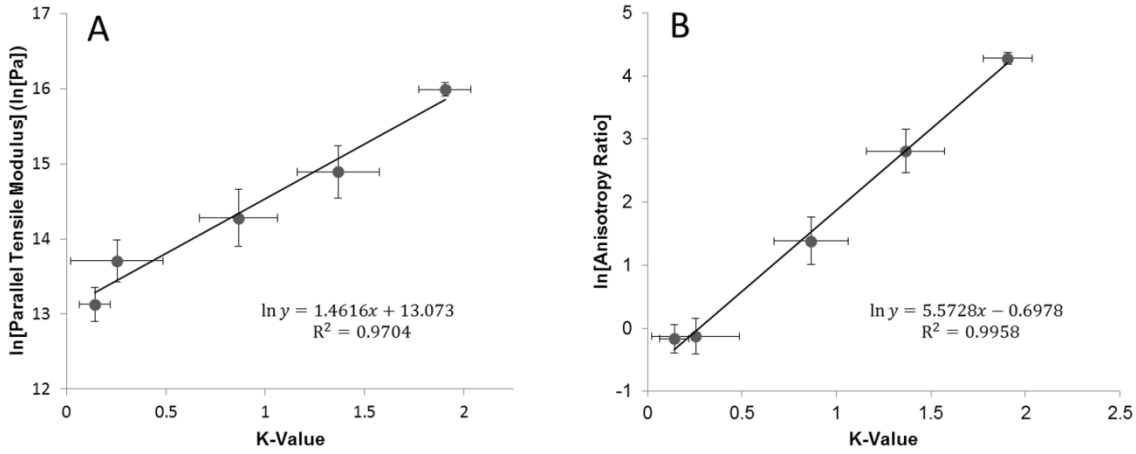

Figure 5. Relationship between the alignment parameter κ and the mechanical properties of the scaffold. **A)** The κ value is linearly related to the log of the modulus parallel to the direction of fiber alignment. Also, **B)** the κ value is linearly related to the log of the anisotropy ratio (defined as the ratio of the modulus in the parallel direction and the perpendicular direction).

DISCUSSION

Nanofibrous tissue engineering scaffolds were produced with controlled degrees of fiber alignment by using a cylindrical collector rotating at various speeds. This procedure yielded four distinct groups of scaffolds with mechanical anisotropy directly modulated by nanofiber alignment within the scaffold. SEM images were analyzed with a novel method of quantifying fiber alignment based on fitting the angles derived from the Sobel approximation of the gradient to a Von Mises distribution. The Von Mises parameter κ can then be used as a metric to quantify the fiber alignment. When compared to other published methods of quantifying alignment within a nanofibrous scaffold, the novel method described above was found to have a better capacity to resolve differences between groups of scaffolds with varying alignments.

The most intuitive method of quantifying fiber alignment in an image is to trace individual fibers with a straight line and record the angle of the line for each fiber, or a sufficiently large random sampling of fibers, and comparing the angular mean of the groups. This method is limited by the fact that SEM images typically contain hundreds of individual fibers, and for most data sets, the p-value approaches zero as N increases. The same issue occurs for quantification methods which generate an observation for each pixel within an image, as sample size increases the p-value becomes increasingly meaningless [13]. The value of the method presented here is the ability to use all the data within an image and generate a single data point, preserving the ability to use traditional

statistical analysis with sample size equal to the number of images, rather than the number of fibers measured or number of pixels within an image.

Using the Von Mises distribution to model the distribution of gradient angles is ideal for several reasons. Firstly, it is a wrapped distribution, which is necessary for angular data. It also varies from a uniform circular distribution when the value κ is small, and approximates the wrapped normal distribution when κ is larger, which permits using a single parameter, κ, to quantify alignment both random and aligned scaffolds.

Uniaxial tensile testing of the scaffolds showed isotropic random scaffolds and an increasing degree of anisotropy as the alignment parameter κ increased. The identification of increasing fiber alignment as the responsible factor induced anisotropy was supported by analysis of SEM images, which indicated no substantial differences in average fiber diameter between the groups. The tensile modulus values observed in our mechanical tests ranged from 0.9 ± 0.26 MPa for randomly oriented scaffolds and increased to 8.8 ± 0.81 MPa for the scaffolds with the highest degree of fiber alignment. The mechanical tensile properties of an electrospun material are dependent upon several parameters including: fiber diameter, fiber orientation, and fiber intersection density [10]. Additionally, it has been shown that the individual fiber properties differ from bulk electrospun materials due to the elimination of alignment and fiber-fiber interactions [14]. Consequently, a relatively broad range of mechanical properties have been previously published for electrospun materials. It has been reported that modulus values for 100% PCL ranging from 7.12 ± 0.8 MPa for random fibers up to 33.2 ± 1.98 MPa for “highly aligned” fibers [15]. It is possible that this research group observed this larger modulus as a result of their scaffolds having an average fiber diameter 100-250 nm larger than the

scaffolds used in this study. It has been previously shown that the incorporation of gelatin into PCL scaffolds alters mechanical properties by decreasing the tensile strength [16]. This is to be expected as electrospun gelatin has been reported to have an ultimate tensile strength no greater than 5 MPa [17]. Random sheets of pure electrospun gelatin have been reported as having a tensile modulus in the range of 116-174 MPa [17]. Adding PCL to Gelatin electrospun scaffolds was shown to decreased mechanical properties [16]. As the gelatin concentration increased from 33% to 66%, the tensile modulus decreased from 38 to 26 MPa for random fibers; the modulus decreased from 45 to 30 MPa for aligned fibers. The numerous factors influencing the mechanical properties of electrospun materials, compounded by the difficulty in measuring the thickness of sub-millimeter sheets, is likely to blame for the wide range of reported values in the literature and is why the modulus values observed in this study do not precisely mimic the values reported for other electrospun materials.

It is important to note that fitting the observed gradient angles to the Von Mises distribution should not be thought of as curve fitting, but rather distribution fitting. In traditional curve fitting using the method of least squares there are two measured parameters (the dependent variable as a function of the independent variable), however distribution fitting is only a single variable (observations from an underlying distribution). This subtle difference implies several factors which violate the assumptions made in the method of least squares. To account for this, the method of maximum likelihood estimation (MLE) was used to fit the observed distribution of angles. The principle of MLE is to estimate the distribution parameters which are most likely to produce the observed data.

Our data has shown that using the dispersion parameter (κ) of the Von Mises distribution, the amount of alignment present within an electrospun scaffold can be quantified from a SEM image. We have also demonstrated a link between the quantified fiber alignment and the anisotropy present within an electrospun material. While this technique was developed using SEM images of nanofibrous scaffolds, it is possible that this technique could be extended to other applications where quantification of alignment is important and not well suited to currently existing techniques.

Because the method we describe relies on MLE for determining statistical parameters, the limitations and assumptions of MLE should be noted. Specifically, MLE produces parameters which are unbiased estimators of the distribution parameters when the number of observations is sufficiently large. For smaller samples, such as a distribution with less than 5 observations for a given angle, the parameters returned by MLE are biased and might not represent the true distribution. This is of little concern in our case as each pixel in the image (with a gradient above a threshold strength) produces an observation, which results in >100000 observations in each of our analyzed images. MLE also requires knowledge or an assumption of the underlying distribution. The Von Mises distribution works very well for our case however, as it smoothly transitions from a wrapped uniform distribution to a wrapped normal distribution. Nevertheless, the Von Mises distribution will not provide a good description of the fiber alignment in cases of non-unimodal alignment.

CONCLUSIONS

In conclusion, we have developed a novel method of quantifying the alignment present within an electrospun scaffold using only SEM images. This method can be used to determine the degree of alignment within a scaffold and can be used to make direct comparisons of scaffold fiber alignment across publications can reduce ambiguity between published results where cells are cultured on “highly aligned” fibrous scaffolds. Additionally, we have shown that quantified alignment predicts the mechanical anisotropy which could reduce the time spent performing mechanical testing of an electrospun scaffold. A simple metric of fiber alignment is clearly a useful tool in the characterization of an electrospun material. This could have important implications for tissue engineering research where scaffold directed cell growth is desired.

ACKNOWLEDGEMENTS

The authors would like to thank the UAB High Resolution Imaging Facility SEM lab. This work was supported in part by the UAB BERM Center Pilot Grant and the EyeSight Foundation of Alabama Research Acceleration Initiative.

REFERENCES

1. Nikkhah M, Edalat F, Manoucheri S, Khademhosseini A (2012) Engineering microscale topographies to control the cell-substrate interface. Biomaterials 33:5230–46. doi: 10.1016/j.biomaterials.2012.03.079
2. Huang C, Fu X, Liu J, et al. (2012) The involvement of integrin β1 signaling in the migration and myofibroblastic differentiation of skin fibroblasts on anisotropic collagen-containing nanofibers. Biomaterials 33:1791–800. doi: 10.1016/j.biomaterials.2011.11.025
3. Cirillo V, Guarino V, Alvarez-Perez MA, et al. (2014) Optimization of fully aligned bioactive electrospun fibers for “in vitro” nerve guidance. J Mater Sci Mater Med 2323–2332. doi: 10.1007/s10856-014-5214-4
4. Huang C, Ouyang Y, Niu H, et al. (2015) Nerve Guidance Conduits from Aligned Nanofibers: Improvement of Nerve Regeneration through Longitudinal Nanogrooves on a Fiber Surface. ACS Appl Mater Interfaces 7:7189–7196. doi: 10.1021/am509227t
5. Safaeijavan R, Soleimani M, Divsalar A, Eidi A (2014) Comparison of random and aligned PCL nanofibrous electrospun scaffolds on cardiomyocyte differentiation of human adipose-derived stem cells. Iran J Basic Med Sci 17:903.
6. Nathan AS, Baker BM, Nerurkar NL, Mauck RL (2011) Mechano-topographic modulation of stem cell nuclear shape on nanofibrous scaffolds. Acta Biomater

7:57–66 ST – Mechano–topographic modulation of stem. doi: S1742-7061(10)00368-5 [pii] 10.1016/j.actbio.2010.08.007

7. Ayres C, Bowlin GL, Henderson SC, et al. (2006) Modulation of anisotropy in electrospun tissue-engineering scaffolds: Analysis of fiber alignment by the fast Fourier transform. Biomaterials 27:5524–34. doi: 10.1016/j.biomaterials.2006.06.014
8. Chaudhuri S, Nguyen H, Rangayyan RM, et al. (1987) A Fourier domain directional filtering method for analysis of collagen alignment in ligaments. IEEE Trans Biomed Eng 34:509–18.
9. Kemeny SF, Clyne AM (2011) A Simplified Implementation of Edge Detection in MATLAB is Faster and More Sensitive than Fast Fourier Transform for Actin Fiber Alignment Quantification. Microsc Microanal 17:156–166. doi: 10.1017/S143192761100002X
10. D'Amore A, Stella JA, Wagner WR, Sacks MS (2010) Characterization of the complete fiber network topology of planar fibrous tissues and scaffolds. Biomaterials 31:5345–54 ST – Characterization of the complete fib. doi: S0142-9612(10)00423-0 [pii] 10.1016/j.biomaterials.2010.03.052
11. Fonck E, Feigl GG, Fasel J, et al. (2009) Effect of aging on elastin functionality in human cerebral arteries. Stroke 40:2552–2556. doi: 10.1161/STROKEAHA.108.528091
12. Feng B, Tu H, Yuan H, et al. (2012) Acetic-Acid-Mediated Miscibility toward Electrospinning Homogeneous Composite Nanofibers of GT/PCL. Biomacromolecules 13:121114071036001. doi: 10.1021/bm3009389

13. Lantz B (2013) The large sample size fallacy. Scand J Caring Sci 27:487–492. doi: 10.1111/j.1471-6712.2012.01052.x

14. Fee TJ, Dean DR, Eberhardt AW, Berry JL (2012) A novel device to quantify the mechanical properties of electrospun nanofibers. J Biomech Eng 134:104503. doi: 10.1115/1.4007635

15. Thomas V, Jose M V, Chowdhury S, et al. (2006) Mechano-morphological studies of aligned nanofibrous scaffolds of polycaprolactone fabricated by electrospinning. J Biomater Sci Polym Ed 17:969–84 ST – Mechano–morphological studies of alig.

16. Guo Z, Xu J, Ding S, et al. (2015) In vitro evaluation of random and aligned polycaprolactone/gelatin fibers via eletrospinning for bone tissue engineering. J Biomater Sci Polym Ed 1–26. doi: 10.1080/09205063.2015.1065598

17. Huang ZM, Zhang YZ, Ramakrishna S, Lim CT (2004) Electrospinning and mechanical characterization of gelatin nanofibers. Polymer (Guildf) 45:5361–5368. doi: 10.1016/j.polymer.2004.04.005

NANOFIBER ALIGNMENT REGULATES NIH3T3 CELL ORIENTATION AND CYTOSKELETAL GENE EXPRESSION ON ELECTROSPUN PCL+GELATIN NANOFIBERS

by

TIMOTHY FEE, SWETHA SURIANARAYANAN, CRAWFORD DOWNS, YONG ZHOU, JOEL BERRY

Submitted to *PLOS ONE*

Format adapted for dissertation

ABSTRACT

To examine the influence of substrate topology on the behavior of fibroblasts, tissue engineering scaffolds were electrospun from polycaprolactone (PCL) and a blend of PCL and gelatin (PCL+Gel) to produce matrices with both random and aligned nanofibrous orientations. The addition of gelatin to the scaffold was shown to increase the hydrophilicity of the PCL matrix and to increase the proliferation of NIH3T3 cells compared to scaffolds of PCL alone. The orientation of nanofibers within the matrix did not have an effect on the proliferation of adherent cells, but cells on aligned substrates were shown to elongate and align parallel to the direction of substrate fiber alignment. A microarray of cyotoskeleton regulators was probed to examine differences in gene expression between cells grown on an aligned and randomly oriented substrates. It was found that transcriptional expression of eight genes was statistically different between the two conditions, with all of them being upregulated in the aligned condition. The proteins encoded by these genes are linked to production and polymerization of actin microfilaments, as well as focal adhesion assembly. Taken together, the data indicates NIH3T3 fibroblasts on aligned substrates align themselves parallel with their substrate and increase production of actin and focal adhesion related genes.

INTRODUCTION

Using electrospun materials as scaffolds for engineering tissue replacements remains a promising research area. Electrospun scaffolds can be fabricated from numerous biodegradable materials and their nanofibrous structure can possess features which mimic the architecture of the native extracellular matrix (ECM) of many tissues. The electrospinning apparatus only requires a few components and is highly customizable to produce tailored nanofibrous matrices. Electrospun scaffolds composed of highly aligned fibers are of particular interest due to their ability to modulate many cellular behaviors. Cells cultured on substrates with an oriented microtopology have been shown to behave differently than cells on randomly oriented or smooth materials [1]. Recent examples of substrate topology regulated cell behaviors include: inducing alignment in nerve regeneration, influencing proliferation of cardiac myocytes, and modulating myofibroblast differentiation [2]–[6].

Many materials have been successfully electrospun into nano-scale fibers. Polycaprolactone (PCL) is frequently used for electrospinning as it possesses several desirable mechanical properties. Specifically, PCL has a high elastic modulus and is simultaneously a hyper-elastic material and can be deformed to over 100% strain prior to failure, though some sources report a lower strain at failure [7]. Additionally, PCL is a biocompatible material with no reported cytotoxicity and is degradable on a timescale of months to years. These properties make PCL an attractive option for electrospun

scaffolds, but scaffolds produced from 100% PCL fibers are limited by poor cell adhesion due to the relatively high hydrophobicity of PCL. To improve the hydrophilicity of PCL scaffolds, researchers have: coated PCL scaffolds with a bioactive molecule such as collagen or fibronectin, or incorporated other materials in to the PCL fibers [8]–[10]. At first, collagen was widely incorporated into the electrospinning solution with PCL, however as questions arose about the secondary structure of collagen post-electrospinning, researchers began replacing collagen with gelatin in electrospinning solutions [11], [12].

Prior studies of substrate induced gene expression identify the cellular substrate as an important regulator of cellular behavior. Substrate topology induced changes in cell morphology have been documented in a litany of cell types including: neural progenitor cells, mesenchymal stem cells, smooth muscle cells, and Schwann cells [13]–[15]. Furthermore, various studies have shown substrate topology to be a regulator of gene expression in adherent cells. Neural progenitor cells have been shown to express neural differentiation markers when grown on aligned nanofibers over random fibers [13], [16]. Additionally, pre-osteoblasts show an increase in bone specific markers on aligned fibers over random fibers [17]. However, there is relatively little literature on the influence of substrate topology on fibroblasts. One study, using NIH3T3 fibroblasts, found that fiber orientation was a strong influence of cell morphology and speculated that this would also induce a change in gene expression [18].

In order to examine the role of the alignment of a nanofibrous substrate on the gene expression profile of adherent fibroblasts, we have fabricated and characterized an electrospun matrix of nanofibrous PCL+Gel fibers possessing a controlled orientation.

We have further quantified the physical properties of the substrate as well as the response of the adherent cells in terms of growth and expression of cytoskeleton regulation genes.

MATERIALS AND METHODS

Electrospinning

The electrospinning solution for 100% PCL fibers was formed from a 10% (w/v) solution of PCL (MW: 70 kDa - 90 kDa, Sigma, St. Louis, MO) in a 50:50 mixture of dichloromethane and dimethylformamide (Fisher Scientific, Pittsburg, PA). Electrospinning solutions used to form PCL+Gel fibers were made from polycaprolactone (PCL, Sigma, St. Louis, MO) and type A gelatin (Sigma) in a 90/10 (w/w) ratio dissolved in Trifluoroethanol (Fisher Scientific, Pittsburg, PA) with 1% acetic acid (Fisher Scientific) to improve miscibility [12]. The PCL+Gel concentration was 10% (w/v) in the electrospinning solution. Either polymer solution was loaded into a 10 mL syringe with a 25 Gauge needle and extruded at a rate of 0.5 mL/hr into a high voltage electric field. The applied static electric potential was +17kV relative to a grounded cylindrical collector 20 cm away. The collector was rotated at high RPMs to collect highly aligned fibers or at very low RPMs to produce randomly oriented fibers. After electrospinning, each sample was put in a vacuum desiccator overnight to remove any residual solvent.

Polymer Characterization

To confirm the presence of gelatin within the scaffold, Fourier Transform Infrared Spectroscopy (FTIR, Nicolet Thermo Scientific, Waltham, MA) operating in ATR mode.

To characterize the effect of gelatin on electrospun PCL crystallinity, samples were analyzed using differential scanning calorimetry (DSC, TA Instruments Q series 100 DSC, New Castle, DE), the temperature was swept from -20°C to 80°C at a rate of 10°C/min. The reference enthalpy of fusion value used for 100% crystalline PCL was 135.44 J/g [19]. The hydrophobicity of PCL and PCL+Gel was quantified by measuring the contact angle formed when a drop of water is placed on the surface of the material. After placing a 20 µl drop of water on the surface, the drop was imaged and the angle was measured using ImageJ (NIH, Bethesda, MD).

Cell Culture

NIH3T3 cells (American Type Culture Collection, Manassas, VA) were cultured in high glucose Dulbecco's Modified Eagle Medium (Fisher Scientific) supplemented with 10% fetal bovine serum (Fisher Scientific) and 1% penicillin and streptomycin (Fisher Scientific) in a humidified 5%CO_2 incubator at 37°C.

Cell Growth Assay

The PicoGreen (Life Technologies, Carlsbad, CA) assay was used to quantify cellular adhesion and proliferation on different substrates according to manufacturer's instructions. In short, adherent cells on different substrate conditions were rinsed with phosphate buffered saline, then lysed using RIPA buffer at day 0 (4 hours post seeding) and day 4. The lysate was collected and mixed with picogreen reagent and the fluorescence intensity was measured in a plate reader (Biotek, Winooski, VT).

Imaging

To observe adherent cells on electrospun scaffolds, samples were fixed in 10% neutral buffered formalin, then permeabilized in 0.05% Triton X-100 and stained with Acti-stain 555 phalloidin (Cytoskeleton Inc, Denver, CO) and 4',6-diamidino-2-phenylindole (DAPI). Stained samples were imaged on a Nikon A1 confocal microscope (Melville, NY). Additionally, cells were imaged using electron microscopy. Samples of cell-laden electrospun matrices were prepared for Scanning Electron Microscopy (SEM) by fixing in 10% neutral buffered formalin and chemically dehydrated via serial dilutions in ethanol followed by serial dilutions of hexamethyldisilazane before drying overnight in a vacuum desiccator. After drying, the samples were sputter-coated with gold-palladium and imaged using a Quanta 650 FEG SEM (FEI, Hillsboro, OR) with an accelerating voltage of 10kV.

Gene Expression Microarray

Gene expression studies were conducted from cells grown on mats of either random or aligned PCL+Gel fibers covering a 10 cm dish. One day after seeding, the cells were rinsed in PBS to remove non-adherent cells and lysed in TriZol reagent (Life Technologies). Total RNA was isolated using manufacturer's protocol, briefly, sample was homogenized in TriZol reagent, chloroform was added to remove the protein and DNA components, RNA was purified from the supernatant by isopropanol precipitation and then washed with ethanol before being resuspended in high quality nuclease-free water. The purity and quantity of the isolated RNA was measured by spectroscopy (Biotek). The RNA was reverse transcribed to cDNA using RT^2 First Strand kit (Qiagen,

Valencia, CA), and qPCR was performed using RT^2 Profiler PCR Array for mouse cytoskeleton regulators (Qiagen). The full list of genes included in the microarray are given in Appendix C.

Statistical Methods

Statistics were implemented in MATLAB (Mathworks, Natick, MA) using a test appropriate for the comparison being made, specifically t-tests for comparing two groups and ANOVA for multiple groups with a post-hoc Tukey HSD test for multiple comparisons (α=0.05). Gene expression data from microarray analysis was examined using the Benjamini–Hochberg method [20] to limit the false discovery rate to no more than 2 expected false discoveries out of all the rejected null hypotheses. To increase the likelihood of biological significance, the genes identified as statistically significant were further limited to genes with a fold change larger than 20%. Sample sizes were: N=4 for contact angle quantification, N=5 for cell growth assay, and N=3 for gene expression microarray tests.

RESULTS

Production of Electrospun Fibers

To probe the influence of substrate topology on fibroblast behavior, nanoscale fibrous matrices were produced by electrospinning. Fig 1 illustrates the electrospinning apparatus set-up. Fibers were produced with random or aligned orientations to mimic the different organization of collagen bundles within various tissues. Fig 1 also shows SEM images of 100% PCL fibers and fibers of PCL blended with gelatin (PCL+Gel).

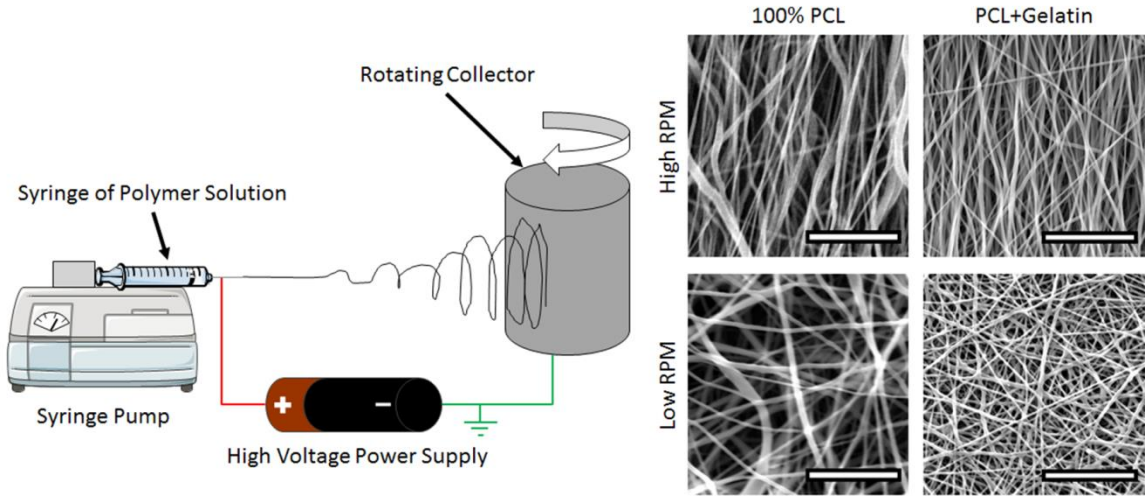

Fig 1. Electrospinning Apparatus and Resulting Nanofibers A) Diagram of the electrospinning set-up: A polymer solution is extruded from a syringe into a high-voltage electric field towards a grounded cylindrical collector. When the collector is rotating at high RPM, aligned fibers are collected; when the collector is rotating at low RPM, randomly oriented fibers are collected. B) Example SEM images of nanofibers collected under various conditions. Scale bars are 10 microns.

Characterization of Fibers

FTIR and DSC were performed to characterize the material properties of the synthesized electrospun nanomatrices. FTIR data (Fig 2A) shows a characteristic peak for amines at 3300 1/cm for the 100% gelatin sample, and no peak for the 100% PCL sample. For the PCL+Gel sample, a smaller peak is present indicating the presence of gelatin within the sample, the height of the smaller peak is 11% of the 100% gelatin peak, which confirms the ratio of PCL to gelatin in the PCL+Gel sample. To characterize the thermal properties of the material, DSC was performed. The DSC data (Fig 2B) indicates that pure PCL melts at 59°C and has a crystallinity of 49%, which is similar to other reported crystallinity values for electrospun PCL [7]. The addition of gelatin to the PCL did not alter the melting point, and only slightly decreased the enthalpy of fusion, indicating that the crystalline structure of the PCL fibers was not substantially altered by the addition of the gelatin.

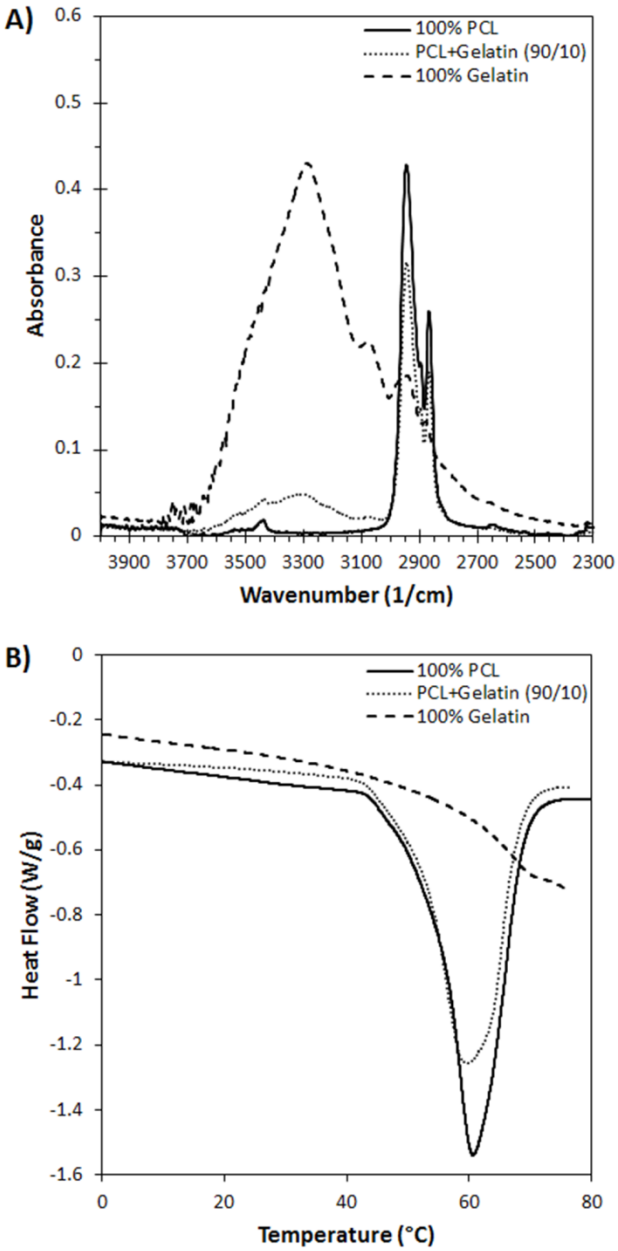

Material	T_m (°C)	ΔH_m (J/g)	%Crystallinity
100% PCL	59.0	66.75	49.28
PCL+Gelatin	59.4	64.67	47.75

Fig 2. Polymer Characterization A) Fourier Transform Infrared Spectroscopy (FTIR) of samples of electrospun gelatin, PCL, and PCL+Gel blend. The data PCL+Gel shows a characteristic N-H stretch peak for amines at 3300 1/cm. This confirms the presence of gelatin within the electrospun matrix. B) Differential Scanning Calorimetry (DSC) of samples of electrospun gelatin, PCL, and PCL+Gel blend. The data indicates that the addition of gelatin to the PCL does not drastically change the crystallinity or melting point of the PCL.

The adsorption of biomolecules to the surface biomaterial is strongly linked to the hydrophilicity of the surface. To quantify the surface hydrophilicity of the electrospun materials, the contact angle was measured as shown in Fig 3. The contact angle for water on 100% PCL was found to be 124.7±8.2°, while the contact angle for water on PCL+Gel was found to be 25.7±6.4°.

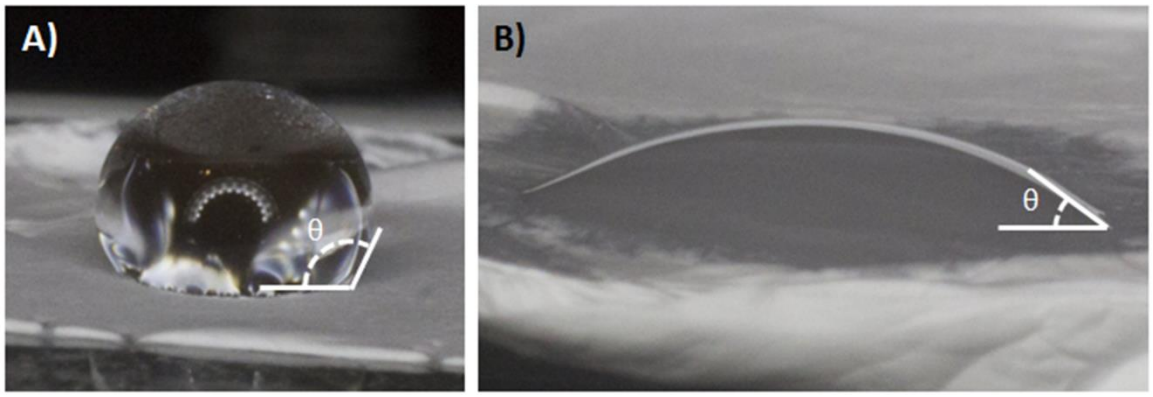

Fig 3. Hydrophilicity Quantification A) A water drop on 100% PCL, the hydrophobic surface produces a large contact angle. B) A water drop on PCL+Gel surface, the gelatin increases the hydrophilicity of the surface producing a smaller contact angle. The data shows a clear change in contact angle induced by the addition of gelatin into the electrospun fiber mat.

Cell Adhesion Response on Fibers

NIH3T3 fibroblast proliferation and growth on electrospun matrices were quantified at 0 and 4 days (FIGURE 4). After cells were seeded on random or aligned PCL or PCL+Gel, they were allowed to adhere for 4 hours then washed and the remaining cells were quantified. The data in Fig 4 shows that on day 0, there is very little difference in cellular adhesion on 100% PCL compared to PCL+Gel. After 4 days, there was a statistically significant difference in the growth rate of fibroblasts on the scaffolds

containing gelatin. At both 0 and 4 days there was no significant difference between groups of random and aligned fibers.

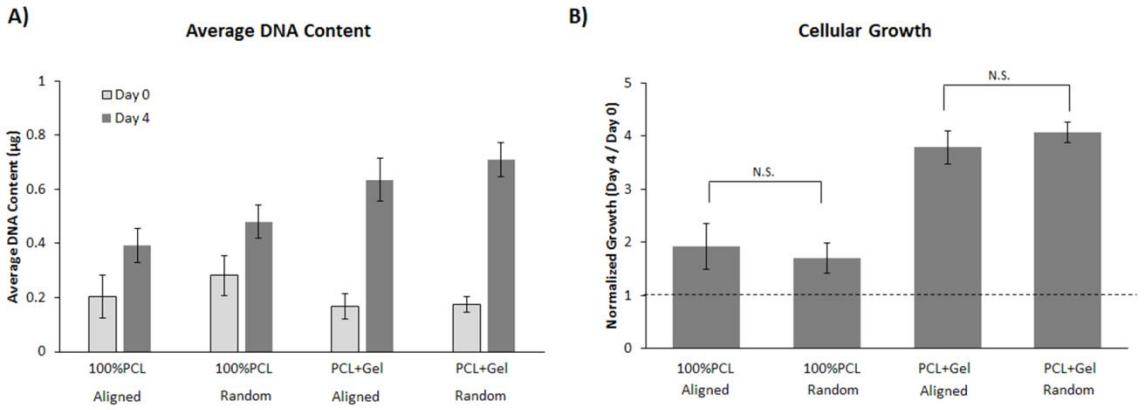

Fig 4. Proliferation assay of NIH 3T3 cells growing on various substrates. A) The average amount of DNA for cells grown on each substrate at 0 and 4 days. The DNA content is directly proportional to the number of cells. B) The cellular growth rate on various substrates as determined by the ratio of DNA content on days 0 and 4. This data indicates that orientation of the fibrous substrate does not influence the initial attachment or growth rate of NIH3T3 cells. However, the addition of gelatin does a substantially increase the growth rate over 100% PCL matrices ($P<0.05$, 2-way ANOVA, Tukey post-hoc). Error bars are ±SD.

Cell Alignment Changes on Fibers

To observe the morphological response of fibroblasts on PCL+Gel to substrate topology, adherent cells were imaged using fluorescent and electron microscopy. Fibroblasts growing on an aligned substrate showed a clear preference to elongate and orient themselves parallel to the direction of fiber alignment, while fibroblasts on randomly oriented fibers show no preferential orientation (Fig 5).

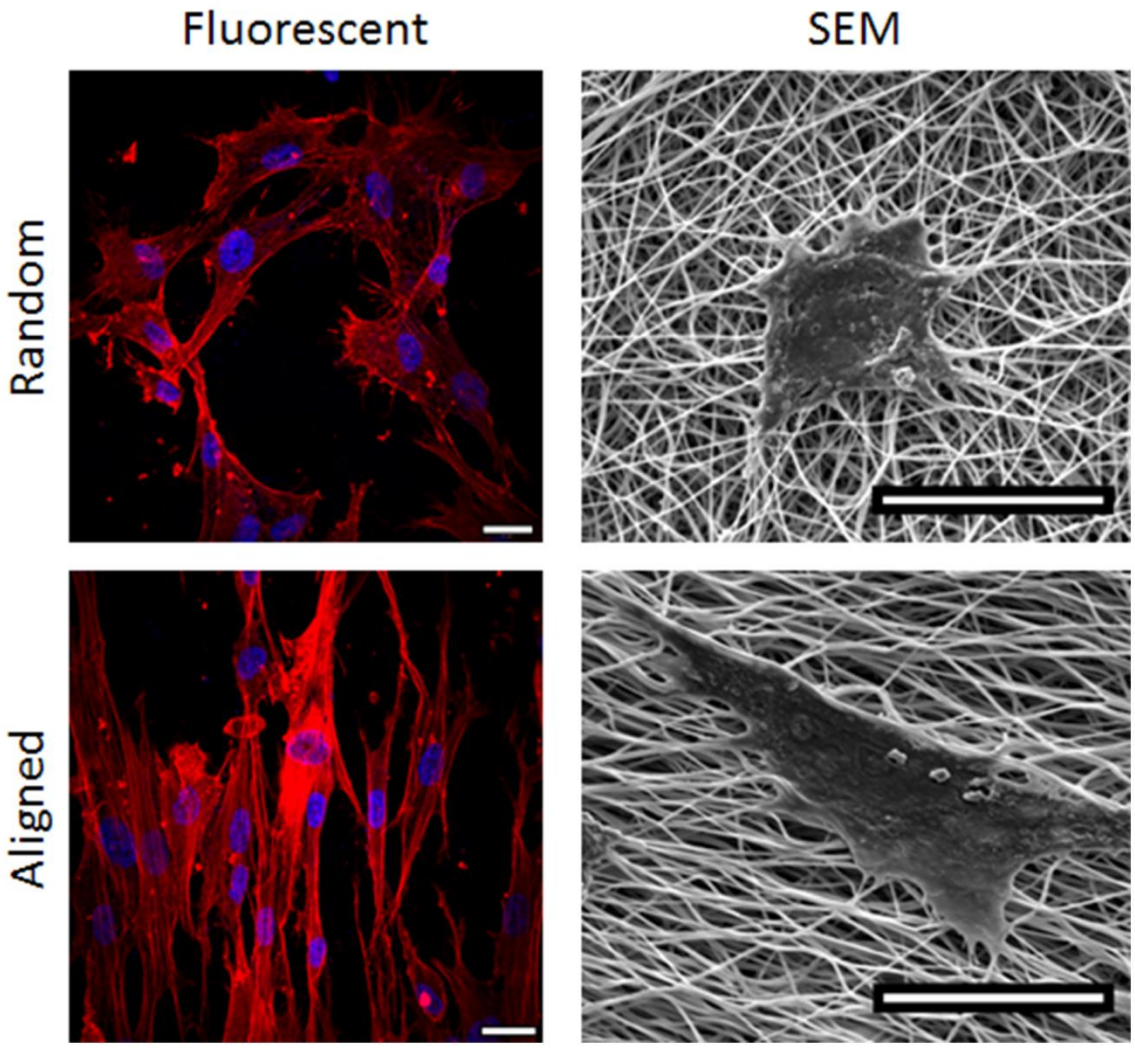

Fig 5. Microscope images showing cells growing on random (top) or aligned (bottom) electrospun PCL+Gel fibers. Fluorescent images are shown on the left with the cells stained to show the nuclei and stress fibers, while electron microscope images are shown on the right to illustrate the cellular interactions with the substrate. All image scale bars are 20μm.

Cell Gene Expression Response on Fibers

To examine how fibroblasts respond to the topological signals of their substrate, a panel of cytoskeletal regulators was probed in a gene expression microarray. Of the 84 genes examined, the expression of 12 were found to be statistically different between the

random and aligned scaffolds. Because statistical significance does not always equate to biological significance in gene expression studies, the genes identified as statistically significant were further limited by the magnitude of the fold change, resulting in 8 genes with altered expression (Fig 6A). Combining a fold-change magnitude threshold with a statistical significance threshold has been previously utilized to identify differentially expressed genes [21], [22]. The protein products of the upregulated genes were associated with actin polymerization and focal adhesion formation (Fig 6B).

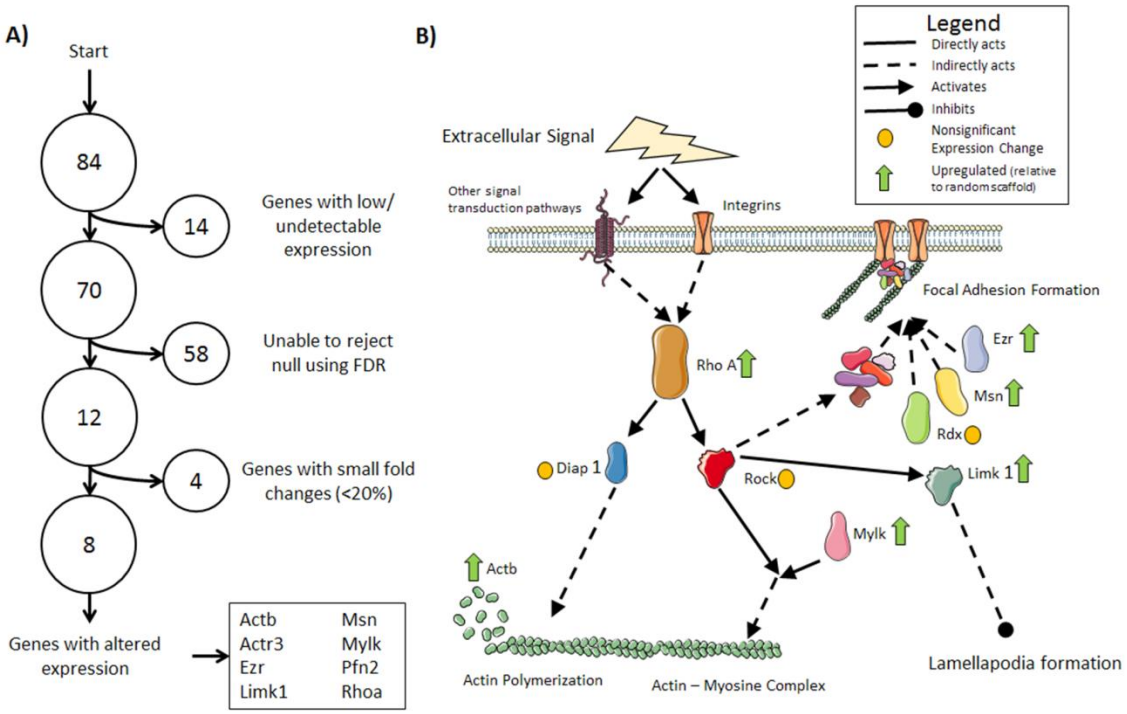

Fig 6. Gene Expression Microarray Results A) A diagram showing the process for identifying genes with altered expression: the false discovery rate (FDR) was calculated using BH method to limit the FDR to at most 2 expected false positive results in the all rejected null hypotheses (FDR=16.6%). These results were further limited to genes with the largest fold changes (fold change > 20%). B) Pathway diagram illustrating where the protein products of several of the identified genes work to promote actin production and polymerization and focal adhesion assembly.

DISCUSSION

An important goal in tissue engineering is the ability to produce a platform which will induce a desired cellular phenotype to replicate that which is observed in the native tissue. One key component of this goal is spatial organization of adherent cells that recapitulates the natural tissue architecture. Electrospun scaffolds are frequently used as a nanoscale biomaterial to provide control over cellular phenotype and behavior through topological and biochemical mechanisms. Here, we have more closely examined how the microtopological properties of electrospun substrates influence the behavior of adherent fibroblasts.

Though often used in electrospun matrices because of its desirable mechanical properties, PCL is a relatively hydrophobic material. This hydrophobicity can lead to impaired cellular adhesion due to the lack of hydrophilic protein adsorption. To remedy this, we fabricated an electrospun scaffold composed of PCL blended with gelatin in a 90/10 ratio. The composition of the resulting scaffold was confirmed using FTIR and DSC. When the hydrophobicity was measured, it was found that the contact angle for the PCL alone was nearly five times larger than the contact angle of PCL+Gel. Typically, the threshold for defining a hydrophobic material is a contact angle of 90° or more, while a hydrophilic material has a contact angle smaller than 90°. The measured contact angle for 100%PCL was about 125° while the addition of gelatin reduced the angle to only 25°.

The addition of gelatin to the electrospun PCL also had a profound impact on cellular growth. While there seems to be no substantial difference in cellular attachment during the first several hours after seeding, a statistically significant difference in growth rate is evident after 4 days of culture. The initial similarity in cell adhesion suggests that the hydrophobicity of 100%PCL does not initially depress cell seeding efficiency, but does negatively influence cell proliferation. It is known that gelatin contains functional peptide sequences associated with integrin binding. The most well-known of these is the RGD sequence of arginine-glycine-aspartic acid, though it has been shown that others exist as well as the ability to bind to sites on fibronectin [23], [24]. It is of interest to note that the orientation of the fibers within the matrix did not have a substantial influence on adhesion or proliferation in either PCL+Gel or PCL alone.

Our experiments have shown that even with similar growth rates, there is a marked difference in cellular behavior when cultured on aligned vs randomly oriented electrospun fibers. The influence of nanoscale fiber orientation on cellular morphology has been described for a variety of cell types, including astrocytes, mesenchymal stem cells, osteoblasts, and smooth muscle cells to name a few. The mechanisms by which this occurs is not fully understood. It has been previously shown that cells on a surface that has been pre-stressed in one direction to yield a smooth anisotropic substrate will elongate preferentially in the direction of highest substrate stiffness [25]. This mechanotransduction explanation for cell reorientation on aligned nanofibers is possible as aligned nanofibers are known to produce anisotropic mechanical properties within the scaffold [26]. It is also possible that topology alone exerts some influence on cell

morphology as cells grown on microgrooved substrates with nearly isotropic mechanical properties also show a preferential orientation [27].

While some genes have been identified as up or down regulated due to electrospun fiber alignment with the substrate in various cell types, the authors are not aware of any such studies using fibroblasts. To identify some of the genes involved in substrate induced cell morphology changes, a microarray study of 84 cytoskeleton regulators was performed. The microarray data indicated 8 genes that were statistically different between random and aligned substrates and had an expression difference above a given threshold. The protein products of these 8 upregulated genes have been previously linked to actin polymerization, focal adhesion formation, actin production, and mechanosensitivity. The full list of genes examined and the microarray results are provided in Appendix C.

One of the genes identified as upregulated on aligned fibers is *Rhoa*. While the gene encoding its kinase, *Rock*, was not found to be statistically different between the groups, the RHOA-ROCK pathway has been identified as an important mechanotransduction pathway in numerous studies [28]. The downstream effects of the *Rhoa* protein product includes actin polymerization, stress-fiber formation, focal adhesion assembly, and actin-myosin complex contraction [29], [30]. In addition to *Rhoa*, we identified *Ezr* and *Msn* to have increased expression in cells grown on aligned fibers. The products of these genes are known to be components of focal adhesions. Our results indicates an increased in expression of genes whose products promote production and polymerization of actin in fibroblasts as well as an increased production of focal adhesion components on aligned nanofibrous scaffolds compared to randomly oriented nanofibers.

The closest comparable published result is a microarray analysis of fibroblasts on microgrooved quartz substrate [31]. The authors of this study did not discuss cytoskeletal regulation changes as they were focused on nuclear reorganization as an explanation for gene expression alterations induced by topographical cues. Additionally, the use of a deformable substrate in our study combines the topological cues with mechanical anisotropy to better recapitulate the environment of both native and engineered tissues.

As with any study, this work is subject to certain limitations. One technical challenge common to all microarray experiments is the multiple comparisons problem. While an uncorrected t-test would seem to suggest a highly statistically significant result, a large number of genes tested increases the likelihood of a type I error. Several approaches have been suggested to correct for multiple comparisons without sacrificing statistical power; the Benjamini–Hochberg (BH) method is well established for increasing the number of null hypothesis rejections at the expense of less stringent control over type I errors. We attempted to mitigate the possibility of false discoveries by applying a fold-change threshold to the genes identified as statistically significant using the BH method. While there is no guarantee that the genes with smaller expression differences are associated with false discoveries, there is a larger confidence in the biological significance of larger changes in gene expression.

CONCLUSIONS

In the present study, we examined the influence of substrate nanofiber orientation on the expression of cytoskeleton regulators in fibroblasts. The nanofibrous substrates used were composed of electrospun PCL+Gel, the composition of which was confirmed by FTIR. It was shown that we have fabricated random and aligned electrospun PCL+Gel scaffolds and shown them to be suitable for cell culture with an increased cell growth rate over scaffolds made from PCL alone. Fibroblasts grown on the matrix of aligned nanofibers altered their morphology to elongate in a preferred orientation parallel to the underlying fibers. Gene expression analysis found that fibroblasts on aligned matrices upregulated genes associated with actin production, actin polymerization, and focal adhesion formation. This is the first time that electrospun substrate modulated gene expression has been shown with fibroblasts, and these results deepen the understanding of the mechanism by which fibroblasts interact with nanofibrous substrates.

ACKNOWLEDGEMENTS

The authors would like to thank the UAB High Resolution Imaging Facility SEM lab. Portions of this work were funded by the UAB BERM Center Pilot Grant and the Eyesight Foundation of Alabama Research Acceleration Initiative.

REFERENCES

[1] M. Nikkhah, F. Edalat, S. Manoucheri, and A. Khademhosseini, “Engineering microscale topographies to control the cell-substrate interface.,” *Biomaterials*, vol. 33, no. 21, pp. 5230–46, Jul. 2012.

[2] C. Huang, X. Fu, J. Liu, Y. Qi, S. Li, and H. Wang, “The involvement of integrin β1 signaling in the migration and myofibroblastic differentiation of skin fibroblasts on anisotropic collagen-containing nanofibers.,” *Biomaterials*, vol. 33, no. 6, pp. 1791–800, Feb. 2012.

[3] V. Cirillo, V. Guarino, M. A. Alvarez-Perez, M. Marrese, and L. Ambrosio, “Optimization of fully aligned bioactive electrospun fibers for ‘in vitro’ nerve guidance,” *J. Mater. Sci. Mater. Med.*, pp. 2323–2332, 2014.

[4] C. Huang, Y. Ouyang, H. Niu, N. He, Q. Ke, X. Jin, D. Li, J. Fang, W. Liu, C. Fan, and T. Lin, “Nerve Guidance Conduits from Aligned Nanofibers: Improvement of Nerve Regeneration through Longitudinal Nanogrooves on a Fiber Surface,” *ACS Appl. Mater. Interfaces*, vol. 7, no. 13, pp. 7189–7196, 2015.

[5] R. Safaeijavan, M. Soleimani, A. Divsalar, and A. Eidi, “Comparison of random and aligned PCL nanofibrous electrospun scaffolds on cardiomyocyte differentiation of human adipose-derived stem cells,” *Iran. J. Basic Med. Sci.*, vol. 17, p. 903, 2014.

[6] A. S. Nathan, B. M. Baker, N. L. Nerurkar, and R. L. Mauck, “Mechano-topographic modulation of stem cell nuclear shape on nanofibrous scaffolds.,” *Acta Biomater*, vol. 7, no. 1, pp. 57–66 ST – Mechano–topographic modulation of stem, Jan. 2011.

[7] T. J. Fee, D. R. Dean, A. W. Eberhardt, and J. L. Berry, “A novel device to quantify the mechanical properties of electrospun nanofibers.,” *J. Biomech. Eng.*, vol. 134, no. 10, p. 104503, Oct. 2012.

[8] N. L. Nerurkar, D. M. Elliott, and R. L. Mauck, “Mechanics of oriented electrospun nanofibrous scaffolds for annulus fibrosus tissue engineering.,” *J. Orthop. Res.*, vol. 25, no. 8, pp. 1018–28, Aug. 2007.

[9] M. C. Phipps, W. C. Clem, S. a Catledge, Y. Xu, K. M. Hennessy, V. Thomas, M. J. Jablonsky, S. Chowdhury, A. V Stanishevsky, Y. K. Vohra, and S. L. Bellis, “Mesenchymal stem cell responses to bone-mimetic electrospun matrices composed of polycaprolactone, collagen I and nanoparticulate hydroxyapatite.,” *PLoS One*, vol. 6, no. 2, p. e16813 ST – Mesenchymal stem cell responses to bo, Jan. 2011.

[10] H. M. Powell and S. T. Boyce, “Engineered human skin fabricated using electrospun collagen-PCL blends: morphogenesis and mechanical properties.,” *Tissue Eng Part A*, vol. 15, no. 8, pp. 2177–87 ST – Engineered human skin fabricated usi, Aug. 2009.

[11] L. Ghasemi-Mobarakeh, M. P. Prabhakaran, M. Morshed, M. H. Nasr-Esfahani, and S. Ramakrishna, “Electrospun poly(ε-caprolactone)/gelatin nanofibrous

scaffolds for nerve tissue engineering," *Biomaterials*, vol. 29, pp. 4532–4539, 2008.

[12] D. I. Zeugolis, S. T. Khew, E. S. Y. Yew, A. K. Ekaputra, Y. W. Tong, L.-Y. L. Yung, D. W. Hutmacher, C. Sheppard, and M. Raghunath, "Electro-spinning of pure collagen nano-fibres - just an expensive way to make gelatin?," *Biomaterials*, vol. 29, no. 15, pp. 2293–305, May 2008.

[13] Y. Yu, X. Lü, and F. Ding, "Influence of Poly(L-Lactic Acid) Aligned Nanofibers on PC12 Differentiation," *J. Biomed. Nanotechnol.*, vol. 11, no. 5, pp. 816–827, May 2015.

[14] J. Han, J. A. Gerstenhaber, P. Lazarovici, and P. I. Lelkes, "Tissue Factor Activity and ECM-Related Gene Expression in Human Aortic Endothelial Cells Grown on Electrospun Biohybrid Sca ff olds," 2013.

[15] S. Y. Chew, R. Mi, A. Hoke, and K. W. Leong, "The effect of the alignment of electrospun fibrous scaffolds on Schwann cell maturation," *Biomaterials*, vol. 29, no. 6, pp. 653–661, 2008.

[16] C. L. Lau, M. Kovacevic, T. S. Tingleff, J. S. Forsythe, H. S. Cate, D. Merlo, C. Cederfur, F. L. Maclean, C. L. Parish, M. K. Horne, D. R. Nisbet, and P. M. Beart, "3D Electrospun scaffolds promote a cytotrophic phenotype of cultured primary astrocytes," *J. Neurochem.*, vol. 130, no. 2, pp. 215–226, Jul. 2014.

[17] X. Chen, X. Fu, J. Shi, and H. Wang, "Regulation of the osteogenesis of pre-osteoblasts by spatial arrangement of electrospun nanofibers in two- and three-dimensional environments.," *Nanomedicine*, vol. 9, no. 8, pp. 1283–92, 2013.

[18] H.-Y. Mi, M. R. Salick, X. Jing, W. C. Crone, X.-F. Peng, and L.-S. Turng, "Electrospinning of unidirectionally and orthogonally aligned thermoplastic polyurethane nanofibers: Fiber orientation and cell migration," *J. Biomed. Mater. Res. Part A*, vol. 103, no. 2, pp. 593–603, 2015.

[19] V. Creszenzi, G. Mazini, G. Calzolari, and C. Borri, "Thermodynamics of fusion of poly-β-propiolactone and poly-ϵ-caprolactone. comparative analysis of the melting of aliphatic polylactone and polyester chains," *Eur. Polym. J.*, vol. 8, pp. 449–463 ST – Thermodynamics of fusion of poly–β–p, 1972.

[20] Y. Benjamini and Y. Hochberg, "Benjamini Y, Hochberg Y. Controlling the false discovery rate: a practical and powerful approach to multiple testing," *J. R. Stat. Soc. B*, vol. 57, no. 1, pp. 289–300, 1995.

[21] C. E. Huggins, a a Domenighetti, M. E. Ritchie, N. Khalil, J. M. Favaloro, J. Proietto, G. K. Smyth, S. Pepe, and L. M. D. Delbridge, "Functional and metabolic remodelling in GLUT4-deficient hearts confers hyper-responsiveness to substrate intervention.," *J. Mol. Cell. Cardiol.*, vol. 44, no. 2, pp. 270–80, 2008.

[22] T. A. Patterson, E. K. Lobenhofer, S. B. Fulmer-Smentek, P. J. Collins, T.-M. Chu, W. Bao, H. Fang, E. S. Kawasaki, J. Hager, I. R. Tikhonova, S. J. Walker, L. Zhang, P. Hurban, F. de Longueville, J. C. Fuscoe, W. Tong, L. Shi, and R. D. Wolfinger, "Performance comparison of one-color and two-color platforms within the Microarray Quality Control (MAQC) project," *Nat. Biotechnol.*, vol. 24, no. 9, pp. 1140–1150, 2006.

[23] Y. Xu, S. Gurusiddappa, R. L. Rich, R. T. Owens, D. R. Keene, R. Mayne, A.

Höök, and M. Höök, “Multiple binding sites in collagen type I for the integrins α1β1 and α2β1,” *J. Biol. Chem.*, vol. 275, no. 50, pp. 38981–38989, 2000.

[24] Y. Katagiri, S. A. Brew, and K. C. Ingham, “All Six Modules of the Gelatin-binding Domain of Fibronectin Are Required for Full Affinity,” *J. Biol. Chem.*, vol. 278, no. 14, pp. 11897–11902, 2003.

[25] C. Liu, S. Baek, J. Kim, E. Vasko, R. Pyne, and C. Chan, “Effect of static pre-stretch induced surface anisotropy on orientation of mesenchymal stem cells,” *Cell. Mol. Bioeng.*, vol. 7, no. 1, pp. 106–121, 2014.

[26] R. L. Mauck, B. M. Baker, N. L. Nerurkar, J. a Burdick, W.-J. J. Li, R. S. Tuan, and D. M. Elliott, “Engineering on the straight and narrow: the mechanics of nanofibrous assemblies for fiber-reinforced tissue regeneration,” *Tissue Eng Part B Rev*, vol. 15, no. 2, pp. 171–93 ST – Engineering on the straight and narro, Jun. 2009.

[27] C. G. Anene-Nzelu, D. Choudhury, H. Li, A. Fraiszudeen, K.-Y. Peh, Y.-C. Toh, S. H. Ng, H. L. Leo, and H. Yu, “Scalable cell alignment on optical media substrates.,” *Biomaterials*, vol. 34, no. 21, pp. 5078–87, Jul. 2013.

[28] M. Chiquet, L. Gelman, R. Lutz, and S. Maier, “From mechanotransduction to extracellular matrix gene expression in fibroblasts.,” *Biochim. Biophys. Acta*, vol. 1793, no. 5, pp. 911–20, May 2009.

[29] M. Kanehisa and S. Goto, “KEGG: Kyoto Encyclopaedia of Genes and Genomes,” *Nucl. Acids Res.*, vol. 28, no. 1, pp. 27–30, 2000.

[30] “Regulation of actin cytoskeleton - Mus musculus,” *KEGG: Kyoto Encyclopedia*

of Genes and Genomes. [Online]. Available: http://www.kegg.jp/pathway/mmu04810. [Accessed: 01-Jan-2015].

[31] L. E. McNamara, R. Burchmore, M. O. Riehle, P. Herzyk, M. J. P. Biggs, C. D. W. Wilkinson, A. S. G. Curtis, and M. J. Dalby, "The role of microtopography in cellular mechanotransduction.," *Biomaterials*, vol. 33, no. 10, pp. 2835–47, Apr. 2012.

CONCLUSIONS

For this work, the mechanical and topological aspects of polycaprolactone based electrospun tissue engineering scaffolds were examined. Electrospun polycaprolactone scaffolds have been gaining interest as a scaffolding material for engineered tissue replacements. The mechanical behavior of electrospun materials is complex and a better understanding is required to produce tissue engineering scaffolds with predictable mechanical properties. Additionally, anisotropic mechanical properties are known to be induced by fiber alignment in electrospun materials. Better descriptors of fiber alignment and the relationship between fiber alignment and mechanical anisotropy and alignment induced gene expression are needed to improve the design of tissue engineered scaffolds.

A novel microtensile testing device has been created which can be used to directly observation strain along an individual electrospun fiber. This device can be used for either natural or synthetic electrospun fibers. Additionally, the mechaincal information collected with this device can be used to develop of a constitutive model of electrospun fibers in various conditions, which can be used to computationally model the dynamic and complex geometries experienced by tissue engineered constructs in vivo. The development of a device capable of recording true strain from arrays of individual electrospun fibers is significant in that an understanding of the materials used in designing tissue engineered implants can lead to improved engineered tissue substitutes.

While the alignment of nanoscale fibers within an electrospun scaffold is well known to produce an anisotropic mechanical behavior, there remain problems with the currently available methods of quantifying fiber alignment within electrospun scaffolds. Therefore, an image-based fiber alignment quantification tool was developed to provide a metric for fiber alignment within electrospun materials. It was found that the developed metric also acted as a predictor of mechanical properties.

Finally, the role of substrate fiber alignment was examined with respect to fibroblast growth and behavior. It was found that while fiber alignment did not significantly influence fibroblast growth, there was a noted difference in the morphology of cells grown on aligned fibers compared to randomly oriented fibrous scaffolds. Additionally, it was found that fibroblasts growing on aligned fibers upregulate several genes related to focal adhesion assembly, microfilament production, and stress fiber assembly.

The information gained from these studies improves the knowledge base available to designers of tissue engineering scaffolds. A more thorough understanding of the mechanical properties of electrospun materials can be used to inform the design of tissue engineering scaffolds to produce scaffolds with mechanical properties and topologies to induce a predictable behavior in adherent cell populations.

GENERAL REFERENCES

[1] J. L. Berry, J. A. Steen, J. Koudy Williams, J. E. Jordan, A. Atala, and J. J. Yoo, "Bioreactors for development of tissue engineered heart valves.," *Ann Biomed Eng*, vol. 38, pp. 3272–9 ST – Bioreactors for development of tissue, 2010.

[2] J. N. Mansbridge, "Tissue-engineered skin substitutes in regenerative medicine.," *Curr Opin Biotechnol*, vol. 20, pp. 563–7 ST – Tissue–engineered skin substitutes in , 2009.

[3] S. Ravi and E. L. Chaikof, "Biomaterials for vascular tissue engineering.," *Regen Med*, vol. 5, pp. 107–20 ST – Biomaterials for vascular tissue engi, 2010.

[4] C. Vinatier, C. Bouffi, C. Merceron, J. Gordeladze, J. M. Brondello, C. Jorgensen, P. Weiss, J. Guicheux, and D. Noël, "Cartilage tissue engineering: towards a biomaterial-assisted mesenchymal stem cell therapy.," *Curr Stem Cell Res Ther*, vol. 4, pp. 318–29 ST – Cartilage tissue engineering: towards, 2009.

[5] A. Boccaccio, A. Ballini, C. Pappalettere, D. Tullo, S. Cantore, and A. Desiate, "Finite element method (FEM), mechanobiology and biomimetic scaffolds in bone tissue engineering.," *Int. J. Biol. Sci.*, vol. 7, no. 1, pp. 112–32 ST – Finite element method (FEM), mechanobi, Jan. 2011.

[6] H. Yoshimoto, Y. M. Shin, H. Terai, and J. P. Vacanti, "A biodegradable nanofiber scaffold by electrospinning and its potential for bone tissue

engineering.,” *Biomaterials*, vol. 24, pp. 2077–82 ST – A biodegradable nanofiber scaffold b, 2003.

[7] B. M. Baker, N. L. Nerurkar, J. A. Burdick, D. M. Elliott, and R. L. Mauck, “Fabrication and modeling of dynamic multipolymer nanofibrous scaffolds.,” *J. Biomech. Eng.*, vol. 131, no. 10, p. 101012, Oct. 2009.

[8] B. Ratner, A. Hoffman, F. Schoen, and J. Lemons, *Biomaterials Science: An Introduction to Materials in Medicine*. New York City: Elsevier Academic Press.

[9] K. Ariga, J. P. Hill, M. V Lee, A. Vinu, R. Charvet, and S. Acharya, “Challenges and breakthroughs in recent research on self-assembly,” *Sci. Technol. Adv. Mater*, vol. 9, no. 1, p. 014109, Jan. 2008.

[10] J. a Matthews, G. E. Wnek, D. G. Simpson, and G. L. Bowlin, “Electrospinning of Collagen Nanofibers,” *Biomacromolicules*, vol. 3, no. 2, p. 7 ST – Electrospinning of Collagen Nanofibers, 2002.

[11] D. I. Zeugolis, S. T. Khew, E. S. Y. Yew, A. K. Ekaputra, Y. W. Tong, L.-Y. L. Yung, D. W. Hutmacher, C. Sheppard, and M. Raghunath, “Electro-spinning of pure collagen nano-fibres - just an expensive way to make gelatin?,” *Biomaterials*, vol. 29, no. 15, pp. 2293–305, May 2008.

[12] S.-W. Tsai, H.-M. Liou, C.-J. Lin, K.-L. Kuo, Y.-S. Hung, R.-C. Weng, and F.-Y. Hsu, “MG63 osteoblast-like cells exhibit different behavior when grown on electrospun collagen matrix versus electrospun gelatin matrix.,” *PLoS One*, vol. 7, no. 2, p. e31200, Jan. 2012.

[13] M. A. Woodruff and D. W. Hutmacher, “The return of a forgotten polymer—Polycaprolactone in the 21st century,” *Prog. Polym. Sci.*, vol. 35, no. 10, pp.

1217–1256, Oct. 2010.

[14] P. Gupta, “Processing-Structure-Property Studies of : I) Submicron Polymeric Fibers Produced By Electrospinning and II) Films Of Linear Low Density Polyethylenes As Influenced By The Short Chain Branch Length In Copolymers Of Ethylene / 1-Butene , Ethylene / 1-Hex,” Virginia Polytechnic Institute and State University, 2004.

[15] R. Seyedmahmoud, A. Rainer, P. Mozetic, S. M. Giannitelli, M. Trombetta, E. Traversa, S. Licoccia, and A. Rinaldi, “A primer of statistical methods for correlating parameters and properties of electrospun poly-l-lactide scaffolds for tissue engineering - PART 1: DOE.,” *J. Biomed. Mater. Res. A*, Mar. 2014.

[16] B. M. Baker, A. M. Handorf, L. C. Ionescu, W. J. Li, and R. L. Mauck, “New directions in nanofibrous scaffolds for soft tissue engineering and regeneration.,” *Expert Rev Med Devices*, vol. 6, pp. 515–32 ST – New directions in nanofibrous scaffol, 2009.

[17] N. J. Amoroso, A. D’Amore, Y. Hong, W. R. Wagner, and M. S. Sacks, “Elastomeric electrospun polyurethane scaffolds: the interrelationship between fabrication conditions, fiber topology, and mechanical properties.,” *Adv Mater*, vol. 23, no. 1, pp. 106–11 ST – Elastomeric electrospun polyurethane , Jan. 2011.

[18] J. Xie, X. Li, J. Lipner, C. N. Manning, A. G. Schwartz, S. Thomopoulos, and Y. Xia, “‘Aligned-to-random’ nanofiber scaffolds for mimicking the structure of the tendon-to-bone insertion site.,” *Nanoscale*, vol. 2, no. 6, pp. 923–6 ST – “Aligned–to–random” nanofiber scaffold, Jun. 2010.

[19] R. L. Mauck, B. M. Baker, N. L. Nerurkar, J. a Burdick, W.-J. J. Li, R. S. Tuan,

and D. M. Elliott, “Engineering on the straight and narrow: the mechanics of nanofibrous assemblies for fiber-reinforced tissue regeneration,” *Tissue Eng Part B Rev*, vol. 15, no. 2, pp. 171–93 ST – Engineering on the straight and narro, Jun. 2009.

[20] E. A. Sander, T. Stylianopoulos, R. T. Tranquillo, and V. H. C.-2764876 Barocas, “Image-based multiscale modeling predicts tissue-level and network-level fiber reorganization in stretched cell-compacted collagen gels.,” *Proc. Natl. Acad. Sci. U. S. A.*, vol. 106, no. 42, pp. 17675–80 ST – Image–based multiscale modeling pre, Oct. 2009.

[21] S. Baker, J. Sigley, C. C. Helms, J. Stitzel, J. L. Berry, K. Bonin, and M. Guthold, “The mechanical properties of dry, electrospun fibrinogen fibers,” *Mater. Sci. Eng. C*, vol. 32, no. 2, pp. 215–221 ST – The mechanical properties of dry, ele, Mar. 2012.

[22] C. R. Carlisle, C. Coulais, M. Namboothiry, D. L. Carroll, R. R. Hantgan, and M. Guthold, “The mechanical properties of individual, electrospun fibrinogen fibers.,” *Biomaterials*, vol. 30, no. 6, pp. 1205–13, Feb. 2009.

[23] T. J. Fee, D. R. Dean, A. W. Eberhardt, and J. L. Berry, “A novel device to quantify the mechanical properties of electrospun nanofibers.,” *J. Biomech. Eng.*, vol. 134, no. 10, p. 104503, Oct. 2012.

[24] J. A. Stella, A. D’Amore, W. R. Wagner, and M. S. Sacks, “On the biomechanical function of scaffolds for engineering load-bearing soft tissues.,” *Acta Biomater.*, vol. 6, no. 7, pp. 2365–81, Jul. 2010.

[25] R. R. Duling, R. B. Dupaix, N. Katsube, and J. Lannutti, “Mechanical

characterization of electrospun polycaprolactone (PCL): a potential scaffold for tissue engineering.," *J. Biomech. Eng.*, vol. 130, no. 1, p. 011006, Feb. 2008.

[26] T. Stylianopoulos, C. A. Bashur, A. S. Goldstein, S. A. Guelcher, and V. H. Barocas, "Computational predictions of the tensile properties of electrospun fibre meshes: effect of fibre diameter and fibre orientation.," *J. Mech. Behav. Biomed. Mater.*, vol. 1, no. 4, pp. 326–35, Oct. 2008.

[27] D. E. Ingber, "Control of Capillary Growth and Differentiation by Extracellular Matrix : Use of a Tensegrity (Tensional Integrity) Mechanism for Signal Processing," *Chest*, vol. 99, p. 34S–40S, 1991.

[28] F. M. Pavalko, S. M. Norvell, D. B. Burr, C. H. Turner, R. L. Duncan, and J. P. Bidwell, "A model for mechanotransduction in bone cells: the load-bearing mechanosome," *J. Cell. Biochem.*, vol. 88, no. 1, pp. 104–112 ST – A model for mechanotransduction in b, Jan. 2003.

[29] D. E. Ingber, "Cellular tensegrity: defining new rules of biological design that govern the cytoskeleton.," *J. Cell Sci.*, vol. 104 (Pt 3, pp. 613–27, Mar. 1993.

[30] S. R. Heidemann, S. Kaech, R. E. Buxbaum, and A. Matus, "Direct Observations of the Mechanical Behaviors of the Cytoskeleton in Living Fibroblasts," *J. Cell Biol.*, vol. 145, no. 1, pp. 109–122, 1999.

[31] D. E. Ingber, S. R. Heidemann, P. Lamoureux, E. Robert, A. D. Bicek, E. Tuzel, A. Demtchouk, M. Uppalapati, W. O. Hancock, D. M. Kroll, D. J. Odde, C. P. Brangwynne, F. C. Mackintosh, S. Kumar, N. A. Geisse, L. Mahadevan, K. K. Parker, and D. A. Weitz, "Opposing views on tensegrity as a structural framework for understanding cell mechanics," *J. Appl. Physiol.*, vol. 89, pp. 1663–1678, 2000.

[32] H.-Y. Tsai, K. Vats, M. Z. Yates, and D. S. W. Benoit, “Two-dimensional patterns of poly(N-isopropylacrylamide) microgels to spatially control fibroblast adhesion and temperature-responsive detachment.,” *Langmuir*, vol. 29, no. 39, pp. 12183–93, Oct. 2013.

[33] K. H. Lee, H. Y. Kim, M. S. Khil, Y. M. Ra, and D. R. Lee, “Characterization of nano-structured poly(caprolactone) nonwoven mats via electrospinning,” *Polymer (Guildf).*, vol. 44, pp. 1287–1294 ST – Characterization of nano–structure, 2003.

[34] M. Nikkhah, F. Edalat, S. Manoucheri, and A. Khademhosseini, “Engineering microscale topographies to control the cell-substrate interface.,” *Biomaterials*, vol. 33, no. 21, pp. 5230–46, Jul. 2012.

[35] A. J. Booth, R. Hadley, A. M. Cornett, A. a Dreffs, S. a Matthes, J. L. Tsui, K. Weiss, J. C. Horowitz, V. F. Fiore, T. H. Barker, B. B. Moore, F. J. Martinez, L. E. Niklason, and E. S. White, “Acellular Normal and Fibrotic Human Lung Matrices as a Culture System for In Vitro Investigation.,” *Am. J. Respir. Crit. Care Med.*, no. C, pp. 1–61, Aug. 2012.

APPENDIX A

ENGINEERING DRAWINGS OF CUSTOM PARTS FOR NOVEL TENSILE TESTING DEVICE

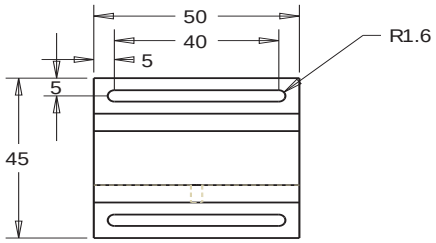

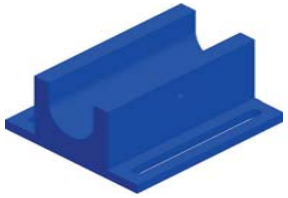

Might want to make 2 holes and move them 2mm up

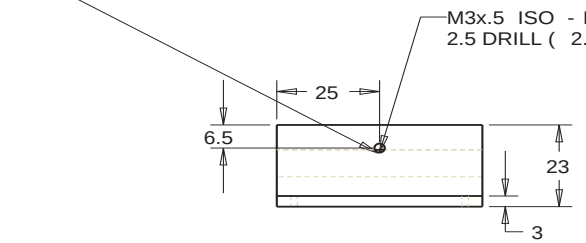

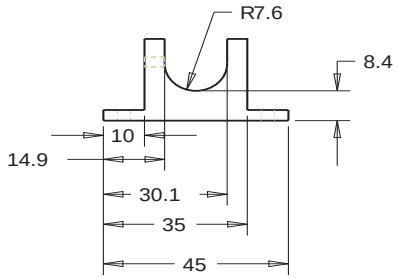

Filename: ACTUATOR_MOUNT | Material: Aluminum | Version: 2 | Drawn By: Timothy Fee | Date: 5-31-11

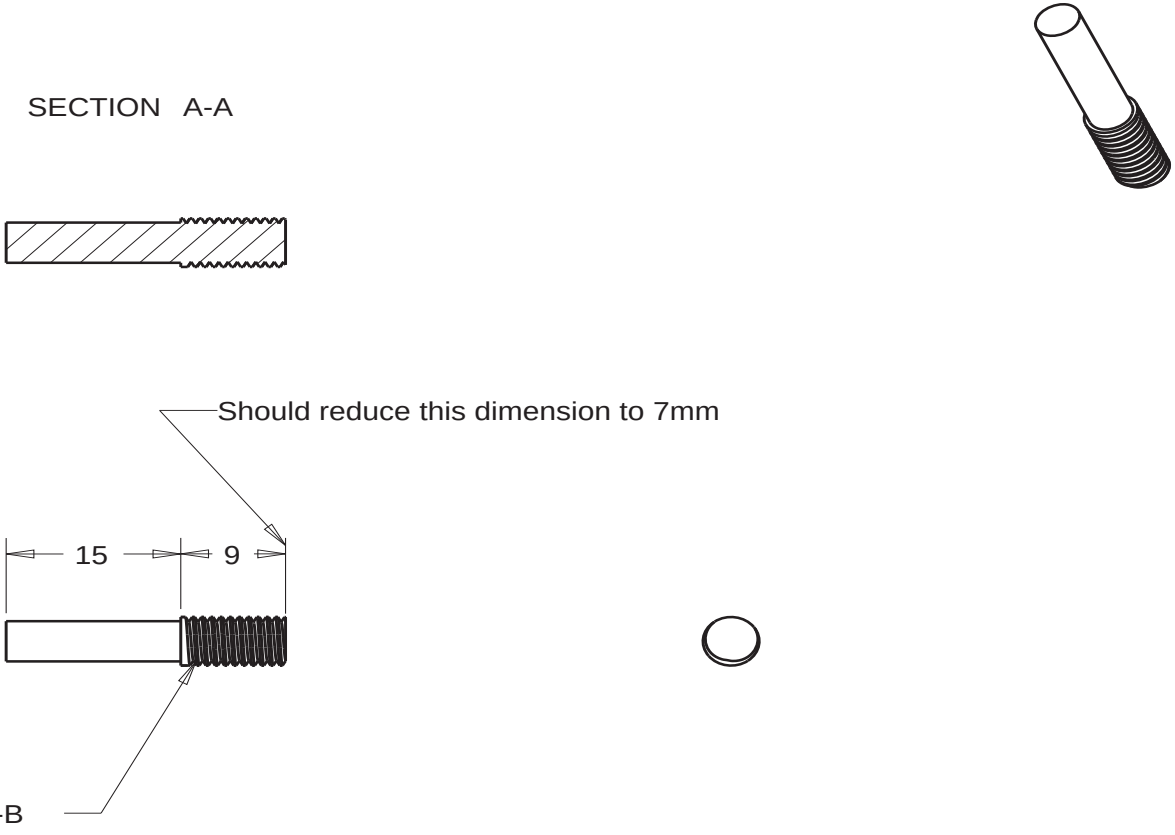

Filename: ADAPTER_LOADCELL_SETSCREW | Material: Aluminum | Version: 3 | Drawn By: Timothy Fee | Date: 5-31-11

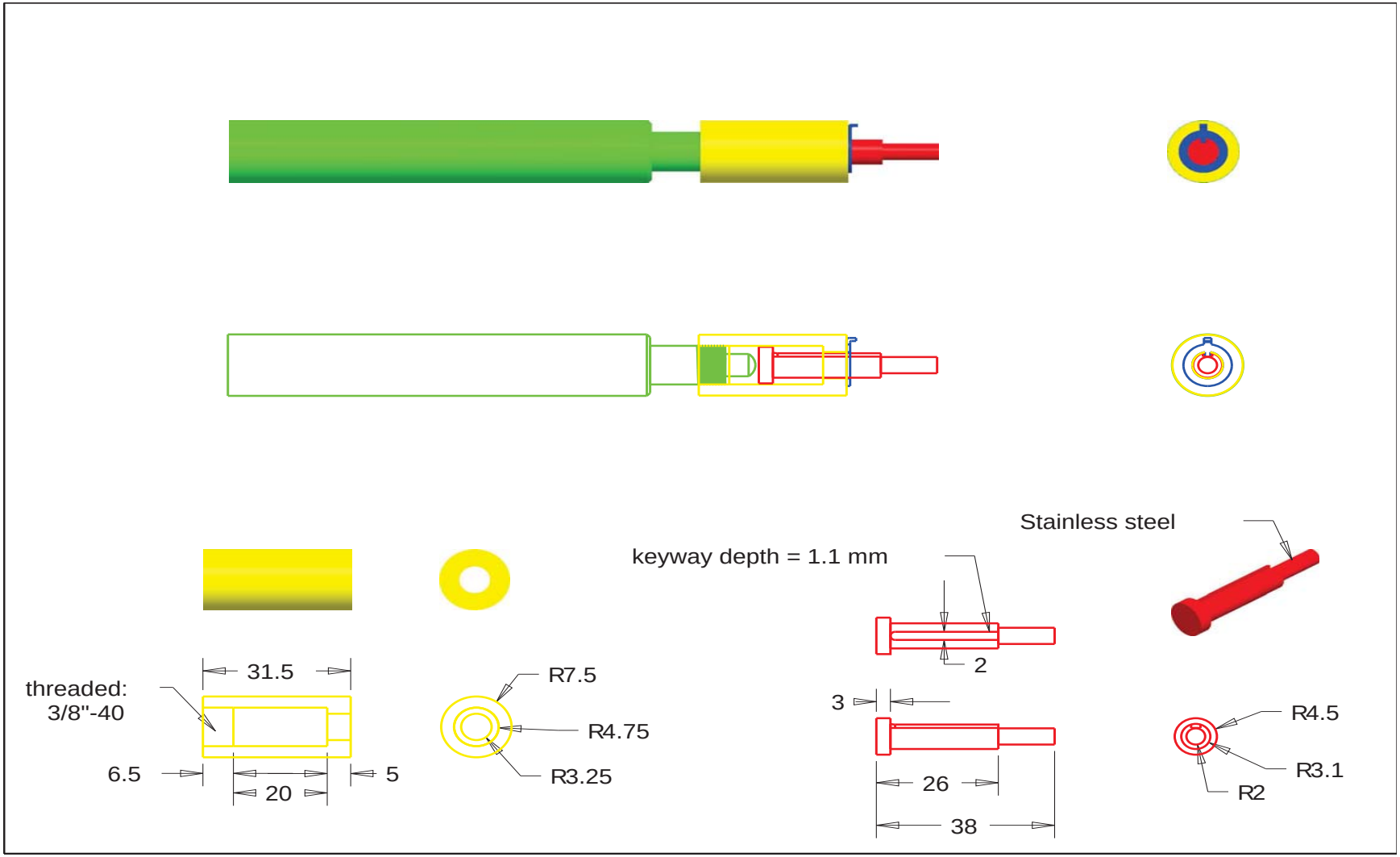
Stainless steel
keyway depth = 1.1 mm
threaded:
3/8"-40
31.5
6.5
20
5
R7.5
R4.75
R3.25
2
3
26
38
R4.5
R3.1
R2

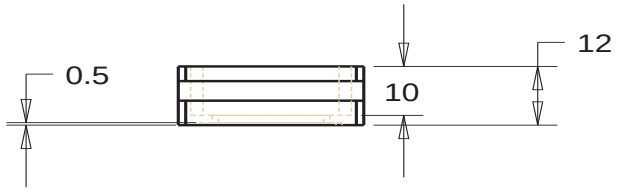

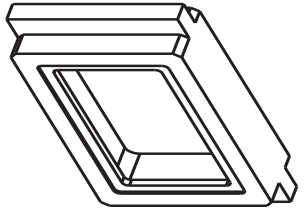

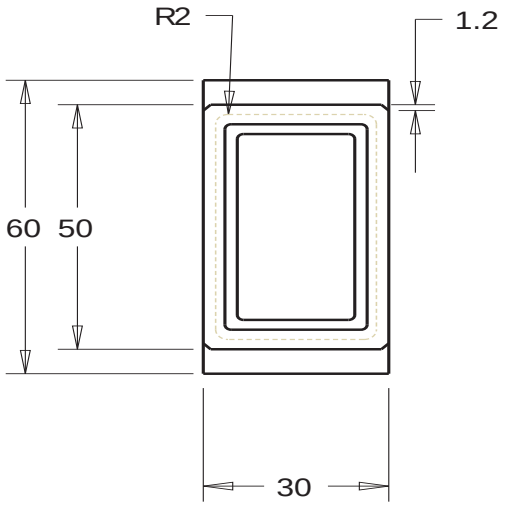

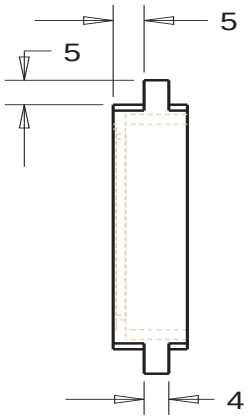

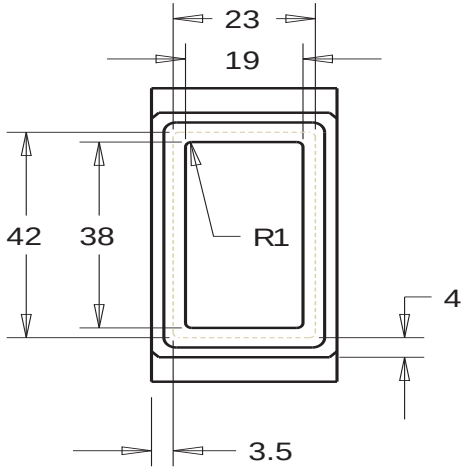

Filename: BATH_CONTAINER | Material: Delrin | Version: 3 | Drawn By: Timothy Fee | Date: 5/26/2011

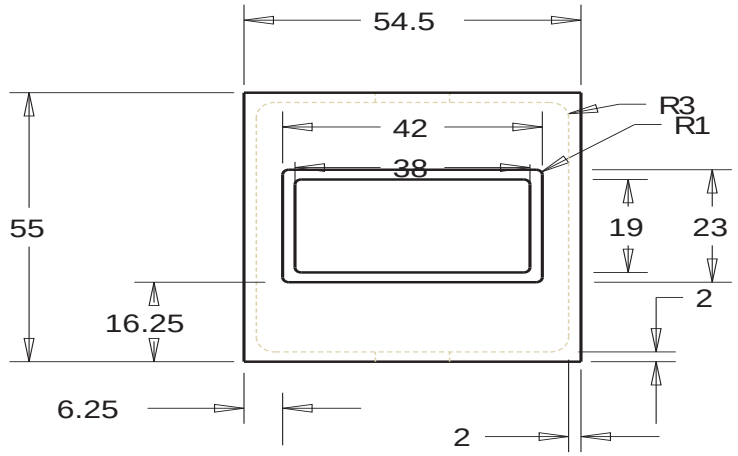

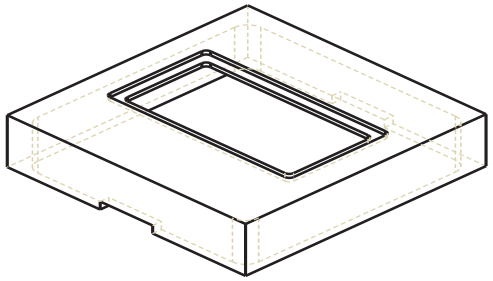

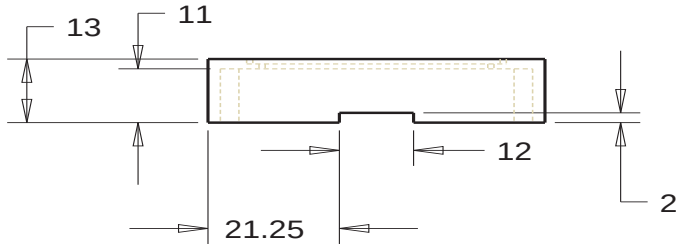

BATH_LID | MATERIAL: DELRIN | VERSION 3 | DRAWN BY: TIMOTHY FEE | DATE 5/26/2011

Filename: Cell_mount | Version: 3 | Material: Aluminum | Drawn By: Timothy Fee | Date: 6-3-2011

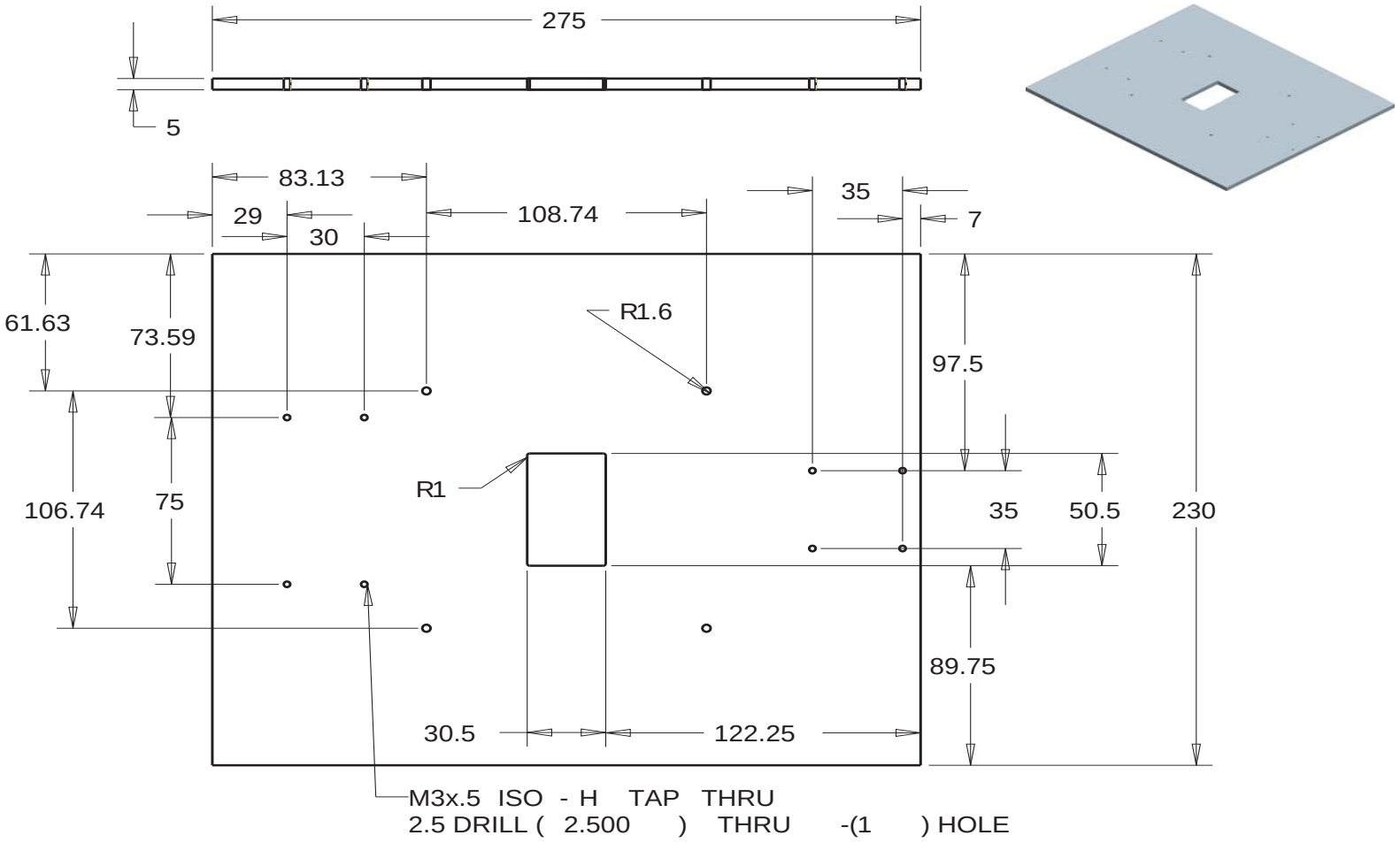

NOTE: small details of this parts have been changed, the overall shape is the same

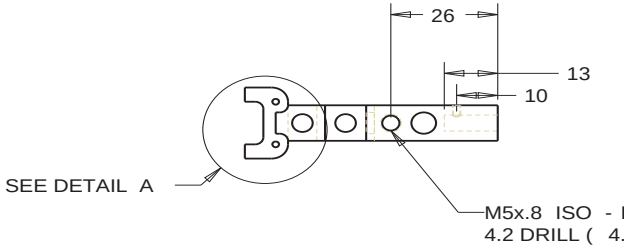

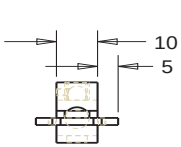

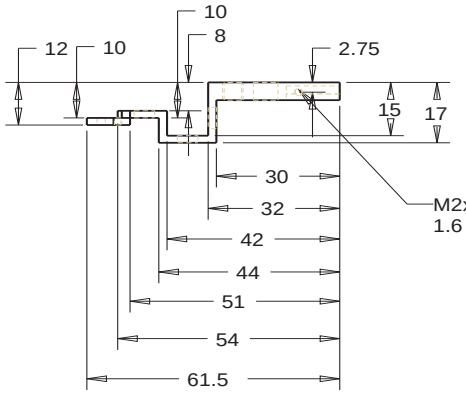

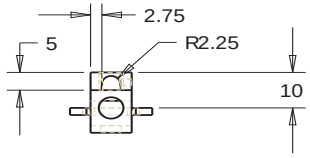

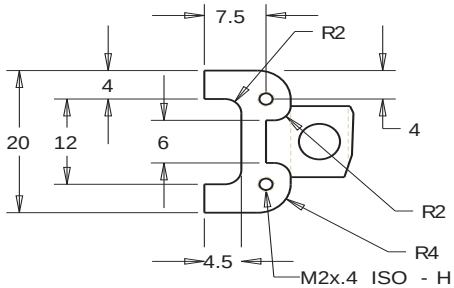

DETAIL A
SCALE 2.000

QUANTITY: 2

Filename: CLAMP_LINKAGE Material: Delrin Version: 13 Drawn: 05-26-2011 By: Timothy Fee

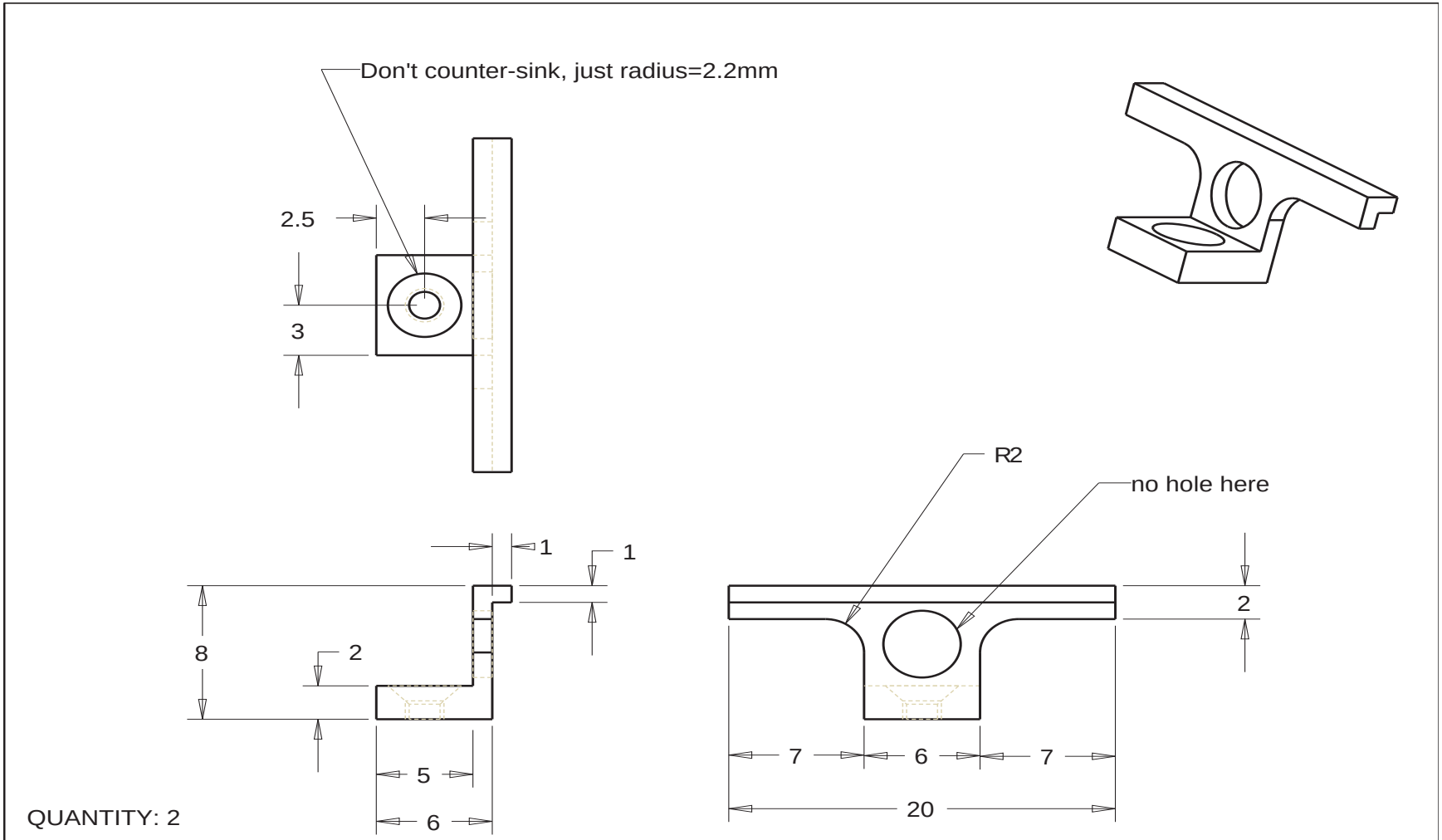

Filename: HOLDING_BARS | Material: Delrin | Version 3 | Drawn By: Timothy Fee | Date: 5-31-11

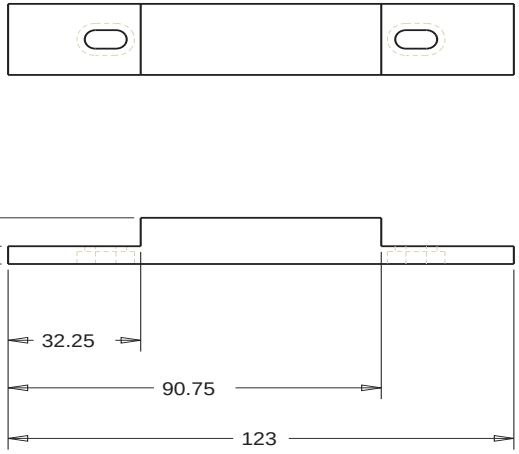

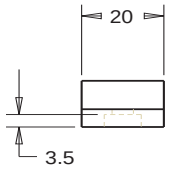

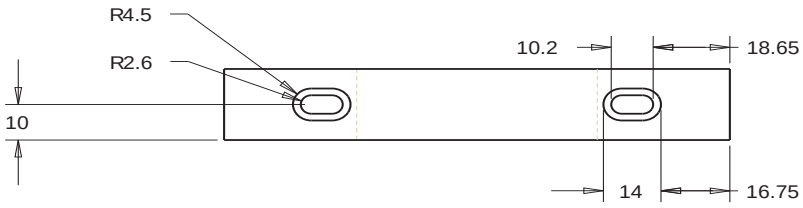

Filename: JIG_FOR_FORKS | Material: delrin | Version: 2 | Drawn By: Timothy Fee | Date: 5-31-11

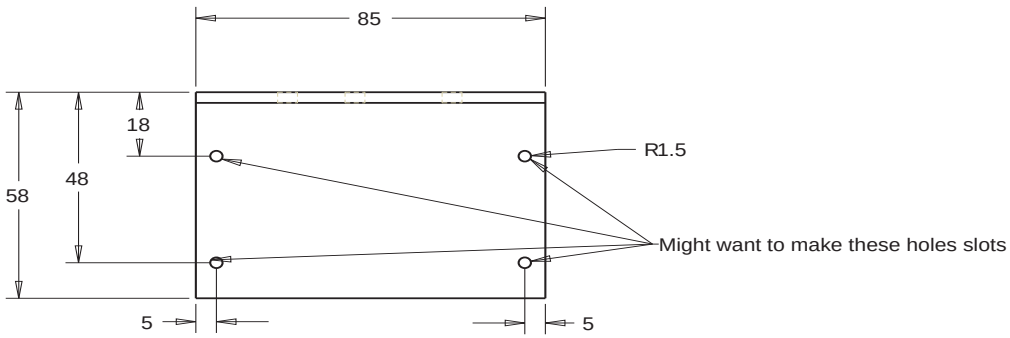

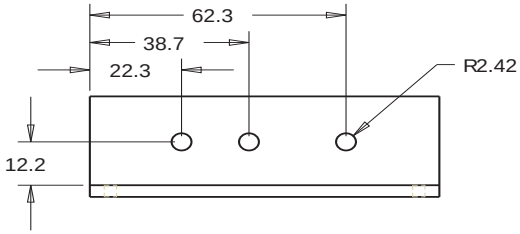

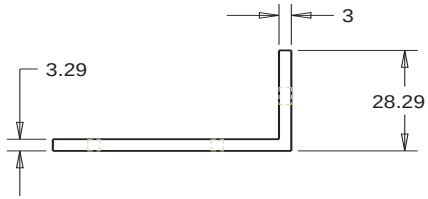

Filename: LOADCELL_BRACKET | Material: Aluminum | Version 1 | Drawn By: Timothy Fee | Date: 5-31-11

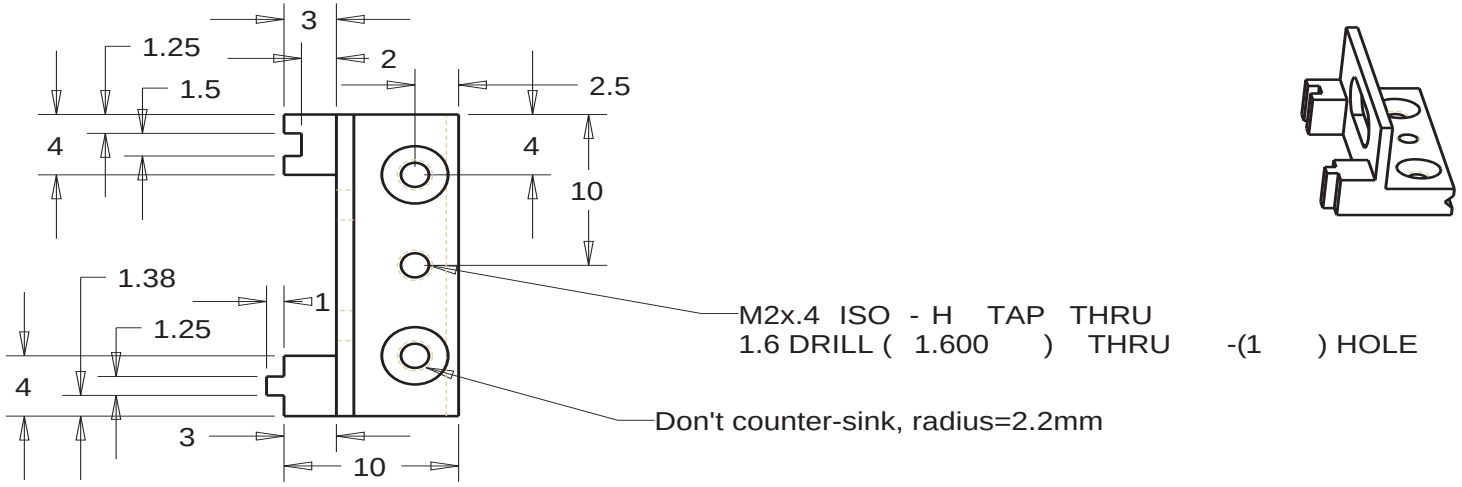

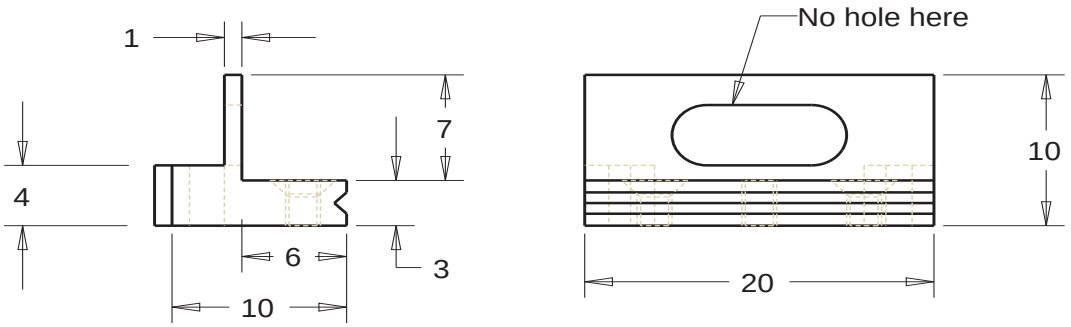

QUANTITY: 2

Filename: NEW_COLLECTOR_RIGHT | Material: Delrin | Version: 5 | Drawn By: Timothy Fee | Date: 6-3-11

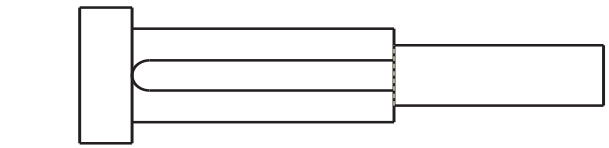

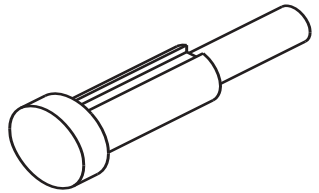

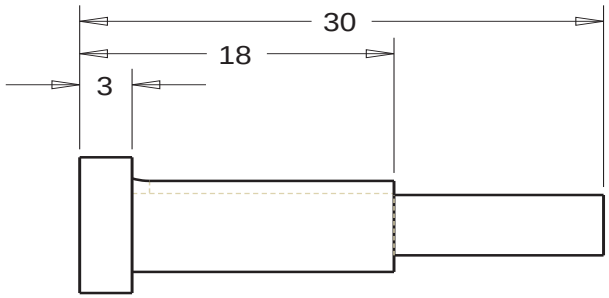

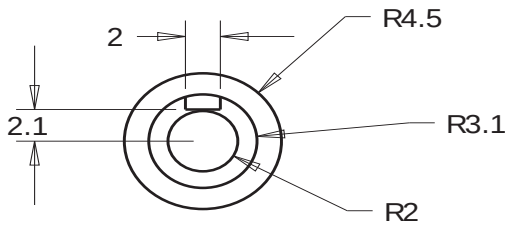

Filename: SHAFT_W_KEYWAY | Material: STAINLESS STEEL | Version: 2 |
Drawn by: Timothy Fee |Date 5-31-11

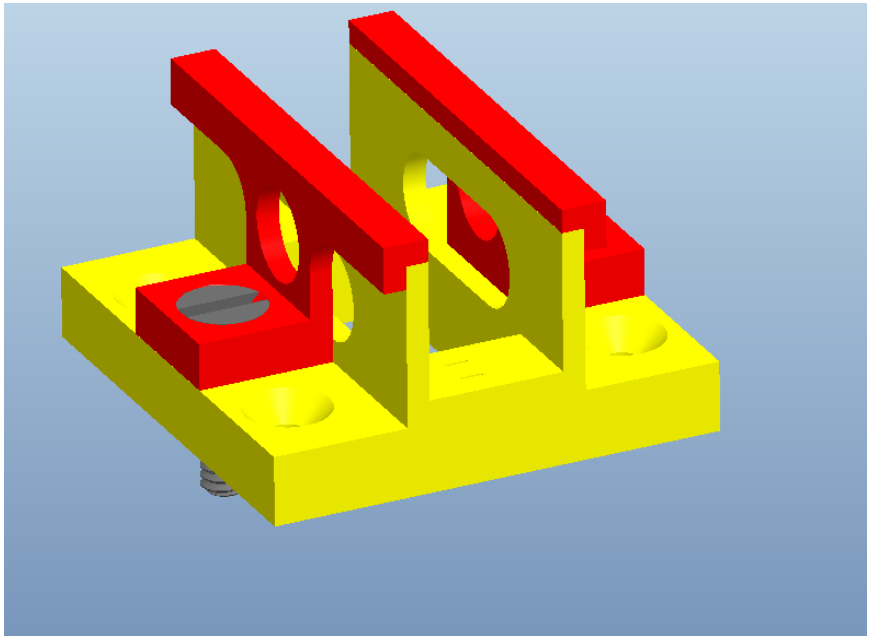

- The fibers are suspended between the yellow bars and clamped between the yellow and red parts
- This assembly can be secured using a clip or a clamp

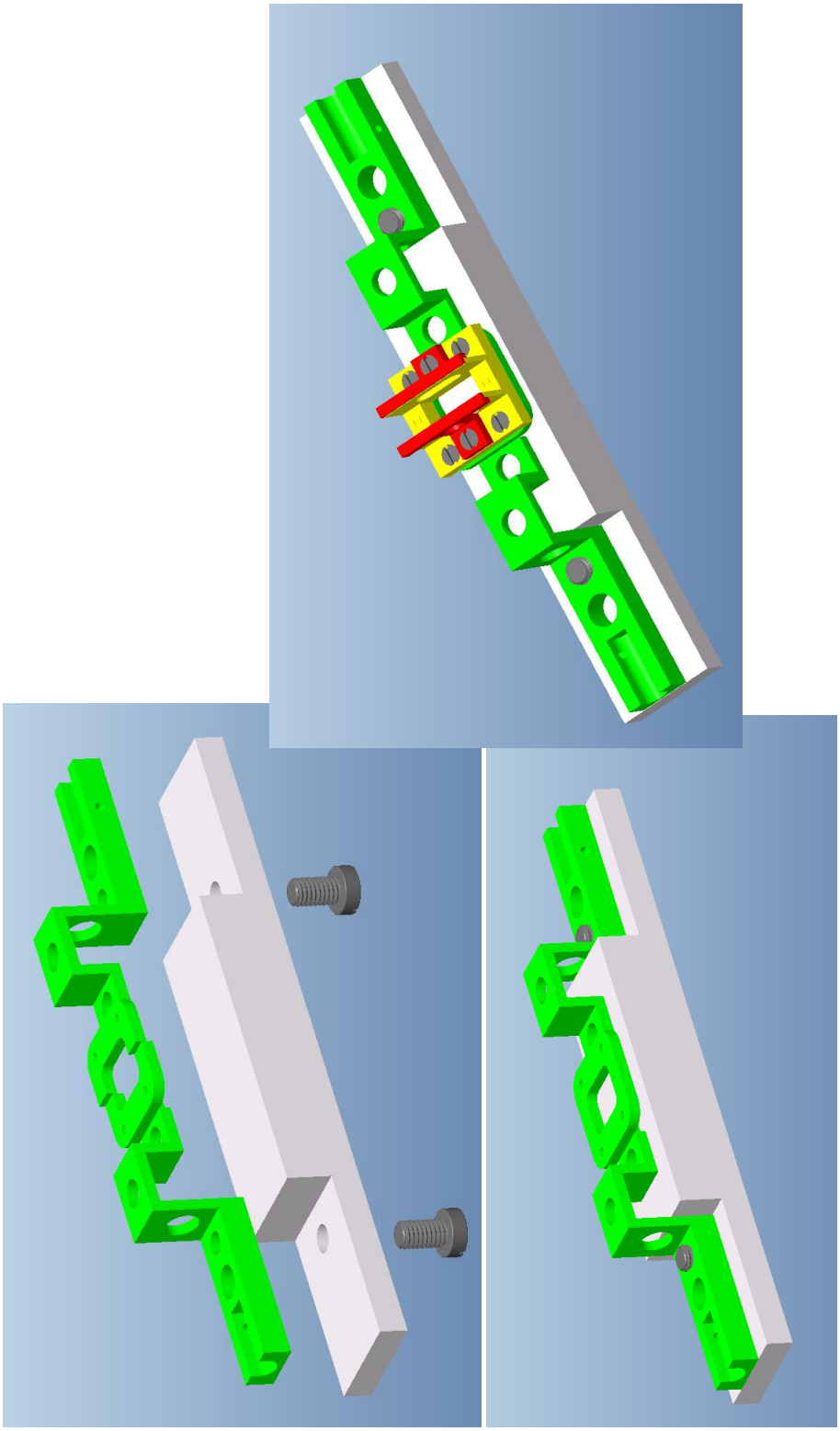

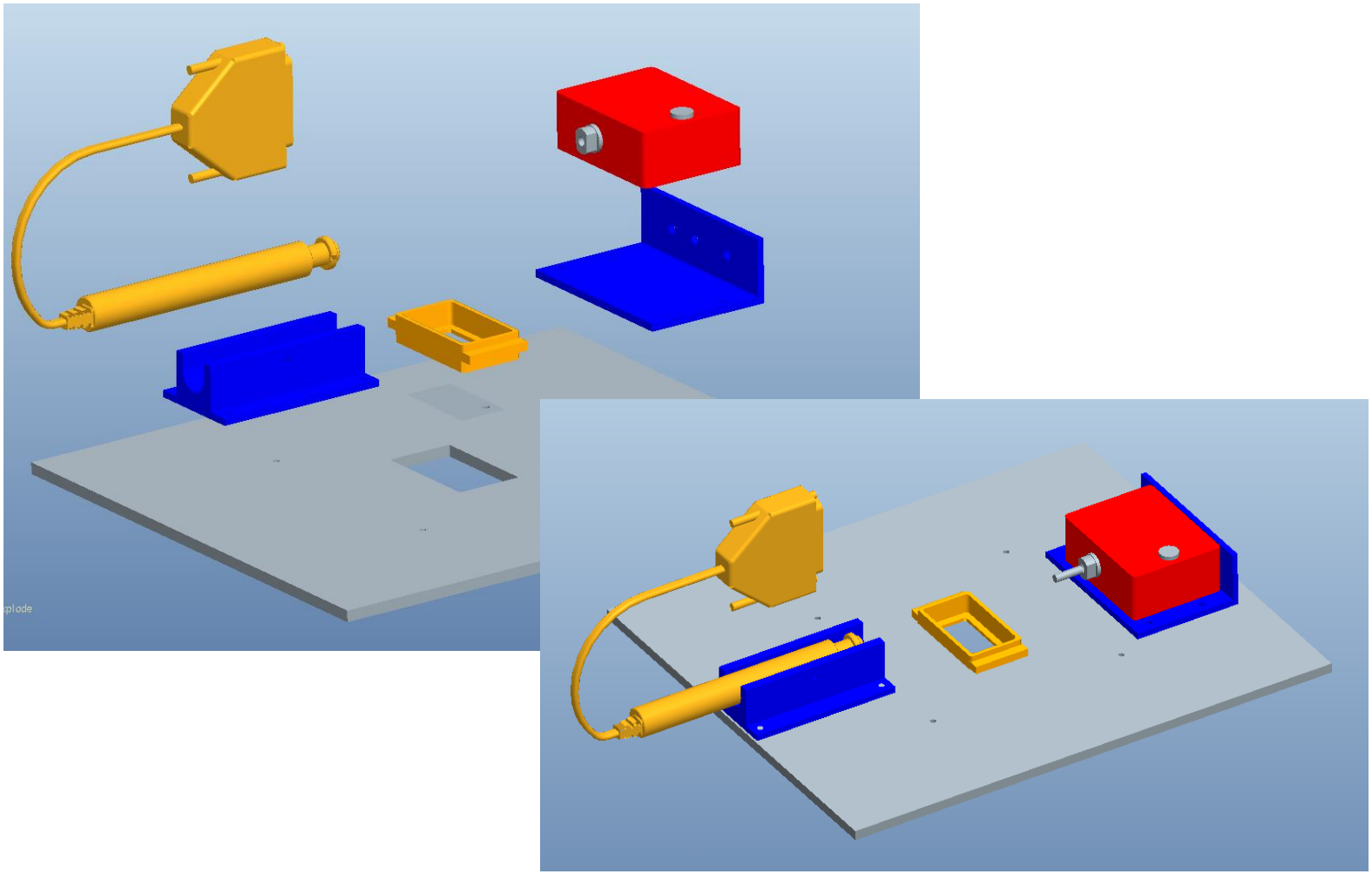

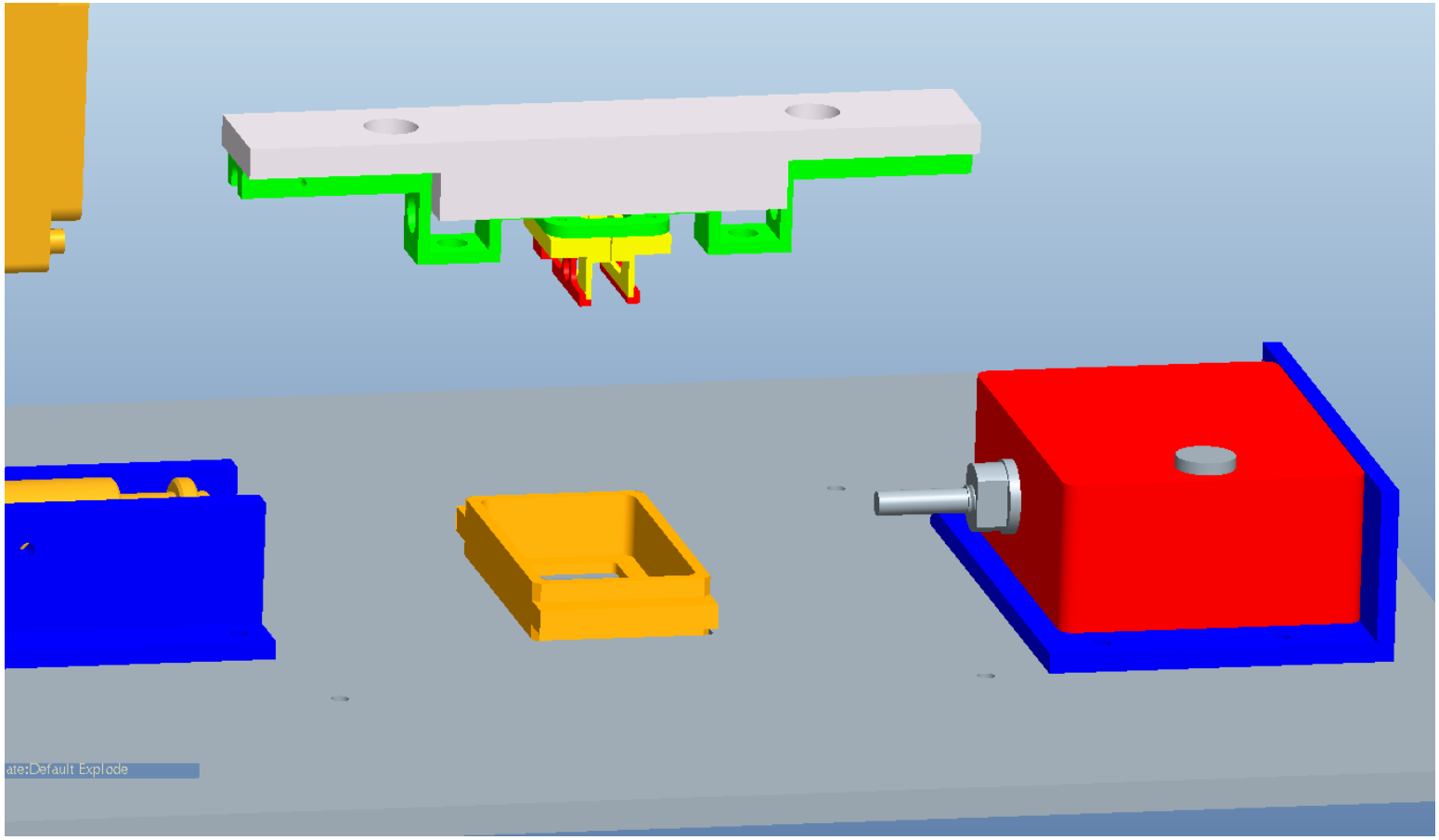
ate:Default Explode

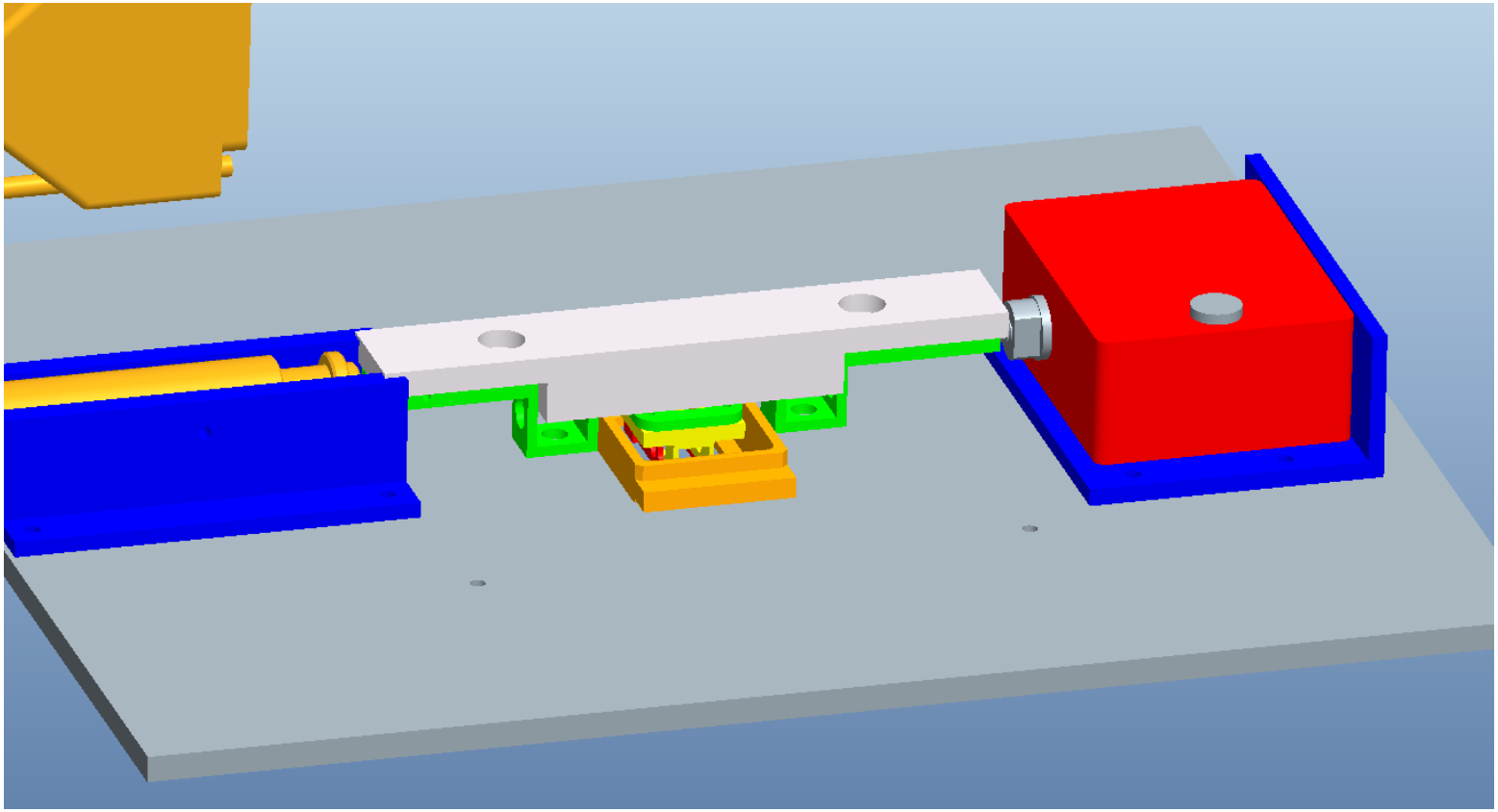

Final Assembly

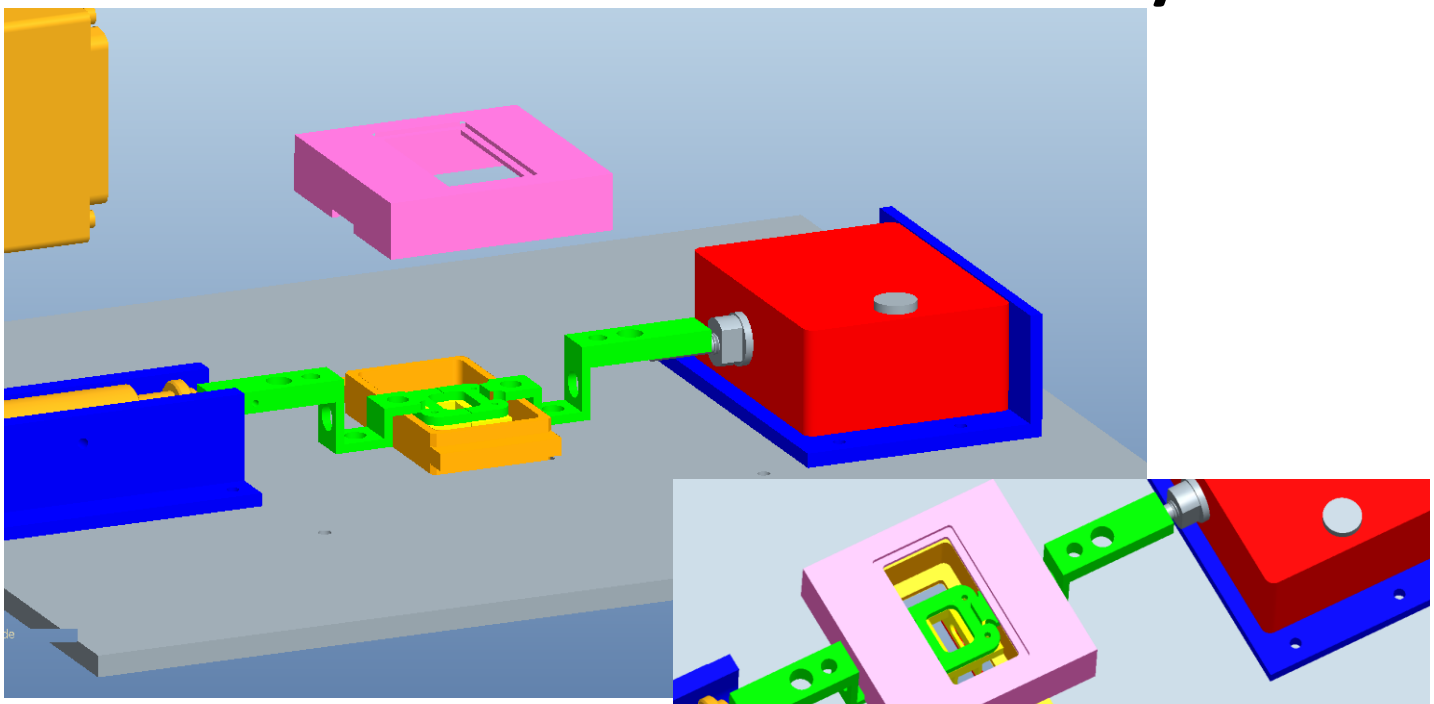

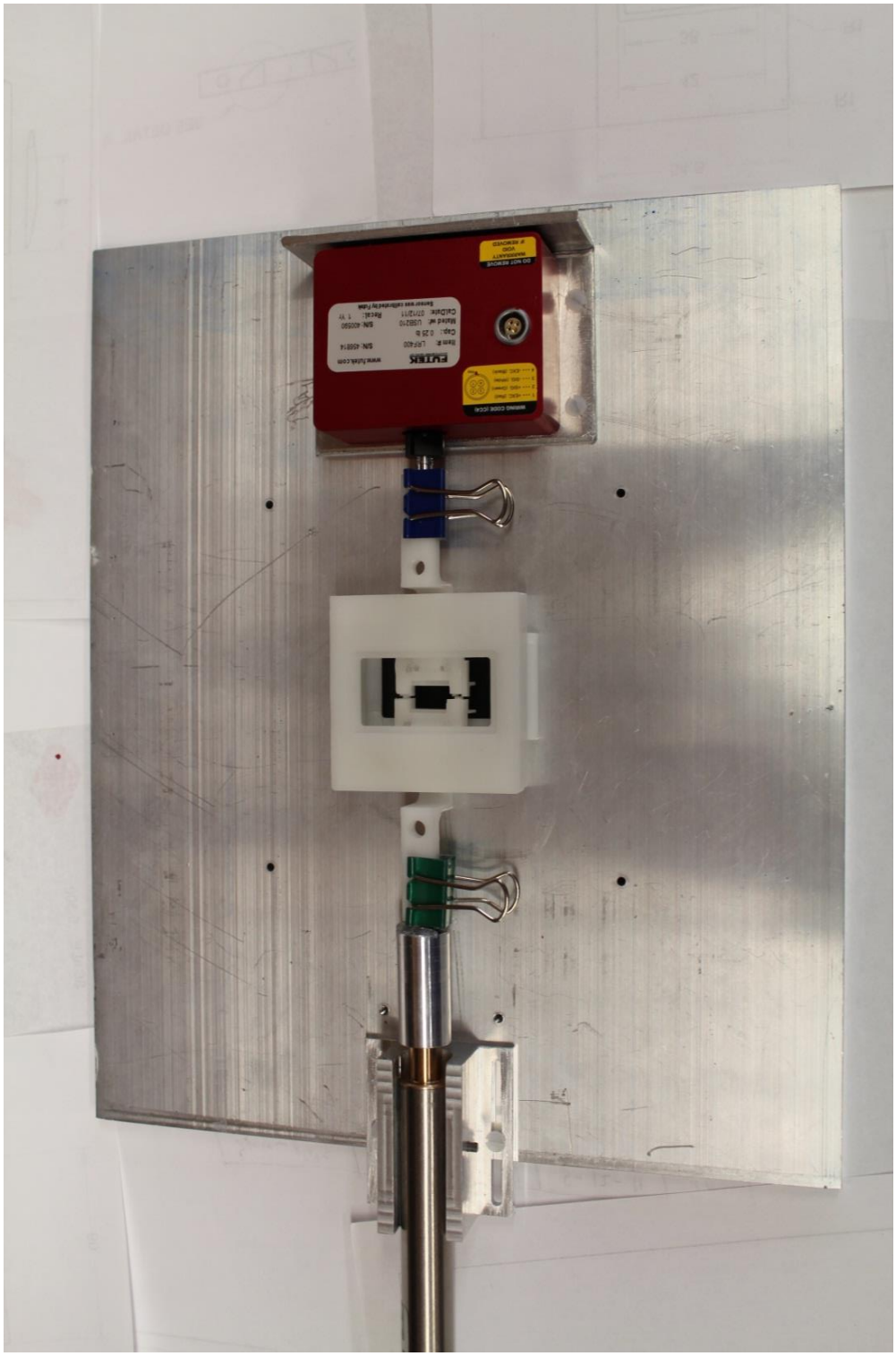

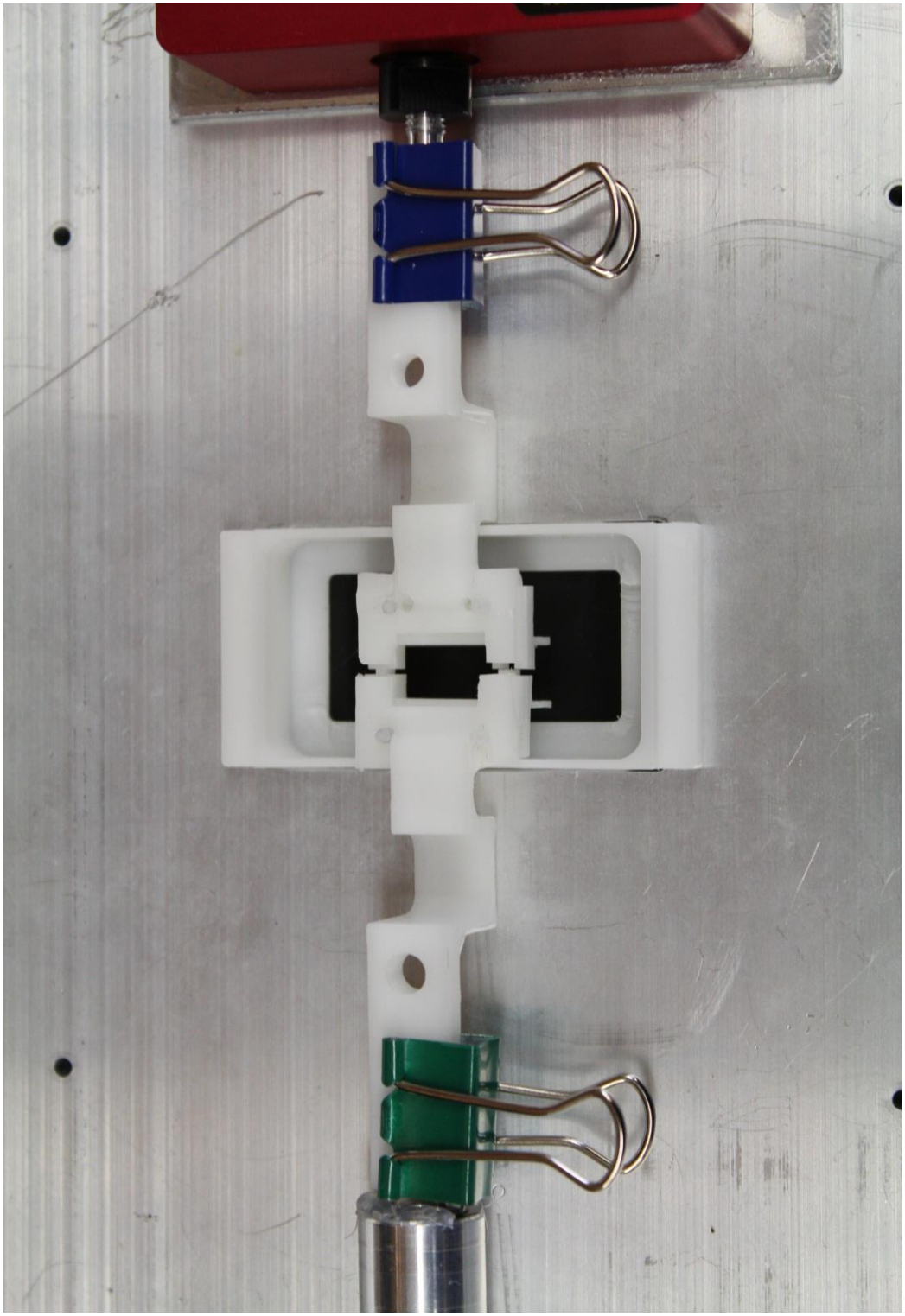

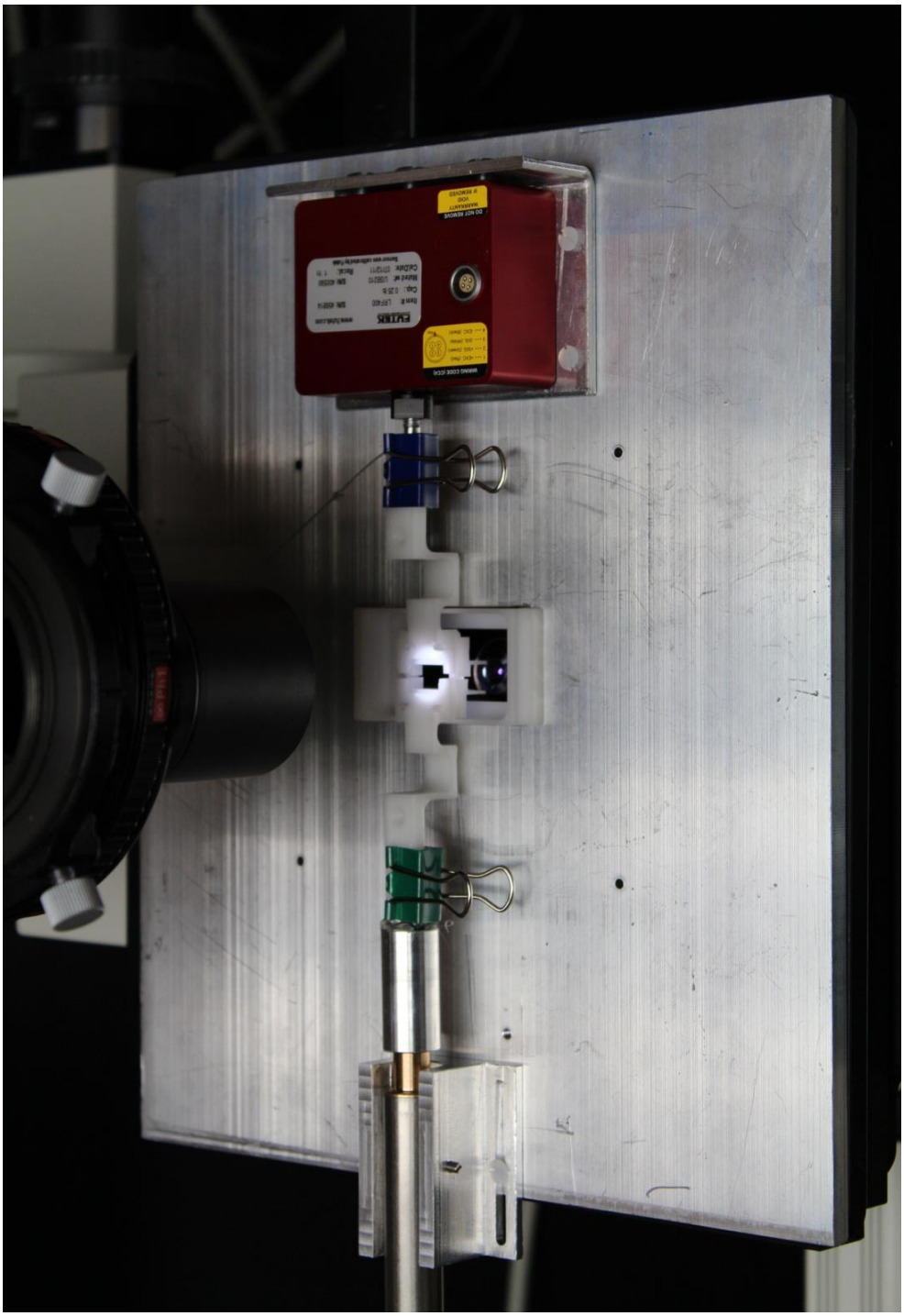

APPENDIX B

CUSTOM MATLAB FUNCTIONS

OPENING_SCRIPT.M

```
%opening_script.m
%image extraction script
%this script calls the function "bfopen.m" (produced by LOCI, Madison,
%WI)and then extracts the images contained the a .nd2 file that is
%output by the microscope used for this research and writes each image
%to a tiff file.
%
%note: the function "bfopen.m" must be present in the current
%directory, as well as the file "loci_tools.jar". Both files are
%available from the LOCI website: http://loci.wisc.edu
%
%this function calls the custom matlab functions "timestampSort.m" and
%"jHashRead.m"

%Copyright (c) 2012, Timothy John Fee
%All rights reserved.
%
%Redistribution and use in source and binary forms, with or without
%modification, are permitted provided that the following conditions are
%met:
%    * Redistributions of source code must retain the above copyright
%      notice, this list of conditions and the following disclaimer.
%    * Redistributions in binary form must reproduce the above
%      copyright notice, this list of conditions and the following
%      disclaimer in the documentation and/or other materials provided
%      with the distribution.
%    * Neither the name of the University of Alabama at Birmingham nor
%      the names of its contributors may be used to endorse or promote
%      products derived from this software without specific prior
%      written permission.
%
%THIS SOFTWARE IS PROVIDED BY THE COPYRIGHT HOLDERS AND CONTRIBUTORS
%"AS IS" AND ANY EXPRESS OR IMPLIED WARRANTIES, INCLUDING, BUT NOT
%LIMITED TO, THE IMPLIED WARRANTIES OF MERCHANTABILITY AND FITNESS FOR
%A PARTICULAR PURPOSE ARE DISCLAIMED. IN NO EVENT SHALL TIMOTHY JOHN
%FEE BE LIABLE FOR ANY DIRECT, INDIRECT, INCIDENTAL, SPECIAL,
%EXEMPLARY, OR CONSEQUENTIAL DAMAGES (INCLUDING, BUT NOT LIMITED TO,
%PROCUREMENT OF SUBSTITUTE GOODS OR SERVICES; LOSS OF USE, DATA, OR
%PROFITS; OR BUSINESS INTERRUPTION) HOWEVER CAUSED AND ON ANY THEORY OF
%LIABILITY, WHETHER IN CONTRACT, STRICT LIABILITY, OR TORT (INCLUDING
%NEGLIGENCE OR OTHERWISE) ARISING IN ANY WAY OUT OF THE USE OF THIS
%SOFTWARE, EVEN IF ADVISED OF THE POSSIBILITY OF SUCH DAMAGE.

%% call bfopen.m

data=bfopen;
```

```
dataSetName=input('Please enter the name of the data set, the image
files will be of the form: name_seriesX_imageX.tif','s');

%% find number of series
numSeries=size(data,1);
fprintf('Found %d image series',numSeries)
numPlanes=zeros(1,numSeries);

for i=1:numSeries
    numPlanes(i)=size(data{i,1},1);
    fprintf('Found %d planes in Series %d',numPlanes(i),i)
end

%% write each of the images to a file (for each series)
% additionally, we need to extract the metadata

labels=cell(numSeries,[]);

for i=1:numSeries
    [m,n]=size(data{i,1}{1,1});
    imstack=zeros(m,n,numPlanes(i),'uint16');
    for j=1:numPlanes(i) %extract each image
        imstack(:,:,j)=data{i,1}{j,1};
        labels{i,j}=data{i,1}{j,2};%also get the image labels
    end
    for j=1:numPlanes(i) %write each image to file

matFilename=sprintf('%s_series%d_image%05d.tif',dataSetName,i,j);
        imwrite(imstack(:,:,j),matFilename,'tif');
    end
    if numSeries == 1
       timstamps=timestampSort(jHashRead(data{i,2})); %get and sort the
                                                      %metadata
    end

end

%% clean up variables
clear numSeries numPlanes imstack matFilename i j dataSetName data
```

JHASHREAD.M

```
function out=jHashRead(in)
%out=jHashRead(in)
%this function reads the contents of a javascript hashtable,
%specifically, the one produced by "bfopen.m" it returns the two column
%matrix with the first being the field name and the second column
%being the value. This function calls the subfunction “hashDisplay”

%Copyright (c) 2012, Timothy John Fee
%All rights reserved.
%
%Redistribution and use in source and binary forms, with or without
```

```
%modification, are permitted provided that the following conditions are
%met:
%    * Redistributions of source code must retain the above copyright
%      notice, this list of conditions and the following disclaimer.
%    * Redistributions in binary form must reproduce the above
%      copyright notice, this list of conditions and the following
%      disclaimer in the documentation and/or other materials provided
%      with the distribution.
%    * Neither the name of the University of Alabama at Birmingham nor
%      the names of its contributors may be used to endorse or promote
%      products derived from this software without specific prior
%      written permission.
%
%THIS SOFTWARE IS PROVIDED BY THE COPYRIGHT HOLDERS AND CONTRIBUTORS
%"AS IS" AND ANY EXPRESS OR IMPLIED WARRANTIES, INCLUDING, BUT NOT
%LIMITED TO, THE IMPLIED WARRANTIES OF MERCHANTABILITY AND FITNESS FOR
%A PARTICULAR PURPOSE ARE DISCLAIMED. IN NO EVENT SHALL TIMOTHY JOHN
%FEE BE LIABLE FOR ANY DIRECT, INDIRECT, INCIDENTAL, SPECIAL,
%EXEMPLARY, OR CONSEQUENTIAL DAMAGES (INCLUDING, BUT NOT LIMITED TO,
%PROCUREMENT OF SUBSTITUTE GOODS OR SERVICES; LOSS OF USE, DATA, OR
%PROFITS; OR BUSINESS INTERRUPTION) HOWEVER CAUSED AND ON ANY THEORY OF
%LIABILITY, WHETHER IN CONTRACT, STRICT LIABILITY, OR TORT (INCLUDING
%NEGLIGENCE OR OTHERWISE) ARISING IN ANY WAY OUT OF THE USE OF THIS
%SOFTWARE, EVEN IF ADVISED OF THE POSSIBILITY OF SUCH DAMAGE.

enum=in.keys();
i=1;
while enum.hasMoreElements
    key=enum.nextElement;
    value=hashDisplay(in.get(key));
    out{i,1}=key;
    out{i,2}=value;
    i=i+1;
end
end


function blat=hashDisplay(entry)
[t,r]=strtok(entry,'^');
blat=[];
while ~isempty(t)
    blat=t;
    [t,r]=strtok(r,'^');
end
end
```

TIMESTAMPSORT.M

```
function out=timestampSort(in)
%out=timstampSort(in)
%this function takes in a 2 column cell array with field names in the
%first column and values in the second column. it searches the field
%names for the string "timestamp" and then sorts the corresponding
```

```
%times by the number at the end of the field name containing
%"timestamp"

%Copyright (c) 2012, Timothy John Fee
%All rights reserved.
%
%Redistribution and use in source and binary forms, with or without
%modification, are permitted provided that the following conditions are
%met:
%    * Redistributions of source code must retain the above copyright
%      notice, this list of conditions and the following disclaimer.
%    * Redistributions in binary form must reproduce the above
%      copyright notice, this list of conditions and the following
%      disclaimer in the documentation and/or other materials provided
%      with the distribution.
%    * Neither the name of the University of Alabama at Birmingham nor
%      the names of its contributors may be used to endorse or promote
%      products derived from this software without specific prior
%      written permission.
%
%THIS SOFTWARE IS PROVIDED BY THE COPYRIGHT HOLDERS AND CONTRIBUTORS
%"AS IS" AND ANY EXPRESS OR IMPLIED WARRANTIES, INCLUDING, BUT NOT
%LIMITED TO, THE IMPLIED WARRANTIES OF MERCHANTABILITY AND FITNESS FOR
%A PARTICULAR PURPOSE ARE DISCLAIMED. IN NO EVENT SHALL TIMOTHY JOHN
%FEE BE LIABLE FOR ANY DIRECT, INDIRECT, INCIDENTAL, SPECIAL,
%EXEMPLARY, OR CONSEQUENTIAL DAMAGES (INCLUDING, BUT NOT LIMITED TO,
%PROCUREMENT OF SUBSTITUTE GOODS OR SERVICES; LOSS OF USE, DATA, OR
%PROFITS; OR BUSINESS INTERRUPTION) HOWEVER CAUSED AND ON ANY THEORY OF
%LIABILITY, WHETHER IN CONTRACT, STRICT LIABILITY, OR TORT (INCLUDING
%NEGLIGENCE OR OTHERWISE) ARISING IN ANY WAY OUT OF THE USE OF THIS
%SOFTWARE, EVEN IF ADVISED OF THE POSSIBILITY OF SUCH DAMAGE.

l=length(in);
tfVect=zeros(1,l,'int8');
pattern='timestamp';

for i=1:l
    tfVect(i)=~isempty(strfind(in{i,1},pattern));
end

times=sum(tfVect); %total number of timestamps
stampdata=zeros(times,2); %preallocate the unsorted values

counter=1;
for i=1:l
    if tfVect(i)==1
        str=in{i,1};
        temp=textscan(str, '%*s %*s %*s %*s %d');
        temp=double(cell2mat(temp));
        stampdata(counter,1)=temp;
        stampdata(counter,2)=(in{i,2});
        counter=counter+1;
    end
end

%now sort the resulting data
out=zeros(times,2);
```

```
[holder1,holder2]=sort(stampdata(:,1));
out(:,1)=holder1;
ind=holder2;
for i=1:times
    out(i,2)=stampdata(ind(i),2);
end
```

POSITIONTRACKER.M

```
function out=positionTracker(imNames)
%out=positionTracker(imNames)
% this function is used to read a series of tiff images one by one and
% allow the user to select points (bright on a dark background) to
%track over time. the returned variable "out" has the form: (N by P by
%2) where N is the number of images, P is the number of points being
%tracked, the 1st layer is the x position of that point, and the 2nd
%layer is the y position of that point.
%
%Note: the variable "test" contains the number of images that should be
%processed
%
%the variable "box" contains the size of the bounding box that is used
%to track the point. therefore, each point being tracked must remain at
%least "box" pixels away from the edge of the image, any pixel being
%tracked should not move more than "box" pixels in any two sequential
%images, and no to points should be within "box" pixels of each other.
%
%This function calls the subfunctions: "findPoints", "centroid", and
%"peak2".
%the function "centroid" uses commands from the MATLAB image processing
%toolbox to find the intensity weighted centroid of the largest region
%of a thresholded region of interest. If your system does not have the
%image processing toolbox, you can replace each the centroid function
%with the peak2 function that tracks the maximum pixel value in a
%region of interest and uses the native MATLAB commands.

%Copyright (c) 2012, Timothy John Fee
%All rights reserved.
%
%Redistribution and use in source and binary forms, with or without
%modification, are permitted provided that the following conditions are
%met:
%    * Redistributions of source code must retain the above copyright
%      notice, this list of conditions and the following disclaimer.
%    * Redistributions in binary form must reproduce the above
%      copyright notice, this list of conditions and the following
%      disclaimer in the documentation and/or other materials provided
%      with the distribution.
%    * Neither the name of the University of Alabama at Birmingham nor
%      the names of its contributors may be used to endorse or promote
%      products derived from this software without specific prior
%      written permission.
%
```

```
%THIS SOFTWARE IS PROVIDED BY THE COPYRIGHT HOLDERS AND CONTRIBUTORS
%"AS IS" AND ANY EXPRESS OR IMPLIED WARRANTIES, INCLUDING, BUT NOT
%LIMITED TO, THE IMPLIED WARRANTIES OF MERCHANTABILITY AND FITNESS FOR
%A PARTICULAR PURPOSE ARE DISCLAIMED. IN NO EVENT SHALL TIMOTHY JOHN
%FEE BE LIABLE FOR ANY DIRECT, INDIRECT, INCIDENTAL, SPECIAL,
%EXEMPLARY, OR CONSEQUENTIAL DAMAGES (INCLUDING, BUT NOT LIMITED TO,
%PROCUREMENT OF SUBSTITUTE GOODS OR SERVICES; LOSS OF USE, DATA, OR
%PROFITS; OR BUSINESS INTERRUPTION) HOWEVER CAUSED AND ON ANY THEORY OF
%LIABILITY, WHETHER IN CONTRACT, STRICT LIABILITY, OR TORT (INCLUDING
%NEGLIGENCE OR OTHERWISE) ARISING IN ANY WAY OUT OF THE USE OF THIS
%SOFTWARE, EVEN IF ADVISED OF THE POSSIBILITY OF SUCH DAMAGE.

%get a list of image files in the current directory
imNames=strcat('*',imNames,'*.tif');
files=dir(imNames);
numImages=length(files) %shows the number of images found.
pause(2)

test=100; %number of images to process, when out=numImages all the
            files will be processed.
box=20; %number of pixels for the bounding box

%now call up the first image
I=imread(files(1).name);
set(gcf, 'OuterPosition', get(0, 'ScreenSize'));
imagesc(I);
title('image 1')
colormap(gray);

%prompt for a point
[X,Y,p]=impixel;
%call subfunction to locate each x and y dot
[X,Y]=findPoints(X,Y,I,box);

%show each point on the image
for z=1:length(X)
    line(X(z),Y(z),'Color','blue','Marker','o','LineStyle','none')
end
pause(0.5)
close
% pre allocate out
out=zeros(test,length(X),2);
%write the data
for i=1:length(X)
    out(1,i,1)=X(i);
    out(1,i,2)=Y(i);
end

%loop for the remaining images
if numImages==1
    error('only one image')
end

for i=2:test
    I=imread(files(i).name);
    set(gcf, 'OuterPosition', get(0, 'ScreenSize'));
    imagesc(I);
```

```
    goo=strcat('image number...',int2str(i));
    title(goo);
    colormap(gray);

    %call subfunction to locate each x and y dot
    [X,Y]=findPoints(X,Y,I,box);

    %show each point on the image
    for z=1:length(X)
        line(X(z),Y(z),'Color','blue','Marker','o','LineStyle','none')
    end
    pause(0.5)
    close

    %write the data
    for j=1:length(X)
        out(i,j,1)=X(j);
        out(i,j,2)=Y(j);
    end
end
end

function [xout,yout]=findPoints(X,Y,I,box)
%this function takes in an image I and two vectors of x and y
%positions. It finds the local maximum for each x-y pair and returns
%those points

l=length(X);
k=box;
xout=zeros(l,1);
yout=zeros(l,1);
for q=1:l
        ROI=I(Y(q)-k:Y(q)+k,X(q)-k:X(q)+k);
        [ix,iy]=centroid(ROI);
        xout(q)=X(q)-k+ix;
        yout(q)=Y(q)-k+iy;
end
end



function [x,y]=peak2(ROIin)
[rowstack, rowindex]=max(ROIin);
[~, col]=max(rowstack);
row=rowindex(col);
x=col;
y=row;
end


function [x,y]=centroid(ROIin)
filteredROI=medfilt2(ROIin,'symmetric');
level = 1.25*mean2(filteredROI);
[cols, rows]=size(filteredROI);
bw = zeros(cols,rows);
for col=1:cols
    for row=1:rows
```

```
        if filteredROI(col,row)>=level
            bw(col,row)=1;
        end
    end
end
stats=regionprops(bw,'Area','Centroid','PixelIdxList', 'PixelList');
biggest=0;
big=0;

for p=1:length(stats)
    if stats(p).Area>biggest
        big=p;
    end
end

if big==0
    [x,y]=peak2(ROIin);
else

%weighted centroid method
k = big;
idx = stats(k).PixelIdxList;
pixel_values = double(filteredROI(idx));
sum_pixel_values = sum(pixel_values);
x_test = stats(k).PixelList(:, 1);
y_test = stats(k).PixelList(:, 2);
xbar = sum(x_test .* pixel_values) / sum_pixel_values;
ybar = sum(y_test .* pixel_values) / sum_pixel_values;
x=round(xbar);
y=round(ybar);
end
end
```

SOBELGRAD.M

```
function [theta, values]=sobelGrad(I)
%this function takes in an image and approximates the image gradient by
%filtering the image using a sobel filter

%Copyright (c) 2015, Timothy John Fee
%All rights reserved.
%
%Redistribution and use in source and binary forms, with or without
%modification, are permitted provided that the following conditions are
%met:
%    * Redistributions of source code must retain the above copyright
%      notice, this list of conditions and the following disclaimer.
%    * Redistributions in binary form must reproduce the above
%      copyright notice, this list of conditions and the following
%      disclaimer in the documentation and/or other materials provided
%      with the distribution.
%    * Neither the name of the University of Alabama at Birmingham nor
%      the names of its contributors may be used to endorse or promote
%      products derived from this software without specific prior
%      written permission.
```

```
%
%THIS SOFTWARE IS PROVIDED BY THE COPYRIGHT HOLDERS AND CONTRIBUTORS
%"AS IS" AND ANY EXPRESS OR IMPLIED WARRANTIES, INCLUDING, BUT NOT
%LIMITED TO, THE IMPLIED WARRANTIES OF MERCHANTABILITY AND FITNESS FOR
%A PARTICULAR PURPOSE ARE DISCLAIMED. IN NO EVENT SHALL TIMOTHY JOHN
%FEE BE LIABLE FOR ANY DIRECT, INDIRECT, INCIDENTAL, SPECIAL,
%EXEMPLARY, OR CONSEQUENTIAL DAMAGES (INCLUDING, BUT NOT LIMITED TO,
%PROCUREMENT OF SUBSTITUTE GOODS OR SERVICES; LOSS OF USE, DATA, OR
%PROFITS; OR BUSINESS INTERRUPTION) HOWEVER CAUSED AND ON ANY THEORY OF
%LIABILITY, WHETHER IN CONTRACT, STRICT LIABILITY, OR TORT (INCLUDING
%NEGLIGENCE OR OTHERWISE) ARISING IN ANY WAY OUT OF THE USE OF THIS
%SOFTWARE, EVEN IF ADVISED OF THE POSSIBILITY OF SUCH DAMAGE.

h1=fspecial('sobel');
h2=h1';

horEdges=imfilter(im2double(I),h1);
verEdges=imfilter(im2double(I),h2);

approxGrad=double(complex(horEdges,verEdges));
strengths=abs(approxGrad);
threshold=mean2(strengths);
mask=strengths>threshold;
allthetas=angle(approxGrad);
theta=allthetas(mask)';

[theta, values]=angleDist(theta);
```

ANGLEDIST.M

```
function [theta, value]=angleDist(varargin)
%this function takes in either:
%   1) a list of angles to be sorted into a histogram
%   2) a set of angles/values with exactly 1 value per angle
% The with either input, the angles domain is 0<=x<2*pi
% The function converts the angles to the domain of 0<=x<pi then
%normalizes
% the height of the values such that the area under the curve is unity.

%Copyright (c) 2015, Timothy John Fee
%All rights reserved.
%
%Redistribution and use in source and binary forms, with or without
%modification, are permitted provided that the following conditions are
%met:
%    * Redistributions of source code must retain the above copyright
%      notice, this list of conditions and the following disclaimer.
%    * Redistributions in binary form must reproduce the above
%      copyright notice, this list of conditions and the following
%      disclaimer in the documentation and/or other materials provided
%      with the distribution.
%    * Neither the name of the University of Alabama at Birmingham nor
%      the names of its contributors may be used to endorse or promote
%      products derived from this software without specific prior
```

```
%      written permission.
%
%THIS SOFTWARE IS PROVIDED BY THE COPYRIGHT HOLDERS AND CONTRIBUTORS
%"AS IS" AND ANY EXPRESS OR IMPLIED WARRANTIES, INCLUDING, BUT NOT
%LIMITED TO, THE IMPLIED WARRANTIES OF MERCHANTABILITY AND FITNESS FOR
%A PARTICULAR PURPOSE ARE DISCLAIMED. IN NO EVENT SHALL TIMOTHY JOHN
%FEE BE LIABLE FOR ANY DIRECT, INDIRECT, INCIDENTAL, SPECIAL,
%EXEMPLARY, OR CONSEQUENTIAL DAMAGES (INCLUDING, BUT NOT LIMITED TO,
%PROCUREMENT OF SUBSTITUTE GOODS OR SERVICES; LOSS OF USE, DATA, OR
%PROFITS; OR BUSINESS INTERRUPTION) HOWEVER CAUSED AND ON ANY THEORY OF
%LIABILITY, WHETHER IN CONTRACT, STRICT LIABILITY, OR TORT (INCLUDING
%NEGLIGENCE OR OTHERWISE) ARISING IN ANY WAY OUT OF THE USE OF THIS
%SOFTWARE, EVEN IF ADVISED OF THE POSSIBILITY OF SUCH DAMAGE.

if length(varargin)==1
    [intensities, thetas]=hist(varargin{1},72);
    intensities=intensities';
    thetas=thetas';
elseif length(varargin)==2
    intensities=varargin{2};
    thetas=varargin{1};
else
    error('could not determine the input format')
end

thetaDeg=round(rad2deg(thetas));

newThetas=mod(thetaDeg,180);

finalThetas=unique(newThetas);
finalValues=zeros(size(finalThetas));

for i=1:length(finalThetas)
    mask=newThetas==finalThetas(i);
    finalValues(i)=sum(intensities(mask));
end

theta=deg2rad(finalThetas);
value=finalValues./trapz(theta,finalValues);

end
```

FFTMETHOD.M

```
function [thetaOut,valueOut]=fftMethod(Iin,varargin)
%this function calculates the alignment shown within an image by the
%fft method.
% It uses the 2D FFT to look for periodicity within an image and
%determines the alignment by the direction of the strongest
%periodicity. It
%takes in an image (Iin) and the following optional name/value pairs:
%   'window'  - either [0] or 1, if set to 1, the image is filtered to
%               provide a smooth transition to the edge to reduce
%artifacts
```

```
%               induced by non-symmetric boundaries
%   'nprofiles'-an integer value of the number of points to sample in
%the
%               2D FFT of the input image. This increases the angular
%               resolution of the analysis. The default is 36.

%Copyright (c) 2015, Timothy John Fee
%All rights reserved.
%
%Redistribution and use in source and binary forms, with or without
%modification, are permitted provided that the following conditions are
%met:
%    * Redistributions of source code must retain the above copyright
%      notice, this list of conditions and the following disclaimer.
%    * Redistributions in binary form must reproduce the above
%      copyright notice, this list of conditions and the following
%      disclaimer in the documentation and/or other materials provided
%      with the distribution.
%    * Neither the name of the University of Alabama at Birmingham nor
%      the names of its contributors may be used to endorse or promote
%      products derived from this software without specific prior
%      written permission.
%
%THIS SOFTWARE IS PROVIDED BY THE COPYRIGHT HOLDERS AND CONTRIBUTORS
%"AS IS" AND ANY EXPRESS OR IMPLIED WARRANTIES, INCLUDING, BUT NOT
%LIMITED TO, THE IMPLIED WARRANTIES OF MERCHANTABILITY AND FITNESS FOR
%A PARTICULAR PURPOSE ARE DISCLAIMED. IN NO EVENT SHALL TIMOTHY JOHN
%FEE BE LIABLE FOR ANY DIRECT, INDIRECT, INCIDENTAL, SPECIAL,
%EXEMPLARY, OR CONSEQUENTIAL DAMAGES (INCLUDING, BUT NOT LIMITED TO,
%PROCUREMENT OF SUBSTITUTE GOODS OR SERVICES; LOSS OF USE, DATA, OR
%PROFITS; OR BUSINESS INTERRUPTION) HOWEVER CAUSED AND ON ANY THEORY OF
%LIABILITY, WHETHER IN CONTRACT, STRICT LIABILITY, OR TORT (INCLUDING
%NEGLIGENCE OR OTHERWISE) ARISING IN ANY WAY OUT OF THE USE OF THIS
%SOFTWARE, EVEN IF ADVISED OF THE POSSIBILITY OF SUCH DAMAGE.

window=0;
nprofiles=36;

if ~isempty(varargin)
    for i=1:2:length(varargin)
        switch varargin{i}
            case 'window'
                if varargin{i+1}==1||varargin{i+1}==0
                    window=varargin{i+1};
                else
                    error('did not understand the provided value for
"window", expected 1 or 0')
                end
            case 'nprofiles'
                nprofiles=varargin{i+1};
            otherwise
                error('could not parse input parameter')
        end
    end
end
```

```
[m,n]=size(Iin);

%makes the input image an even number of pixels in size
if rem(m,2)==1
    m=m-1;
end
if rem(n,2)==1
    n=n-1;
end

Iin=Iin(1:m,1:n);

if window==1
    J=windowedFFT2(Iin);
else
    J=fftshift(fft2(im2double(Iin)));
end

[angles, radialSums]=ovalProfile(J,nprofiles);

for i=1:length(angles)
    if angles(i)>=pi/2
        angles(i)=angles(i)-pi/2;
    else
        angles(i)=angles(i)+3*pi/2;
    end
end

[thetaOut, valueOut]=angleDist(angles,radialSums);

end
```

OVALPROFILE.M

```
function [theta, Rsums]=ovalProfile(FFTin,nlines)
%this function calculates the sums along lines from the center of a
%FFT
%of an image to a point along an inscribed circle. This can be used in
%the
%fft method of determining fiber alignment in an image.

%Copyright (c) 2015, Timothy John Fee
%All rights reserved.
%
%Redistribution and use in source and binary forms, with or without
%modification, are permitted provided that the following conditions are
%met:
%    * Redistributions of source code must retain the above copyright
%      notice, this list of conditions and the following disclaimer.
%    * Redistributions in binary form must reproduce the above
%      copyright notice, this list of conditions and the following
%      disclaimer in the documentation and/or other materials provided
%      with the distribution.
%    * Neither the name of the University of Alabama at Birmingham nor
```

```
%      the names of its contributors may be used to endorse or promote
%      products derived from this software without specific prior
%      written permission.
%
%THIS SOFTWARE IS PROVIDED BY THE COPYRIGHT HOLDERS AND CONTRIBUTORS
%"AS IS" AND ANY EXPRESS OR IMPLIED WARRANTIES, INCLUDING, BUT NOT
%LIMITED TO, THE IMPLIED WARRANTIES OF MERCHANTABILITY AND FITNESS FOR
%A PARTICULAR PURPOSE ARE DISCLAIMED. IN NO EVENT SHALL TIMOTHY JOHN
%FEE BE LIABLE FOR ANY DIRECT, INDIRECT, INCIDENTAL, SPECIAL,
%EXEMPLARY, OR CONSEQUENTIAL DAMAGES (INCLUDING, BUT NOT LIMITED TO,
%PROCUREMENT OF SUBSTITUTE GOODS OR SERVICES; LOSS OF USE, DATA, OR
%PROFITS; OR BUSINESS INTERRUPTION) HOWEVER CAUSED AND ON ANY THEORY OF
%LIABILITY, WHETHER IN CONTRACT, STRICT LIABILITY, OR TORT (INCLUDING
%NEGLIGENCE OR OTHERWISE) ARISING IN ANY WAY OUT OF THE USE OF THIS
%SOFTWARE, EVEN IF ADVISED OF THE POSSIBILITY OF SUCH DAMAGE.

[m,n]=size(FFTin);

if m~=n
    error('expected FFTin to be a square image')
end

if isempty(nlines)
    nlines=72;
end

Xc=(n/2)+1; %coordinates of center pixel in image
Yc=(m/2)+1;

if Xc>Yc
    R=floor(Yc)-3; %length of radius (in pixels)
else
    R=floor(Xc)-3;
end

increment=2*pi/nlines;

theta=zeros(nlines,1);
Rsums=zeros(nlines,1);

for i=1:nlines
    x=R*cos((i-1)*increment) + Xc;
    y=-R*sin((i-1)*increment) + Yc;
    theta(i)=increment*(i-1);

    values=improfile(FFTin,[Xc,x],[Yc,y],R);

    Rsums(i)=sum(abs(values));
    %plot(x,y,'rx')
end
```

FITTOHALFVONMISES.M

```
function [mu,kappa]=fitToHalfVonMises(theta,frequency)
%this function is designed to take in a set of angles and
%frequencies on the range 0<=x<=pi and fits them to a half-
%Von Mises distribution using maximum likelihood estimation.

%Copyright (c) 2015, Timothy John Fee
%All rights reserved.
%
%Redistribution and use in source and binary forms, with or without
%modification, are permitted provided that the following conditions are
%met:
%    * Redistributions of source code must retain the above copyright
%      notice, this list of conditions and the following disclaimer.
%    * Redistributions in binary form must reproduce the above
%      copyright notice, this list of conditions and the following
%      disclaimer in the documentation and/or other materials provided
%      with the distribution.
%    * Neither the name of the University of Alabama at Birmingham nor
%      the names of its contributors may be used to endorse or promote
%      products derived from this software without specific prior
%      written permission.
%
%THIS SOFTWARE IS PROVIDED BY THE COPYRIGHT HOLDERS AND CONTRIBUTORS
%"AS IS" AND ANY EXPRESS OR IMPLIED WARRANTIES, INCLUDING, BUT NOT
%LIMITED TO, THE IMPLIED WARRANTIES OF MERCHANTABILITY AND FITNESS FOR
%A PARTICULAR PURPOSE ARE DISCLAIMED. IN NO EVENT SHALL TIMOTHY JOHN
%FEE BE LIABLE FOR ANY DIRECT, INDIRECT, INCIDENTAL, SPECIAL,
%EXEMPLARY, OR CONSEQUENTIAL DAMAGES (INCLUDING, BUT NOT LIMITED TO,
%PROCUREMENT OF SUBSTITUTE GOODS OR SERVICES; LOSS OF USE, DATA, OR
%PROFITS; OR BUSINESS INTERRUPTION) HOWEVER CAUSED AND ON ANY THEORY OF
%LIABILITY, WHETHER IN CONTRACT, STRICT LIABILITY, OR TORT (INCLUDING
%NEGLIGENCE OR OTHERWISE) ARISING IN ANY WAY OUT OF THE USE OF THIS
%SOFTWARE, EVEN IF ADVISED OF THE POSSIBILITY OF SUCH DAMAGE.

[~,n]=size(theta);
if n~=1
    theta=theta';
end
[~,n]=size(frequency);
if n~=1
    frequency=frequency';
end
[~,index]=max(frequency);

[values, ~]=mle(theta,'pdf',@(x,mu,k)exp(k*cos(2*(x-
mu)))./(pi*besseli(0,k)),'start',[theta(index),2],...
    'frequency',frequency*10000,'lowerbound',[0,-
0.1],'upperbound',[pi,Inf]);

mu=values(1);
kappa=values(2);

end
```

APPENDIX C

LIST OF GENES INCLUDED IN MICROARRAY

Table 1. Full list of genes included in the expression microarray. The listed fold change and results are for the cells on the aligned scaffold relative to cells on the random scaffold.

Unigene	Refseq	Symbol	Full Name	Fold Change	p-value from t-test	Result
Mm.391967	NM_007393	Actb	Actin, beta	1.2592	0.007756	upregulated
Mm.259045	NM_146243	Actr2	ARP2 actin-related protein 2 homolog (yeast)	1.0204	0.689969	unable to reject null
Mm.183102	NM_023735	Actr3	ARP3 actin-related protein 3 homolog (yeast)	1.239	0.005799	upregulated
Mm.277687	NM_027180	Arap1	ArfGAP with RhoGAP domain, ankyrin repeat and PH domain 1	1.0087	0.891749	excluded, Ct>30
Mm.41637	NM_029802	Arfip2	ADP-ribosylation factor interacting protein 2	1.1115	0.19521	unable to reject null
Mm.441810	NM_009707	Arhgap6	Rho GTPase activating protein 6	1.3096	0.509456	excluded, Ct>30
Mm.2241	NM_007486	Arhgdib	Rho, GDP dissociation inhibitor (GDI) beta	1.1776	0.073306	unable to reject null
Mm.287267	NM_001003912	Arhgef11	Rho guanine nucleotide exchange factor (GEF) 11	0.9721	0.853505	unable to reject null
Mm.30010	NM_023142	Arpc1b	Actin related protein 2/3 complex, subunit 1B	1.0911	0.138586	unable to reject null
Mm.337038	NM_029711	Arpc2	Actin related protein 2/3 complex, subunit 2	1.1722	0.038195	fold change < 20%
Mm.275942	NM_019824	Arpc3	Actin related protein 2/3 complex, subunit 3	1.0886	0.232668	unable to reject null
Mm.472172	NM_026552	Arpc4	Actin related protein 2/3 complex, subunit 4	1.1695	0.011824	fold change < 20%
Mm.288974	NM_026369	Arpc5	Actin related protein 2/3 complex, subunit 5	1.0987	0.719136	unable to reject null
Mm.249363	NM_011497	Aurka	Aurora kinase A	1.0937	0.076088	unable to reject null
Mm.3488	NM_011496	Aurkb	Aurora kinase B	1.1141	0.076641	unable to reject null

Unigene	Refseq	Symbol	Full Name	Fold Change	p-value from t-test	Result
Mm.261572	NM_020572	Aurkc	Aurora kinase C	1.8478	0.172677	excluded, Ct>30
Mm.197534	NM_130862	Baiap2	Brain-specific angiogenesis inhibitor 1-associated protein 2	1.0987	0.029595	fold change < 20%
Mm.482600	NM_145575	Cald1	Caldesmon 1	1.1722	0.043772	fold change < 20%
Mm.285993	NM_009790	Calm1	Calmodulin 1	1.2361	0.102433	unable to reject null
Mm.474948	NM_009806	Cask	Calcium/calmodulin-dependent serine protein kinase (MAGUK family)	1.0861	0.413376	unable to reject null
Mm.4815	NM_007628	Ccna1	Cyclin A1	1.3096	0.509456	excluded, Ct>30
Mm.22592	NM_007630	Ccnb2	Cyclin B2	1.0886	0.321739	unable to reject null
Mm.447553	NM_009861	Cdc42	Cell division cycle 42 homolog (S. cerevisiae)	1.1192	0.14589	unable to reject null
Mm.259655	NM_001033285	Cdc42bpa	Cdc42 binding protein kinase alpha	1.1115	0.419869	unable to reject null
Mm.491103	NM_026772	Cdc42ep2	CDC42 effector protein (Rho GTPase binding) 2	1.1749	0.129348	unable to reject null
Mm.140601	NM_026514	Cdc42ep3	CDC42 effector protein (Rho GTPase binding) 3	1.2333	0.053639	unable to reject null
Mm.445256	NM_007668	Cdk5	Cyclin-dependent kinase 5	1.1454	0.625	excluded, Ct>30
Mm.474282	NM_009871	Cdk5r1	Cyclin-dependent kinase 5, regulatory subunit 1 (p35)	0.9282	0.551336	excluded, Ct>30
Mm.329655	NM_007687	Cfl1	Cofilin 1, non-muscle	1.1803	0.287661	unable to reject null
Mm.426282	NM_007708	Cit	Citron	1.0064	0.898104	unable to reject null
Mm.138740	NM_001081276	Clasp1	CLIP associating protein 1	1.0712	0.457774	unable to reject null
Mm.222272	NM_029633	Clasp2	CLIP associating protein 2	1.0761	0.533289	unable to reject null
Mm.441802	NM_019765	Clip1	CAP-GLY domain containing linker protein 1	1.0041	0.903416	unable to reject null
Mm.255138	NM_009990	Clip2	CAP-GLY domain containing linker protein 2	1.2857	0.035648	unable to reject null
Mm.280125	NM_133656	Crk	V-crk sarcoma virus CT10 oncogene homolog (avian)	1.0911	0.634088	unable to reject null

Unigene	Refseq	Symbol	Full Name	Fold Change	p-value from t-test	Result
Mm.490123	NM_007803	Cttn	Cortactin	1.1218	0.199605	unable to reject null
Mm.333893	NM_011370	Cyfip1	Cytoplasmic FMR1 interacting protein 1	1.1038	0.01295	fold change < 20%
Mm.454389	NM_133769	Cyfip2	Cytoplasmic FMR1 interacting protein 2	0.9049	0.56485	excluded, Ct>30
Mm.195916	NM_007858	Diap1	Diaphanous homolog 1 (Drosophila)	1.2163	0.045112	unable to reject null
Mm.28919	NM_019771	Dstn	Destrin	1.0564	0.267389	unable to reject null
Mm.277812	NM_009510	Ezr	Ezrin	1.2219	0.012021	upregulated
Mm.470230	NM_153118	Fnbp1l	Formin binding protein 1-like	1.0937	0.472834	unable to reject null
Mm.481403	NM_172802	Fscn2	Fascin homolog 2, actin-bundling protein, retinal (Strongylocentrotus purpuratus)	1.2886	0.139339	excluded, Ct>30
Mm.21109	NM_146120	Gsn	Gelsolin	0.9477	0.314111	unable to reject null
Mm.207619	NM_016721	Iqgap1	IQ motif containing GTPase activating protein 1	1.0937	0.263415	unable to reject null
Mm.38878	NM_027711	Iqgap2	IQ motif containing GTPase activating protein 2	1.3096	0.509456	excluded, Ct>30
Mm.15409	NM_010717	Limk1	LIM-domain containing, protein kinase	1.3036	0.030005	upregulated
Mm.390323	NM_010718	Limk2	LIM motif-containing protein kinase 2	1.1803	0.012605	fold change < 20%
Mm.285453	NM_008502	Llgl1	Lethal giant larvae homolog 1 (Drosophila)	1.1115	0.361225	unable to reject null
Mm.485351	NM_001199136	Macf1	Microtubule-actin crosslinking factor 1	1.0087	0.868628	unable to reject null
Mm.185026	NM_022012	Map3k11	Mitogen-activated protein kinase kinase kinase 11	1.2276	0.038258	unable to reject null
Mm.27970	NM_011950	Mapk13	Mitogen-activated protein kinase 13	1.4431	0.457409	excluded, Ct>30
Mm.143877	NM_007896	Mapre1	Microtubule-associated protein, RP/EB family, member 1	1.1296	0.191148	unable to reject null
Mm.132237	NM_153058	Mapre2	Microtubule-associated protein, RP/EB family, member 2	1.0937	0.191317	unable to reject null
Mm.1287	NM_010838	Mapt	Microtubule-associated protein tau	1.2163	0.583826	excluded, Ct>30

Unigene	Refseq	Symbol	Full Name	Fold Change	p-value from t-test	Result
Mm.258986	NM_007928	Mark2	MAP/microtubule affinity-regulating kinase 2	1.0786	0.48498	unable to reject null
Mm.34441	NM_010797	Mid1	Midline 1	1.2023	0.281265	unable to reject null
Mm.138876	NM_010833	Msn	Moesin	1.239	0.015974	upregulated
Mm.443428	NM_008633	Map4	Microtubule-associated protein 4	1.1507	0.121304	unable to reject null
Mm.33360	NM_139300	Mylk	Myosin, light polypeptide kinase	1.3433	0.007512	upregulated
Mm.250604	NM_001081044	Mylk2	Myosin, light polypeptide kinase 2, skeletal muscle	1.3096	0.509456	excluded, Ct>30
Mm.181485	NM_010878	Nck1	Non-catalytic region of tyrosine kinase adaptor protein 1	1.0962	0.158754	unable to reject null
Mm.483157	NM_010879	Nck2	Non-catalytic region of tyrosine kinase adaptor protein 2	1.1885	0.173444	unable to reject null
Mm.260227	NM_011035	Pak1	P21 protein (Cdc42/Rac)-activated kinase 1	1.1776	0.174303	unable to reject null
Mm.21876	NM_027470	Pak4	P21 protein (Cdc42/Rac)-activated kinase 4	1.0299	0.810644	unable to reject null
Mm.271744	NM_019410	Pfn2	Profilin 2	1.2276	0.014362	unable to reject null
Mm.211477	NM_153412	Phldb2	Pleckstrin homology-like domain, family B, member 2	1.3249	0.031067	unable to reject null
Mm.38370	NM_011086	Pikfyve	Phosphoinositide kinase, FYVE finger containing	1.2191	0.132433	unable to reject null
Mm.489819	NM_027892	Ppp1r12a	Protein phosphatase 1, regulatory (inhibitor) subunit 12A	1.1375	0.128761	unable to reject null
Mm.451578	NM_001081307	Ppp1r12b	Protein phosphatase 1, regulatory (inhibitor) subunit 12B	1.1322	0.291733	excluded, Ct>30
Mm.331389	NM_008913	Ppp3ca	Protein phosphatase 3, catalytic subunit, alpha isoform	1.0937	0.225859	unable to reject null
Mm.274432	NM_008914	Ppp3cb	Protein phosphatase 3, catalytic subunit, beta isoform	1.1534	0.067274	unable to reject null

Unigene	Refseq	Symbol	Full Name	Fold Change	p-value from t-test	Result
Mm.469963	NM_009007	Rac1	RAS-related C3 botulinum substrate 1	1.0861	0.671401	unable to reject null
Mm.273804	NM_012025	Racgap1	Rac GTPase-activating protein 1	1.1641	0.037405	fold change < 20%
Mm.472057	NM_009041	Rdx	Radixin	1.2219	0.080542	unable to reject null
Mm.318359	NM_016802	Rhoa	Ras homolog gene family, member A	1.2191	0.028556	upregulated
Mm.6710	NM_009071	Rock1	Rho-associated coiled-coil containing protein kinase 1	1.1401	0.101461	unable to reject null
Mm.389682	NM_198109	Ssh1	Slingshot homolog 1 (Drosophila)	0.9218	0.530802	excluded, Ct>30
Mm.440381	NM_177710	Ssh2	Slingshot homolog 2 (Drosophila)	1.3907	0.085916	unable to reject null
Mm.378957	NM_019641	Stmn1	Stathmin 1	1.0515	0.273928	unable to reject null
Mm.310902	NM_009384	Tiam1	T-cell lymphoma invasion and metastasis 1	1.2248	0.276148	unable to reject null
Mm.9684	NM_009499	Vasp	Vasodilator-stimulated phosphoprotein	0.9609	0.586824	unable to reject null
Mm.4735	NM_009515	Was	Wiskott-Aldrich syndrome homolog (human)	1.3096	0.509456	excluded, Ct>30
Mm.41353	NM_031877	Wasf1	WASP family 1	1.0347	0.662419	unable to reject null
Mm.1574	NM_028459	Wasl	Wiskott-Aldrich syndrome-like (human)	1.1401	0.113133	unable to reject null
Mm.163	NM_009735	B2m	Beta-2 microglobulin	0.8904	0.161803	Housekeeping
Mm.304088	NM_008084	Gapdh	Glyceraldehyde-3-phosphate dehydrogenase	1.0836	0.540205	Housekeeping
Mm.3317	NM_010368	Gusb	Glucuronidase, beta	1.0371	0.756475	Housekeeping
Mm.2180	NM_008302	Hsp90ab1	Heat shock protein 90 alpha (cytosolic), class B member 1	0.9994	0.966986	Housekeeping